Abstract

Title of dissertation: MOLECULAR AND GENETIC ANALYSIS OF FLOWER DEVELOPMENT IN *ARABIDOPSIS THALIANA* AND THE DIPLOID STRAWBERRY, *FRAGARIA VESCA*

Courtney Allison Hollender, Doctor of Philosophy, 2012

Dissertation directed by: Professor Zhongchi Liu
Department of Cell Biology and Molecular Genetics

In a world with a warming climate and a rapidly growing population, plant biology is becoming a field of increasing importance. Deciphering the molecular and genetic mechanisms behind the development of the flower, the fruit and seed progenitor, will enhance the agricultural productivity needed to ensure a sustainable food supply. My PhD research ties in with this need by furthering the basic knowledge of the mechanisms underlying flower development in two ways.

First, using *Arabidopsis thaliana*, the classic model plant, I investigated the regulation of a gene, *SPATULA (SPT),* necessary for the proper development of the gynoecium, the female flower organ that, upon fertilization, directly gives rise to fruit. For flower and fruit to properly develop, the expression of *SPT*, must be tightly regulated both spatially and temporally. My research examined the mechanism of transcriptional repression of *SPT* in the sepals and petals by several interacting transcription factors (LEUNIG,

SEUSS, APETALA2) and the molecular and genetic interaction between ETTIN and SPT in patterning gynoecium.

The second focus of my research was to develop *Fragaria vesca* (the diploid strawberry), as a model Rosaceae for the study of flower and fruit development. *Arabidopsis* has much value as a small, fast growing, flowering plant with a multitude of genetic and genomic resources, however the flower of this mustard family weed is not representative of all crop flowers. The Rosaceae family, including many agriculturally important fruit trees such as apple, peach, blackberry, and strawberry, warrants its own model plant to investigate the distinct mechanisms behind their unique reproductive biology. Toward developing *F. vesca* as the model plant for studying Rosaceae flowers, I characterized and described developmental progression of *F. vesca* flowers morphologically through scanning electron microscopy and histological analysis as well as molecularly through transcriptomes and *in situ* hybridization. In addition, I pioneered a small-scale mutagenesis screen of *F. vesca* that will lead to future genetic resources. My thesis work places the groundwork for future discoveries in *F. vesca* and Rosaceae and benefits research, education, and agricultural applications for the *Rosaceae* and the plant biology communities.

MOLECULAR AND GENETIC ANALYSIS OF FLOWER DEVELOPMENT IN *ARABIDOPSIS THALIANA* AND THE DIPLOID STRAWBERRY, *FRAGARIA VESCA*

by

Courtney Allison Hollender

Dissertation submitted to the Faculty of the Graduate School of the
University of Maryland, College Park in partial fulfillment
Of the requirements for the degree of
Doctor of Philosophy
2012

Advisory Committee:

Professor Zhongchi Liu, Chair
Professor Gary Colman
Professor Stephen Miller
Professor Louisa Wu
Professor Shunyuan Xiao

©Copyright by
Courtney Allison Hollender
2012

Acknowledgements

I would like to acknowledge several people that supported and helped me along the way, making this process a lot easier than it could have been. First and foremost, I would like to acknowledge my advisor, Dr. Zhongchi Liu. She has spent an innumerable amount of hours working with me over the past several years, teaching me how to think critically, be a good scientist, and to write like one. I am grateful to have her as a mentor and believe that I am leaving her lab well trained. Second, I would like to thank the past and present members of the Liu lab. Over the years, their support and willingness to help when needed, has made this experience not just enjoyable, but also fun. Specifically, I would like to acknowledge Dr. Paja Sijacic, who not only taught me lab techniques, but also taught me to question every result. In addition, Paja let me ask him many, many questions I already knew the answer to, and was a good friend to me throughout our 5+ years sitting next to each other. I would also like to acknowledge Aviva Geretz, who worked with me for 2 years on everything from genotyping to microdissection. Her careful lab hands, critical thinking, problem solving, and constant questioning helped move my research along faster than I could have done on my own. Additionally, I would like to thank Liu lab member Chunying Kang for sharing the responsibility of the strawberry project with me and for moving it forward, as well as for her help with bioinformatics. Next, I would like to acknowledge Dr. Janet Slovin from the USDA. She taught me the strawberry system from the ground up, helped with dissections and imaging, and had a genuine enthusiasm for science that was refreshing to be around. Dr. Nadim Alkarouf from Towson University, his graduate student Omar Darwish, and several of his undergraduates, were responsible for the RNA-Seq sequence alignments

and some analysis; none of the transcriptome work described in Chapter V could not have been done without their help. I would to thank Xiaoning Zhang for teaching me how to perform protoplast transfection at her lab at St. Bonaventure University, and for rekindling my enthusiasm for science every time we worked together. Additionally, my work could not have been completed with out the help of Tim Maugel, in the Laboratory for Biological Ultrastructure, who trained me on the SEM, and Ben Matthews at the USDA for both advice and use of the laser capture microscope. Further, Dr. Heven Sze and Dr. Robert Su greatly enriched my experience here with many thoughtful discussions about science, teaching, and life. I would also like to thank Dr. Bob Slocum from Goucher College for introducing me to plant biology, encouraging my desire to enter this field, and exposing me to graduate program at the University of Maryland. Finally, I would like to acknowledge the wonderful plant science community in the department of Cell Biology and Molecular Genetics. This has been a highly collaborative, welcoming, and friendly atmosphere. I feel privileged to have been a part of it and will miss the monthly happy hours and celebrations.

Table of Contents

List of Tables

List of Figures

Appendix A

Appendix B

Chapter I: Introduction

Part 1: Regulation of *ABCE* genes in *Arabidopsis thaliana* flower development

The *Arabidopsis thaliana* Flower

The *Arabidopsis thaliana* flower is a typical dicot flower, consisting of four concentric whorls of distinct organs: sepals, petals, stamen and carpels (Fig. 1-1). The inner whorls, the stamen and carpels, are the reproductive organs. The stamen produce pollen, the male gametes, while the carpels develop the ovules which pollen will fertilize. In the model plant *Arabidopsis thaliana* (here after referred to as *Arabidopsis*), the two carpels at the center of the flower fuse with each other, forming a structure known as a gynoecium (Fig. 1-1).

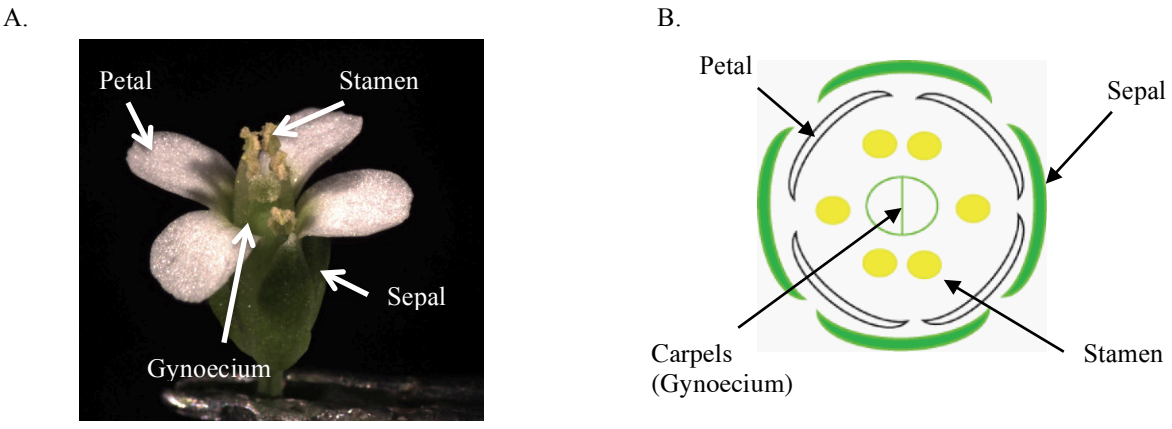

Fig. 1-1 The *Arabidopsis* flower (A) is comprised of 4 concentric whorls of four floral organ types, illustrated in a cartoon (B) of a cross section of a flower

The ABC Model of Flower Development

In the flower, as with all specialized tissues or structures in multicellular eukaryotes, proper development is dependent on strict temporal and spatial regulation of gene expression. Much past research in the field of floral development was dependent on the genetic analysis of floral homeotic mutants (Bowman et al., 1989; Bowman et al., 1991b), whose floral organs take on the identity of organs in a different position or whorl of the flower. For example the class C mutant *agamous* (*ag*) develops petals in place of stamens and sepals in place of carpels (Bowman et al., 1989). The genetic analysis of single, double, and triple *abc* flower mutants led to the establishment of an elegant model, the ABC model, that describes how A, B, and C classes of genes direct the development of each type of floral organ in their proper spatial position in a flower (Coen and Meyerowitz, 1991).

This "ABC" model works as follows: the activity of class A genes in a group of cells will result in sepal development, the combined activity of class A and class B genes results in petal development, the activity of class B and class C genes together will produce stamens, and the activity of C genes alone will cause carpels development (Fig 1-2A). In *Arabidopsis,* there are two main A genes, *APETALA1* and *APETALA2* (*AP1* and *AP2*); two B genes, *APETALA3* and *PISTILLATA* (*AP3* and *PI*); and one main C gene, *AGAMOUS* (*AG*). Genes in all three of these classes code for transcription factors that regulate downstream genes necessary for specific floral organ identity.

An important aspect of the ABC model is that the A and C class genes negatively regulate each other's expression, in addition to conferring sepal/petal and stamen/carpel identity, respectively (Bowman et al., 1991b; Coen and Meyerowitz, 1991). Class A proteins repress C class gene expression in the outer floral whorls, and the C class proteins repress class A gene expression in the inner two whorls (Fig1-2A). In *ap2* mutants (class A mutant), sepals were converted to carpels and petals to stamen, owing to expansion of *AG* expression into outer floral whorls (Bowman et al., 1989; Bowman et al., 1991a; Drews et al., 1991). In *ag* flowers (class C mutants), stamen are converted to petals and carpels to sepals and a new flower (Bowman et al., 1989). Transgenic plants with ectopic expression of *AG* (in *35S::AG* plants) phenocopied *ap2* mutants, showing that AG is sufficient to repress A function in sepal and petal whorls (Mandel et al., 1992; Mizukami and Ma, 1992).

MADS proteins

The ABC genes, with the exception of *AP2*, all encode MADS proteins (Becker and Theissen, 2003), which are transcription factors found in plants, animals and fungi with a highly conserved MADS domain. The name originates from the four founding members MCM1 (in yeast), AGAMOUS (in *Arabidopsis*), Deficiens (in *Antirrhinum*), and SRF (in humans) (Becker and Theissen, 2003; Parenicová et al., 2003).

MADS proteins are commonly grouped into two types, I & II, although other categorizations exist (Theissen et al., 2000; Becker and Theissen, 2003; Parenicová et al., 2003). Type I MADS proteins have only the MADS box domain. In animals and yeast,

the type I MADS are involved in a range of functions including response to growth factors, tracheal development, metabolism, cell cycle, cell growth, and cell type determination. Little to nothing is known about the few Type I MADS genes in plants (Becker and Theissen, 2003). Type II MADS proteins contain additional conserved regions. In plants, the majority of MADS proteins (including the ABC classes of MADS proteins) are the plant specific MIKC class belonging to the Type II MADS proteins. MIKC MADS proteins contain three additional domains C-terminal to the MADS domain: the I box, the K-box, and a C-terminal domain. The ~58 amino acid MADS box domain at the N-terminus is involved in both DNA binding and protein dimerization. While both the Intervening (I-box) and the Keratin-like domain (K-box) are involved in protein dimerization, the highly variable C-terminal domain is believed to play a role in transcription activation (Riechmann and Meyerowitz, 1997; Theissen et al., 2000; Becker and Theissen, 2003). In flowering plants, many–but not all–MADS proteins are involved in flowering (Riechmann and Meyerowitz, 1997; Becker and Theissen, 2003). *In vitro* binding assays determined that the MADS domain (from MADS proteins in multiple species) binds to CArG box ($CC(A/T)_6GG$) regulatory elements in the promoters of target genes (Wynne and Treisman, 1992; Riechmann et al., 1996a; Riechmann et al., 1996b; Riechmann and Meyerowitz, 1997) (Fig.1-2B). Hetero- or homo-dimers of the ABC MADS proteins could bind to this element *in vitro*. An electrophoretic mobility-shift assay showed that homodimers of AP1 or AG and heterodimers of AP3/PI could bind the CArG box, while homodimers of AP3 or PI could not (Riechmann et al., 1996a).

AP2 proteins

AP2, the only non-MADS protein belonging to class A, is the founding member of the AP2-EREBP family transcription factors. The AP2 family proteins are unique to plants and contain over 130 members in *Arabidopsis*. All members of this family contain either one or two 68 amino acid AP2 domains (Jofuku et al., 1994; Ohme-Takagi and Shinshi, 1995; Okamuro et al., 1997b; Riechmann and Meyerowitz, 1998; Fujimoto et al., 2000; Nole-Wilson and Krizek, 2000). The AP2 domain is also involved in DNA binding. However the single AP2 domain–containing proteins (the EREBP proteins) bind ethylene response elements (GCC boxes) or dehydration response elements (CCGAC) (Nole-Wilson and Krizek, 2000). In contrast double AP2 domain containing proteins such as AINTEGUMENTA and AP2 tend to bind loosely conserved target sequences (Nole-Wilson and Krizek, 2000; X. Chen personal communication). However, the second AP2 domain in AP2 was recently shown to bind an AT-rich element (TTTGTT / AACAAA) (X. Chen, personal communication). AP2 domain proteins are involved in regulating a wide range of processes including disease resistance, abiotic stress, and ethylene and jasmonic acid signaling (Gutterson and Reuber, 2004; Pre et al., 2008; Xu et al., 2011).

The revision of ABC model: The discovery of the E class genes

Based purely on observation, over two hundred years ago Goethe hypothesized that flowers were merely modified leaves (Coen, 2001). The ABC model supports this concept, as *abc* triple mutants produce whorls of leaf-like organs (Coen and Meyerowitz, 1991). Yet, if the ABC model was wholly entirely correct, then one should be able to convert leaves into floral organs by expressing A, B, and C genes in leaves. However,

such attempts failed, suggesting that additional essential factors might be missing in leaves but present in flowers (Mizukami and Ma, 1992; Krizek and Meyerowitz, 1996).

The missing factors were the class E genes encoded by four functionally redundant MADS proteins. Two different labs identified the class E genes simultaneously using different approaches. The Yanofsky lab took a reverse genetic approach and successively knocked out a group of three to four highly homologous MADS box proteins (or *AGAMOUS-LIKE* or AGL proteins). Single mutants of these genes had no phenotype due to functional redundancy among them (Pelaz et al., 2000). It wasn't until they constructed a triple mutant for three of the AGL genes that they observed a flower phenotype with sepals in every whorl. These AGL genes were renamed *SEPALLATA1, 2* and *3* (*SEP1, 2, 3*) (Pelaz et al., 2000). The *sep1 sep2 sep3* phenotype resembled the *b* and *c* double mutants (*ap3 ag*, and *pi ag)* (Bowman et al., 1991b), suggesting that the SEP genes work in concert with B and C class genes to specify petal, stamen, and carpel identity. When mutation of the fourth E gene, *SEP4,* was introduced into the triple mutants, the quadruple *sep1 sep2 sep3 sep4* mutants produced whorls of leaves instead of organs (Ditta et al., 2004), indicating that in the absence of E function, A, B, and C genes are all dysfunctional. The Goto lab on the other hand identified class E genes by a yeast two hybrid screen using both B class proteins AP3 and PI as co-baits. Subsequently, they and the Yanofsky lab both showed that constitutive expression of the SEP gene together with *ABC* genes in plants could transform leaves into floral organs (Honma and Goto, 2001; Pelaz et al., 2001). The co-expression of 35S::PI/AP3/SEP3 (B and E genes) produced petaloid leaves, while *35S::PI/AP3/AG/SEP3* (B, C, and E genes) produced stamenoid

leaves (Honma and Goto, 2001). Additionally, rosette leaves of plants expressing *35S::SEP3/AP1/AP3/PI* (A, B, and E genes) were transformed into petals (Pelaz et al., 2001). These findings led to the revision of the ABC model into to the ABCE model (Fig. 1-2) (Theissen and Saedler, 2001).

The E genes are expressed in all four whorls, with SEP3 only in the inner three whorls, and SEP 4 primarily expressed in the carpels and young sepal primordia. E proteins interact with the ABC proteins to form organ-specific transcriptional complexes that specify different organ types (Krizek and Fletcher, 2005).

This ABCE model of flower development is also known as "quartet model" because of the physical interactions between the ABCE proteins that occur to activate their downstream targets (Theissen and Saedler, 2001; Smaczniak et al., 2012). To specify

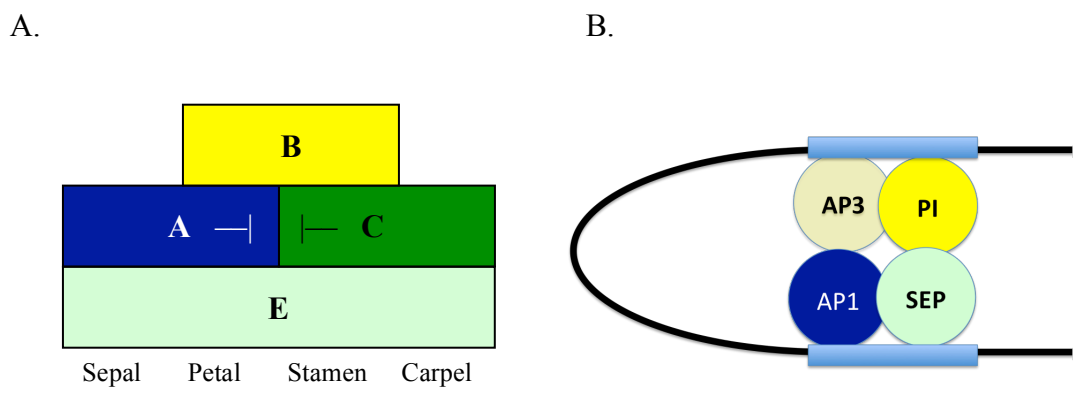

Figure 1-2.The ABCE model of flower development. (A) Cartoon illustrating spatial expression of ABCE genes and the antagonism between the A and C class. (B) Cartoon illustrating the "quartet" model of the ABCE protein complex that binds two CArG-boxes in DNA, bending the DNA in the process. The protein complex in (B) specifies petal identity. SEP represents SEP1, 2, or 3.

organ identity, the respective ABCE proteins for each whorl first form specific homo or heterodimers (i.e. AP1/AP1, AG/AG, AP3/PI, AP1/SEP, or SEP/AG) (Goto and Meyerowitz, 1994; Riechmann et al., 1996a; Fan et al., 1997). Next, these dimers interact with each other in specific arrangements, to form heterotetramers and bridge two CArG boxes from the regulatory regions of their target genes, bending the DNA in the process (Fig. 1-2B) (Honma and Goto, 2001; Theissen and Saedler, 2001; Krizek and Fletcher, 2005; Smaczniak et al., 2012). Specifically, sepal identity is specified by a protein tetramer (quartet) consisting of A + E proteins (ie. AP1/AP1/SEP/SEP). Petal identity is specified by a quartet of A + B + E proteins (AP1/SEP/PI/AP3). B + C + E protein quartets (PI/AP3/AG/SEP) cause stamen identity, and C + E protein quartets (AG/AG/SEP/SEP) specify carpel identity (Fig.1-2). ABCE proteins in other angiosperms, such as *Antirrhinum* and petunia, also form similarly organized complexes in specifying respective floral organs (Tröbner et al., 1992; Davies et al., 1996; Egea-Cortines et al., 1999; Krizek and Fletcher, 2005). In *Arabidopsis*, these quartets have been shown to associate with numerous chromatin remodeling factors including the histone H3K27 demethylase REF6, Chromatin Remodeling 4 (CH4), and histone deacetylase 19 (HDA19) (Gonzalez et al., 2007; Smaczniak et al., 2012). It's likely that the regulatory role of these tetramers is dependent on these interactions.

The involvement of a miRNA in flower development

Adding another dimension to the ABCE model is the interesting role of microRNA172 (*miR172)*. Initially expressed in all four floral whorls, *mir172* is later concentrated in the inner whorls starting around the time of carpel initiation (Chen, 2004). When *miR172*

was overexpressed, the resulting flowers resembled the phenotype of a strong *ap2* mutant (Aukerman and Sakai, 2003; Chen, 2004). Additionally, *miR172* has been shown to post-transcriptionally down regulate AP2, and act at the same time as a target of AP2-regulation (Chen, 2004; Wollmann et al., 2010; Grigorova et al., 2011). The mutual antagonism between A class gene AP2 and *miR172*, in addition to the *35S::miR172* phenotype, suggests that *miR172* functions as a C gene. This C function was shown to be independent of *AG* (Zhao et al., 2007a).

LEUNIG and SEUSS as co-repressors for C gene expression in *Arabidopsis*

One important aspect of the ABCE model is the antagonism between A and C class genes. As mentioned above, in an A class mutant, C expression expands to all flour whorls, leading transformation of sepals to carpels or carpelloid organs. Our lab's research has been focused on understanding the mechanism of A - C gene antagonism, in which the C gene in question is not only *AG*, but also the non-traditional C genes *miR172* and *SPATULA* (*SPT*). Thus far, the SEUSS and LEUNIG proteins (SEU/LUG) have been shown genetically and molecularly to repress *AG* and *miR172* (Liu and Meyerowitz, 1995; Conner and Liu, 2000; Franks et al., 2002; Sridhar et al., 2004; Sridhar et al., 2006; Grigorova et al., 2011). In *lug* or *seu* mutants, *AG* expression expands to the outer floral whorls, causing carpelloid sepals and stamenoid petals. The removal of *AG* function from *lug* single, *seu* single, and *seu lug* mutants reduced their outer whorl carpelloidy and produced a flower that resembled *ag* single mutant (Liu and Meyerowitz, 1995; Franks et al., 2002). Likewise, *miR172* expression expands to the outer whorls of *seu* and *lug* mutant flowers (Grigorova et al., 2011). Further, both SEU and LUG have been shown to

interact with the cis-regulatory regions of *AG* and *miR172* through ChIP (Sridhar et al., 2006; Grigorova et al., 2011) (see Chapter III for interaction between LUG and *AG* element).

The *lug* loss-of-function mutant has reduced fertility, carpelloid sepals and petals, and gynoecium deformities including lack of full carpel fusion (Liu and Meyerowitz, 1995). However, LUG is not strictly a flower development gene, and it is expressed in all four floral whorls as well as throughout the *Arabidopsis* plant (Conner and Liu, 2000; Schmid et al., 2005). LUG is a member of the Groucho(Gro)/Tup1 family of co-repressors that functions in part to regulate flower development (Liu and Karmarkar, 2008). Members of this repressor family (found in plants, animals, and fungi) are capable of regulating diverse genes and developmental processes. The co-repressor specificity depends on the DNA-binding transcription factors that the co-repressors interact with via their multiple C-terminal WD domains (Liu and Karmarkar, 2008). For example, when the *Drosophila* co-repressor Groucho (Gro) interacts with the bHLH transcription factor Hairy it regulates segmentation genes, but when Gro interacts with Deadpan, it regulates genes involved in sex determination (Jiménez et al., 1997). The yeast co-repressor Tup1 functions similarly to regulate diverse genes, but with one exception, Tup1 cannot directly interact with DNA-binding transcription factors. Instead, Tup1 binds through its N-terminal domain to the glutamine (Q)-rich protein Ssn6; Ssn6 in turn binds to various DNA-binding transcription factors (Liu and Karmarkar, 2008). In yeast, Ssn6 acts as an adapter protein that links the co-repressor Tup1 with various DNA sequence-specific transcription factors. LUG, which is one of 13 Gro/Tup1 co-

repressors in *Arabidopsis*, works in a similar fashion as Tup1. The LUG protein has repressor ability, but it neither directly binds to DNA nor DNA-binding transcription factors. Rather, LUG is recruited to transcription factors via its interaction with SEU (similar to the interaction between Tup1 and Ssn6) (Sridhar et al., 2004).

SEU encodes a glutamine (Q) rich protein that is expressed throughout the plant (Franks et al., 2002; Schmid et al., 2005). The flowers of *seu* mutants have a similar, although weaker, phenotype compared to *lug* mutants (carpelloid outer whorls and unfused carpels), and *lug seu* double mutants have a severe homeotic conversion of all flower whorls to carpelloid sepals. In *seu*, *lug*, single and *lug seu* double mutants, *AG* mRNA is ectopically expressed in the outer whorls contributing to the floral homeotic phenotypes of the *seu* and *lug* mutants (Liu and Meyerowitz, 1995; Conner and Liu, 2000; Franks et al., 2002).

Together, SEU and LUG physically interact to form a co-repressor complex (Franks et al. 2002; Sridhar et al. 2004). The repressor ability of LUG occurs through interactions with histone deacetylases or the mediator complex, LUG could not regulate target genes in the absence of SEU (Sridhar et al., 2004; Gonzalez et al., 2007). Further, this co- repressor complex was recruited to negatively regulate C class genes. SEU/LUG interacts with the A class protein AP1 and the E class protein SEP3 to repress *AG* in the outer whorls of *Arabidopsis* flowers via the histone deacetylase HDA19 (Figure 1-3) (Sridhar et al., 2006). Recently, our lab showed that SEU/LUG also negatively regulates the microRNA *miR172* in the outer floral whorls, and this regulation is mediated by AP2, which provides

the DNA-binding activity for SEU/LUG (Grigorova et al., 2011). Other work has implicated SEU/LUG mediated repression in petal vasculature and abaxial/adaxial polarity genes in the petal (Franks et al., 2006). SEU and LUG likely regulate numerous other genes throughout the plant, with their specificity determined by the tissue specific DNA-binding transcription factors they interact with. My work described in Chapters II and III is aimed at testing if the gene *SPATULA (SPT)* is a target of SEU/LUG repression. *SPT* is what I would consider a non-traditional C class gene. *SPT* is essential for the identity of specific carpel tissues, but not the carpel identity itself. *spt* mutants develop malformed carpels, while plants with null mutations in *AG*, the traditional C class gene, do not develop carpels at all.

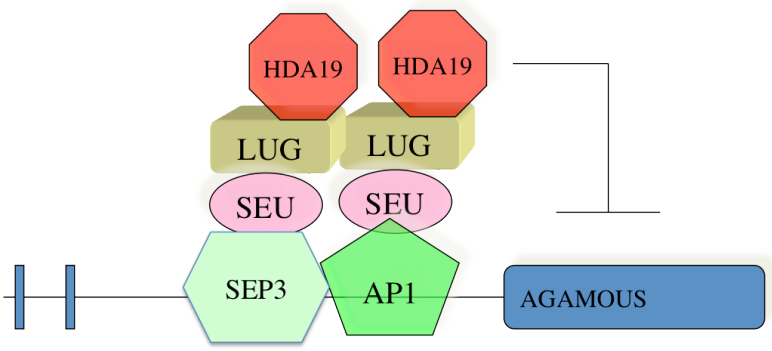

Figure 1-3. Cartoon of SEU/LUG mediated repression of AG

The structure of gynoecium, the female reproductive organ

Although small in size, the *Arabidopsis* gynoecium is comprised of over 6 types of tissue (Figs.1-1 and 1-4), all of which need to develop properly to ensure fertilization and eventual seed production (the epitome of evolutionary success). The cartoons in Fig. 1-4 illustrate the parts and organization of the gynoecium. The uppermost, or apical, region of the gynoecium is known as the stigma. This is the region where the male pollen will land, germinate, and begin to grow pollen tubes downwards towards the ovules. Pollen tubes grow through a specialized tissue in the gynoecium called the transmitting tract, which runs vertically through the entire gynoecium and secretes an extracellular polysaccharide matrix that aids in their growth. Beneath the stigma is a short region known as the style. The enlarged tube basal to the style is the ovary that contains the ovules.

The gynoecium is made up of two carpels that fused post-genitally. All tissues derived from the region of carpel fusion are referred to as 'marginal tissues.' These 'marginal tissues (indicated in yellow in Fig. 1-4) include the stigma, the septum, which bisects the interior of the gynoecium, and the replum, which connects the two valves on the exterior of the gynoecium. Each valve is the exterior of one of the two fused carpels, and together they encase the ovary. Within the ovary, ovules extend from both sides of the septum connected by the funiculus. The transmitting tract, which runs through the center of the ovary, and the ovules, which develop from the septum, are also considered marginal tissues.

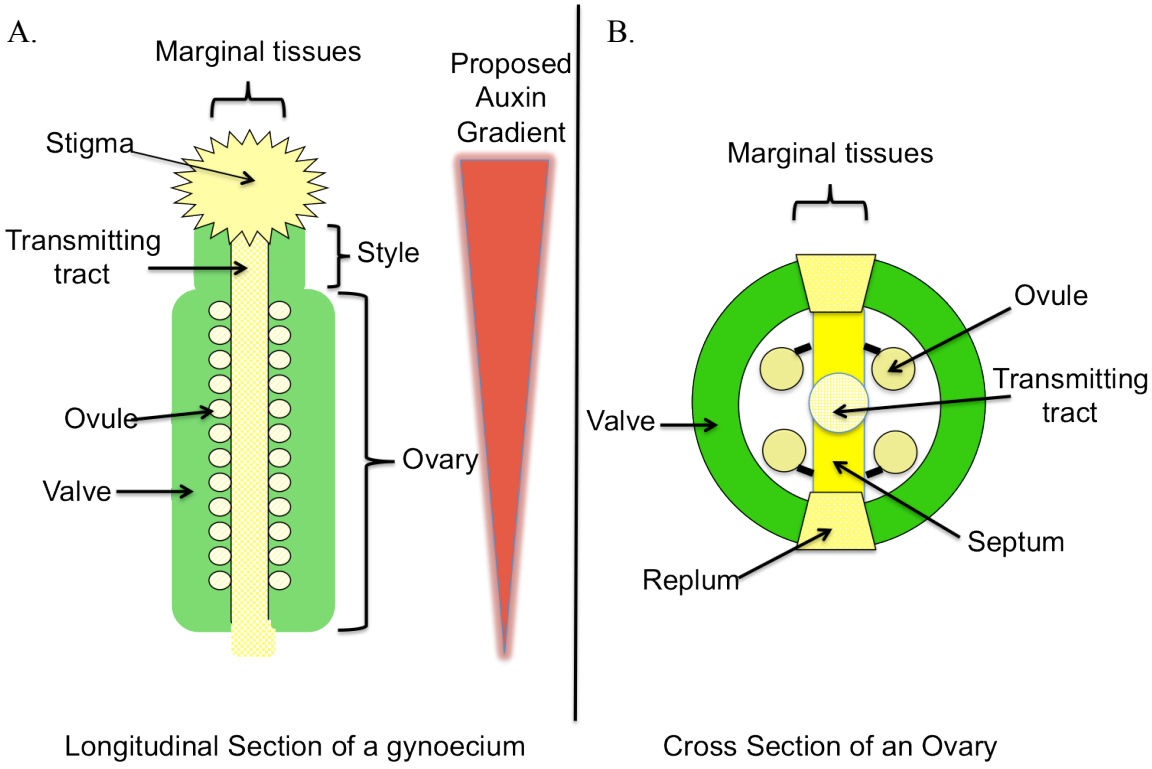

Figure 1-4. Cartoons depicting the tissue organization of the *Arabidopsis* gynoecium. (A) Longitudinal Section. (B) Cross section of the ovary. The proposed apical-basal auxin gradient is indicated in (A) by the red triangle. Auxin level is believed to be at the highest at the apex of the gynoecium and the lowest at the base. In both (A) and (B) marginal tissues are indicated by yellow coloring.

Auxin in gynoecium development

An apical to basal gradient of the plant hormone auxin was proposed for specifying the distinct tissues along the apical-basal axis (Nemhauser et al., 2000). Auxin is a small but essential plant hormone that is transported throughout plants and is involved in regulating diverse processes including embryonic development; phototropism and gravitropism; and cell division, elongation, and differentiation, among others (Teale et al., 2006). Auxin is transported from cell-to-cell via membrane bound influx and efflux transporters such as the PIN and AUX1 proteins, respectively. Auxin signaling involves interactions between intracellular auxin receptors, Aux/IAA repressor proteins, and auxin response factors (ARFs) that bind DNA (Guilfoyle and Hagen, 2007). In the absence of auxin, Aux/IAA repressor proteins bind to ARFs situated on DNA, blocking their activating ability (Fig 1-5, top). When auxin is available, the hormone binds to a TIR1 auxin receptor attached to an E3-ligase complex, triggering the E3 ligase complex to ubiquitinate Aux/IAA proteins, thereby causing IAA degradation by the proteasome and releasing ARFs from the Aux/IAA inhibition (Fig. 1-5, bottom) (Guilfoyle and Hagen, 2007). Not all ARFs are activators, however, and those that have repressor function may act by competing with the activator ARFs for binding to auxin response elements (AuxRE sequences) and/or through physical interactions with activating ARFs (Guilfoyle and Hagen, 2007).

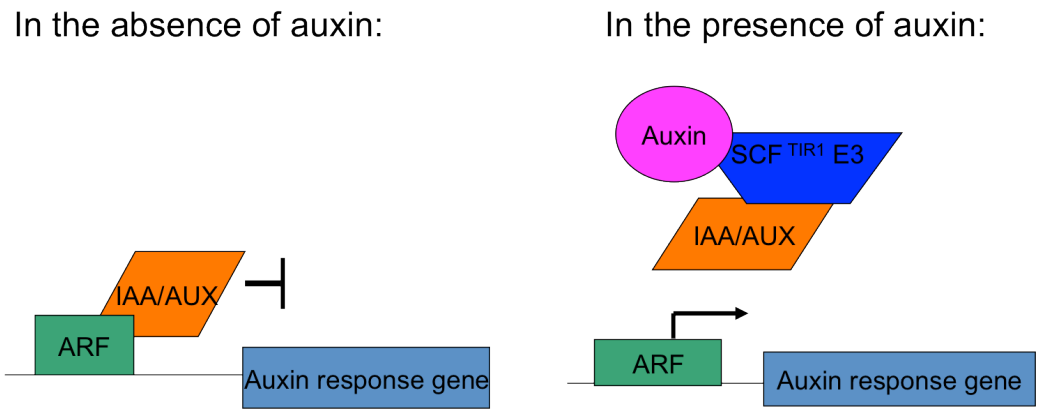

Figure 1-5. Cartoon depicting a simplified mechanism for auxin-mediated gene regulation. In the absence of auxin, ARFs are inhibited by Aux/IAA proteins (left). The presence of auxin triggers the ubiquitination and removal of the Aux/IAA repressors by the SCF^{TIR1}E3 ligase complex, allowing ARFs to perform their normal functions.

The belief that an apical-basal auxin gradient is needed to specify the distinct gynoecium tissues along this axis is the result of experiments using the polar auxin transport inhibitor NPA as well as analysis of auxin signaling mutants (Nemhauser et al., 2000). When a developing gynoecium is treated with NPA, auxin pools at the apex and depletes in the ovary, resulting in a gynoecium with an increase in stigmatic tissue at the apex and a severely decreased valve. Loss-of-function mutants for an ARF (ARF3), also named *ETTIN* (*ETT*), produce a similar valveless phenotype (Sessions and Zambryski, 1995; Nemhauser et al., 2000). It is believed that highest concentration of auxin accumulates in the apical region and promotes stigma development, while the polar transport of auxin downward (basally) results in a medium level of auxin that specifies the development of ovary tissues (Nemhauser et al., 2000). Previous studies have implicated a role for SEU in ETT-mediated auxin signaling in flower development (Pfluger and Zambryski, 2004).

Chapter III further investigates the relationship between SEU and ETT in connection with the expression of the C class gene *SPT*.

Part 2: Toward establishing *Fragaria vesca* as a model for studying flower and fruit development in Rosaceae

Why strawberry?

Arabidopsis is very convenient model plant to study flower development, and it comes with 20+ years of genetic and genomic tools in addition to substantial literature resources. However, the *Arabidopsis* flower is not representative of all flowers, nor does the fruit it produces have any agricultural importance. For these reasons, I chose to simultaneously work on *Arabidopsis* as well as strawberry, a plant with more agricultural significance. In addition to being an important crop, the strawberry plant offers aspects of biology that could not be studied in *Arabidopsis*, including vegetative propagation and a unique auxin-dependent fruit development (described below), among other features. Further, *F. vesca* flowers differ from *Arabidopsis* in the number and arrangement of their carpels and stamens. As the other aspects of my research focused on C class gene regulation (essential for stamen and carpel development), I was interested to explore C function in a different species. The switch into strawberry flower development also enabled me to be part of, and influence the development of a model system from the ground up (an experience not too many molecular biology students get to have), as well as gain experience with techniques that my *Arabidopsis* project may not have exposed me to such as histological staining, laser capture microscopy, and RNA-Seq, and bioinformatics.

F. vesca as a new model for Rosaceae flower development

The commercial strawberry, *Fragaria* × *ananassa,* is of significant agricultural importance. In 2009 alone, strawberry production in the United States was valued at over $2 billion (Economic Research Service, USDA). Most strawberry research in the US and Europe has focused on economically important issues such as genetic markers, growing and packaging practices, pest and pathogen control, aroma, flavor, and nutritional properties (Hummer and Hancock, 2009; Sargent et al., 2009; Schwab et al., 2009; Reganold et al., 2010; Slovin and Michael, 2011). In comparison, basic knowledge of strawberry development on a molecular and cellular level is lacking. With the availability of new genomic and genetic resources and the development of new inbred diploid strawberry lines, the strawberry research community is poised to make major advances in research on all aspects of strawberry biology.

Of particular interest and importance, both from a scientific as well as a practical point of view, is the biology of strawberry sexual and asexual reproduction. *F. vesca* is self-fertile and can produce many seeds per fruit. However, strawberry is also capable of asexual clonal propagation through the production of runners, or stolons, and by the production of branch crowns. The true fruit of strawberry, in the botanical sense, are the achenes that dot the surface of an enlarged receptacle (Fig 1-6). Each achene is the product of an individual carpel and contains a single seed. The fleshy, flavorful tissue is the receptacle, a modified stem tip (Darrow, 1966; Hancock, 1999). For the purposes of this thesis, I refer to the enlarged receptacle with the attached achenes as the berry or fruit. Ripening

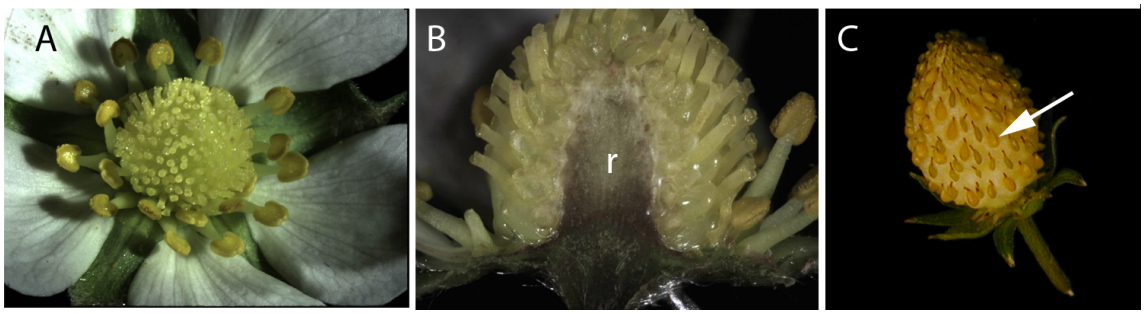

Figure 1-6. The *F. vesca* flower and fruit. (A) Open flower with 5 petals, 20 stamen, and ~160 carpels in the center. (B) Bisected flower revealing receptacle (r) beneath the carpels. (C) Berry with an arrow pointing to a true fruit, an achene.

of the fruit is considered non-climacteric (Darrow, 1966; Hancock, 1999). Although the influence of ethylene on the development of aromatic volatiles, color, and the production of softening enzymes associated with ripening is not yet clear, ethylene does not have a major influence on the ripening of strawberry as it does in apple, banana, peach, and tomato (Perkins-Veazie, 1995; Perkins-Veazie et al., 1995; Giovannoni, 2001; Castillejo et al., 2004; Trainotti et al., 2005; Taiz and Zeiger, 2006). In strawberry, berry enlargement is dependent on auxin secreted from developing fertilized achenes (Nitsch, 1950). Removal of the achenes from the receptacle resulted in failure of the fleshy fruit (receptacle) to enlarge and develop unless auxin was applied (Fig. 1-7) (Nitsch, 1950). Ripening, or reddening and softening of the berry is associated with a reduction of auxin levels (Archbold and Dennis, 1984; Archbold and Dennis, 1985). The molecular mechanisms triggering post-fertilization auxin production by the achenes, and the signaling leading to cessation of such production, are still unknown. Tissue or cellular localization of auxin production within the achene also remains unknown.

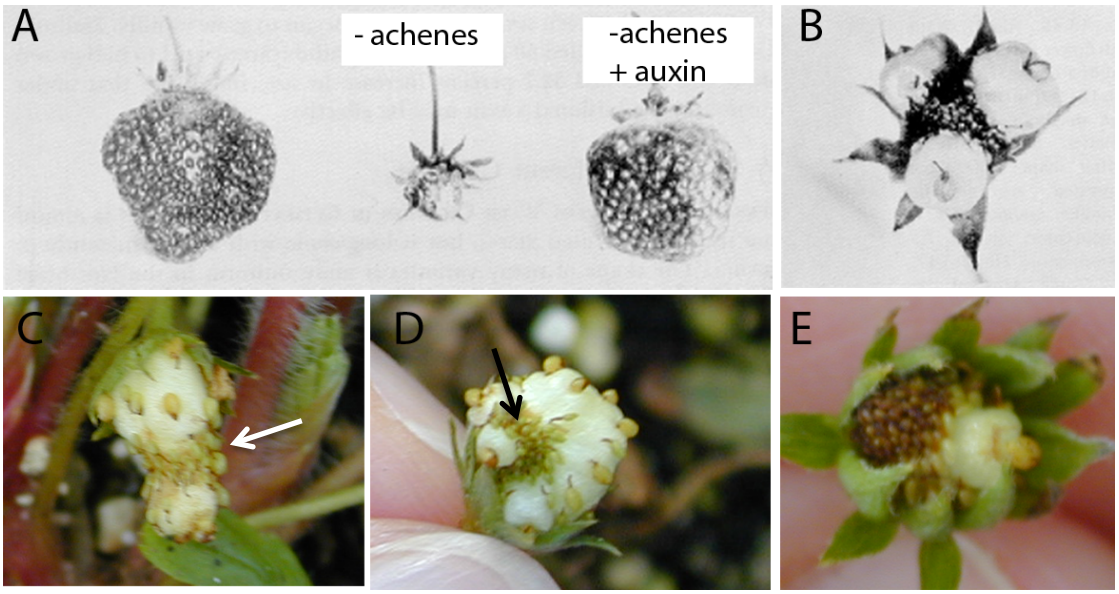

Figure 1-7. The role of auxin and fertilization on berry development. (A) Nitsch's classic experiment, in which removing fertilized achenes from a berry stunts it's growth (center) but applying auxin to a berry without achenes rescues the phenotype (right). (B) A berry with only three fertilized achenes produces three corresponding enlargements of the receptacle. (A) and (B) are taken from Darrow 1966. (C-E) Irregular *F. vesca* berry development due to improper fertilization. In (C), carpels in the center of the berry (arrow) were not fertilized. In (D) a ring of carpels was not fertilized (arrow). In (E) only the carpel at the tip of the berry was fertilized and is developing into an achene.

The commercial strawberry, *Fragaria* × *ananassa,* is an octoploid, hindering its use in molecular, genetic, and functional studies. This limitation led to the development of the smaller diploid strawberry, in particular the woodland strawberry *F. vesca*, as a useful tool for genomics and genetics (Slovin et al., 2009; Slovin and Michael, 2011). *F. vesca*, like its octoploid relative, is a perennial. In addition to having a small physical size, it has a small genome size (~240 MB; $x = 7$), and a draft genome sequence was recently published (Shulaev et al., 2011). *F. vesca* has a short seed to fruit cycle (~3.5 months),

high seed production (~160 per primary berry), inbred lines capable of clonal vegetative propagation via runners or branch crowns, and several lines that are amenable to *Agrobacterium*-mediated transformation (Oosumi et al., 2006; Folta and Dhingra, 2007; Qin et al., 2008; Slovin et al., 2009; Slovin and Michael, 2011). The high-level of co-linearity between the genomes of octoploid and diploid *Fragaria* suggests that genomic information from diploid *F. vesca* is transferable to the octoploid (Rousseau-Gueutin et al., 2008). Apart from their larger size, the floral structure, sepal and petal numbers, floral organ arrangement, floral organ morphology and coloring, and early fruit development in *F.* × *ananassa* are basically the same as *F. vesca.* The exception is the stamen number. While *F.* × *ananassa* has an average 25 stamens per flower*, F. vesca* has 20 stamens per flower.

Inbred lines of three F. vesca cultivars, Reugen F7-4, Yellow Wonder 5AF7 (YW5AF7), and Hawaii 4 (H4 × 4) have been developed specifically for genetic and genomic studies (Oosumi et al., 2006; Shulaev et al., 2008; Mouhu et al., 2009; Shulaev et al., 2011). All three cultivars are day neutral. YW5AF7, which bears yellow berries (Fig. 1-5C) and Ruegen, which bears red berries, are runnerless, whereas H4 × 4 bears yellow berries and develops runners. Despite differences in berry color and aroma, floral development and morphology with respect to size, organ arrangement, and organ number, as well as fruit development, are identical in these three cultivars (J. Slovin, unpublished). In red-fruited *Fragaria*, the red color develops in the later stages of fruit development, when the seed within the achene is mature and the receptacle has reached mature size (Fait et al., 2008; Slovin and Michael, 2011). YW5AF7 was chosen for the present study as it was more

inbred than H4 × 4 and Ruegen at the inception of this study and the runnerless phenotype of YW5AF7 permits growing large numbers of plants in a small space, an essential feature for future mutagenesis screens (Slovin et al., 2009). The yellow berry of YW5AF7 has the added advantage that red fruit color, which is a dominant trait, can serve as a selection marker for transformation and genetic crosses (Williamson et al., 1995; Davis and Yu, 1997; Deng and Davis, 2001).

Staging *F. vesca* flower development

Using YW5AF7, a standardized developmental staging of morphological changes associated with flower and early fruit development was created (Chapter IV). Developmental stages were defined based on macroscopic and microscopic landmark events including changes in tissue and organ structure, shape, size, and cellular events including meiosis and tissue degeneration. A majority of the landmark events proposed by Bugozo et al. (2004) were incorporated to facilitate comparisons across flowering plants. In addition, the expression of the *F. vesca* homolog of *AGAMOUS* (*FvAG*), a molecular marker for stamen and carpel primordia, was examined by in situ hybridization during YW5AF7 flower development. The work reported in Chapter IV lays the foundation for future molecular analysis of *F. vesca* flower development, characterization of floral or fruit mutants, and investigations of the molecular mechanisms underlying strawberry floral organ initiation, differentiation, gametophyte development, and fruit growth and ripening. In addition, the staging is critical for comparing data across different laboratories and different data sets.

The creation of *F. vesca* flower transcriptomes

A transcriptome, a snapshot of the expression levels of every gene in a tissue at one point in time, can serve as a map to understand the connection between genes and development. For example, with tissue-specific transcriptomes (maps of gene expression), the phenomenon that Nitsch found with the removal of young achenes from a berry and the application of auxin (Fig. 1-6) could be studied in terms of gene regulation. Isolating RNA from the achene or the receptacle may reveal higher expression of auxin biosynthesis or response genes, giving further insight into this developmental process.

After the completion of the *F. vesca* flower staging (Chapter IV), a next step was to utilize it as a reference to investigate the connection between transcriptomes and their effect on development. As part of a large-scale project, RNA was isolated from both developing flower and young true fruit (achenes). As my interests are in flower development, my role in this project was to create the RNA-seq libraries to establish the young and developing flower tissue transcriptomes (Chapter V). Transcriptomes reveal gene expression levels, however they do not capture any of the essential post-transcriptional regulation that may be occurring, such as repression by microRNA or protein degradation pathways. These genomic resources will be freely available to the scientific community, and will act as a stepping off point for discovering interesting biological and developmental processes.

Creating a *F. vesca* mutagenesis population

Lastly, I worked to create preliminary populations of mutagenized *F.* vesca plants. Such populations could serve as tool for both forward and reverse genetic approaches to investigate *F. vesca* development. The details of this work are described in Appendix A.

Chapter II: APETALA2 may directly recruit SEUSS/LEUNIG to repress SPATULA expression in flowers

Introduction

The *Arabidopsis* SPATULA (SPT) protein is a basic-Helix-Loop-Helix transcription factor with activator function that is essential for proper carpel development (Alvarez and Smyth, 1999; Heisler et al., 2001; Alvarez and Smyth, 2002; Groszmann et al., 2010; Groszmann et al., 2011). In wildtype flowers two carpels fuse with each other to form the gynoecium (Figure 1-1 and 1-4). The fusion relies on the proper development of carpel marginal tissues including septum, transmitting tract, replum, and stigma. In *spt-2,* a null allele (Alvarez and Smyth, 1999; Alvarez and Smyth, 2002), the septum tissue is partially or completely absent, resulting in the abnormally flat gynoecium structure from which the gene gets its name. The stigma and style of *spt-2* are partially or completely unfused, and there is a severe reduction of stigmatic tissue (arrows and asterisk in Fig 2-1 D and E). There is also an absence of the transmitting tract, the nutrient rich matrix in the center of the septum that aids in pollen tube growth (Alvarez and Smyth, 1999; Alvarez and Smyth, 2002). As a result, *spt-2* gynoecia have reduced fertility.

Based on *spt* mutant phenotype, it can be inferred that *SPT* is required for marginal tissue, in particular, the stigmatic tissue formation. *SPT's* role in promoting stigma formation is further supported by genetic analysis. In *ap2-2* mutants, ectopic expression of carpel promoting gene *AGAMOUS (AG)* in all four floral whorls, resulted in the

conversion of outer whorl sepals to carpelloid sepals with stigmatic tissues on their margins (Bowman et al., 1991b; Liu and Meyerowitz, 1995). When this ectopic *AG* was removed in *ap2-2* by constructing the *ag-1; ap2-2* double mutants, the stigmatic tissues on the margins of (carpelloid) sepals remained. The introduction of *spt-2* allele into the *ag-1; ap2-2* background (i.e., in the triple mutant), was able to remove this stigmatic tissue almost completely from the first whorl carpelloid sepals (Alvarez and Smyth 1999). This suggests that that the development of stigmatic tissue is regulated by *SPT* independently of *AG*, and that the A class gene *AP2* works in part to suppress both *SPT* and *AG* in the outer whorls. This was supported by an *in situ* hybridization experiment showing ectopic *SPT* expression in the sepals of *ap2-2* mutants (Heisler et al., 2001). Thus, *SPT* can be considered a C class gene, as it is necessary for the specification of carpel tissues in parallel with *AG* (and not downstream of *AG*) and both *SPT* and *AG* are repressed by the A class gene *AP2* (Alvarez and Smyth, 1999).

The mRNA expression pattern of *SPT* correlates well with its role as a C class gene with a positive regulatory role for carpel development. Using GUS reporter constructs driven by various lengths of the *SPT* promoter (gifted to us from David Smyth, Monash University), I was able to visualize *SPT* expression in developing *Arabidopsis* flowers. Like *AG*, *SPT* is initially expressed throughout young (~stage 2) undifferentiated floral meristem before being restricted to the center of slightly older stage 4 floral meristem, after sepal primordia develop (Fig. 2-1 F). As wildtype flowers mature and carpels develop, *SPT* is entirely restricted to the gynoecium–most strongly at the apex, where

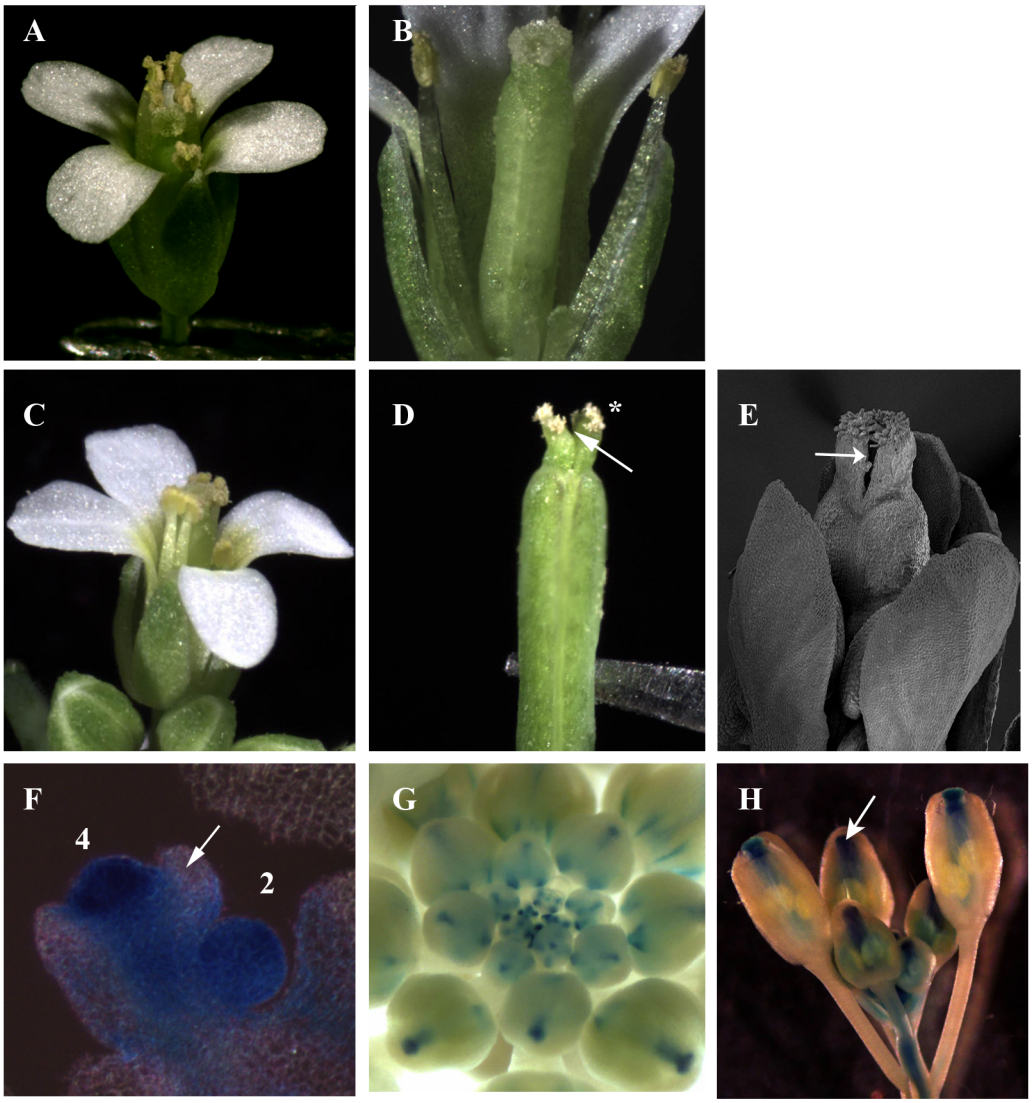

Figure 2-1. *SPATULA* is a carpel development gene. (A) A wild type flower, (B) A wild type gynoecium showing two fused carpels, (C) A *spt-2* flower similar to wild type, (D) *spt-2* gynoecium showing unfused carpels (arrow) and reduced stigmatic tissue (asterisk). (E) Scanning electron micrograph of *spt-2*. Arrow indicates split stigma. (F) Dark field micrograph of longitudinal section of stage 4 and stage 2 flowers with a *pSPT::GUS* reporter expression in blue. SPT is expressed in the inner whorls of stage 4 flower and not the sepals (arrow), as well as in the entire stage 2 flower. (G-H) Whole mount images of wild type flowers expressing *pSPT::GUS. SPT* is expressed in carpels only. Arrow in (H) indicates strong expression in gynoecium apex. *Arabidopsis* seeds containing *pSPT::GUS* reporter constructs were a gift from David Smyth (Monash University). Flowers in F and H have *pSPT6072::GUS* in Col-0 background. Flowers in G have *pSPT1270::GUS* in Ler background.

the stigma develops (Fig. 2-1 G-H). This temporal and spatial-specific expression of *SPT* is consistent with *SPT's* role in stigma and carpel margin tissue development.

Although genetics and gene expression analysis indicated that *AP2* negatively regulates *SPT* expression (Alvarez and Smyth, 1999; Heisler et al., 2001), the mechanism for the repression of *SPT* by *AP2* is still unknown. Based on previous work of our lab on the repression of *AG* by the two interacting co-repressors SEU/LUG, we hypothesize that *AP2* may recruit SEU/LUG co-repressors to repress *SPT* expression in the outer floral whorls.

To test if the SEU/LUG co-repressor complex plays a role in restricting *SPT* to the inner whorls, *in situ* hybridization was performed to determine if *SPT* expression is altered in *seu, lug,* single and *seu; lug* double mutants. In addition, yeast two hybrid, yeast three hybrid, and bi-molecular fluorescent complementation (BiFC) assays were used to test for the physical interactions between AP2 and SEU/LUG. Finally, genetic analyses were performed on *seu-1; spt-2* and *lug-3 spt-2* double mutants. The majority of our data support the hypothesis of *SPT* repression by AP2 and SEU/LUG.

Results

SEUSS (SEU) and LEUNIG (LUG) repress *SPATULA* expression in the outer floral whorls

To determine if *SPT* expression is negatively regulated by *SEU/LUG* in flowers, *in situ* hybridization was carried out to examine *SPT* mRNA in *seu-1* and *lug-3* single as well as *seu-1;lug-8* double mutant flowers. *SPT* expression in wild type flowers was restricted to

the stamen and carpels (Fig. 2-2A). In the *seu-1* and *lug-3* single mutants and *seu-1;lug-8* double mutants, ectopic expression of *SPT* in outer floral whorls (particularly in the sepals) was detected (Fig. 2-2 B-D). The degree of ectopic *SPT* expression in the outer floral whorls directly correlates with the degree of carpelloidy found in their outer whorl. *seu-1* flowers, which have a very mild carpelloid phenotype in first whorl, ~ 7.4% of outer whorl organs (Franks et al., 2002), showed only slight *SPT* expression in their sepals (Fig 2-2B). The *lug-3* and *seu-1;lug-8* mutant flowers had a much higher degree of ectopic *SPT* expression (Fig 2-2 C,D), which correlates with their more severe outer whorl carpelloidy (40% in *lug*, and 88% in *seu; lug*) (Franks et al., 2002). My result suggests that both *SEU* and *LUG* are required (directly or indirectly) for the repression of *SPT* in outer floral whorls.

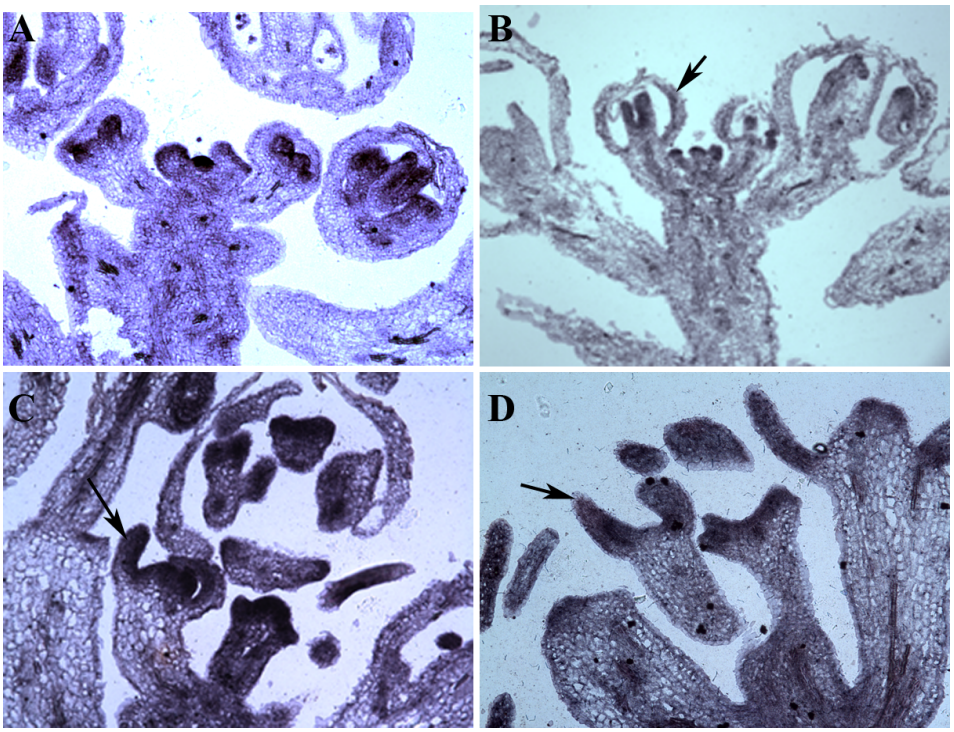

Figure 2-2. *in situ* hybridization illustrating *SPATULA* expression patterns in (A) wild type , (B) *seu-1*, (C) *lug-3,* and (D) *seu-1; lug-8* flowers. Arrows indicate ectopic expression of *SPT* in sepals/outer whorls.

APETALA2 (AP2) physically and specifically interacts with SEUSS (SEU)

Since SEU and LUG encode co-repressors that require the help of DNA-binding transcription factors to be tethered to their target genes, we tested if AP2 serves as the DNA-binding partner of SEU/LUG in *SPT* repression. This is based on the earlier work indicating *AP2* as a repressor of *SPT* expression in outer floral whorls (Alvarez and Smyth, 1999). The yeast-two hybrid system was used to test if a physical interaction between SEU or LUG and AP2 was possible. I showed that there was a direct interaction of AP2-AD with SEU-BD (Fig. 2-3A, sector 2). In contrast, AP2-AD failed to interact with LUG-BD (Fig 2-3A, sector 5). To further investigate the specificity of the interaction between AP2 and SEU, SEU-BD was also tested against AINTEGUMENTA (ANT), another AP2 domain-containing protein, however, they did not interact (Fig 2-3A, sector 4; Fig 2-5), indicating that SEU specifically interacts with AP2. To determine the region of the AP2 protein required for the interaction with SEU, I tested for an interaction between SEU-BD and a truncated version of AP2 (AP2Δ), containing primarily the two AP2 domains (Fig. 2-5). The truncated AP2Δ failed to interact with SEU-BD (Fig 2-3A, sector 3), suggesting that this interaction requires the N and/or C-terminal region of AP2.

Bimolecular fluorescence complementation (BiFC) was used to confirm the interaction between SEU and AP2 in plants. SEU and AP2 were each fused to the N-terminal and C-terminal fragments of YFP using the pUC- SPYNE and pUC-SPYCE vectors, respectively (Walter et al., 2004) and bombarded into onion epidermal cells. The fusion proteins SEU-N and AP2-C were observed to interact in nuclei, whereas the negative controls did not (Fig. 2-3B). The reciprocal combination of SEU-C with AP2-N was also tested, which yielded the same positive interaction (Fig. 2-4).

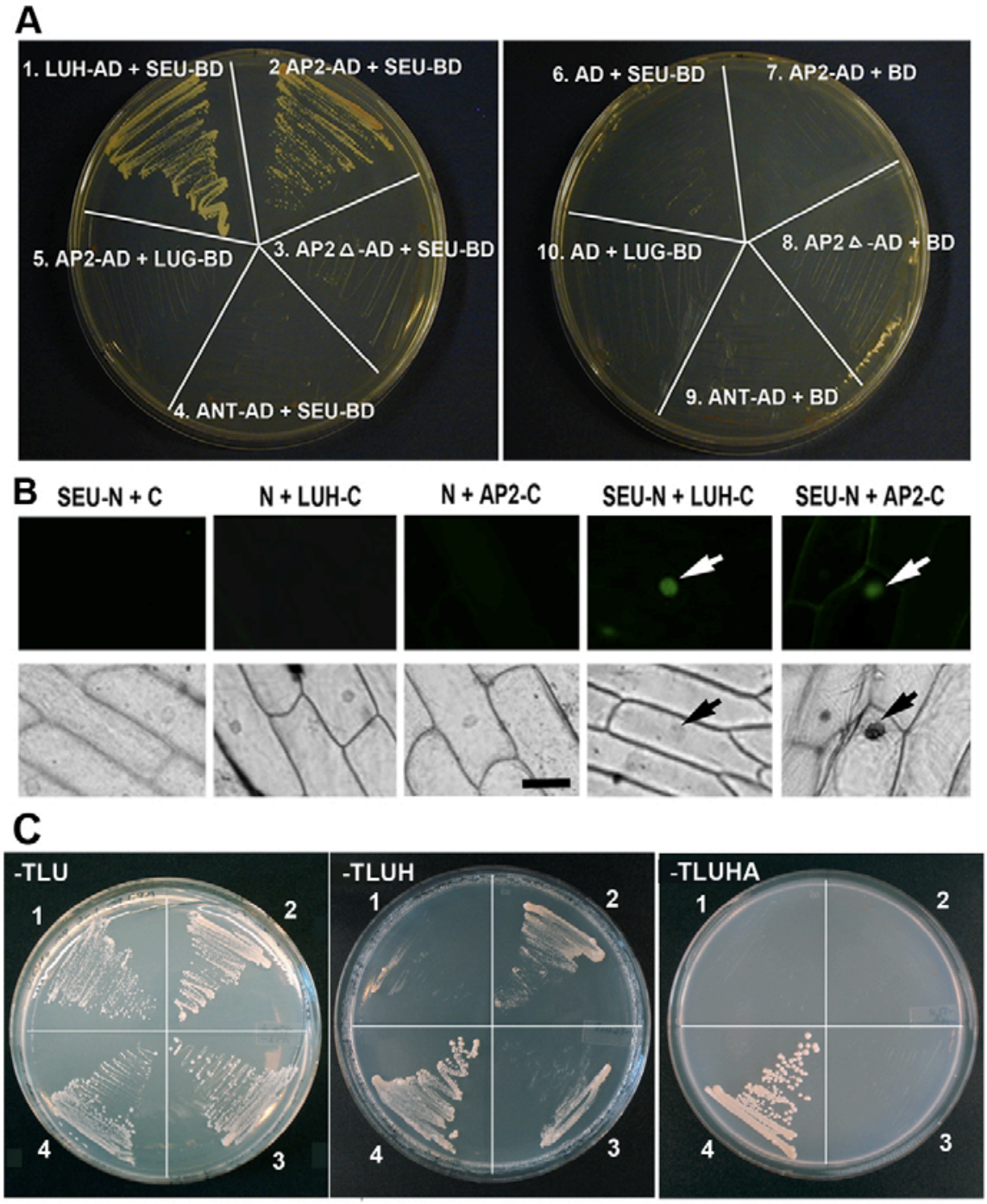

Fig. 2-3. AP2 interacts with SEU but not LUG.

Fig. 2-3. AP2 interacts with SEU but not LUG. (**A**) A yeast two hybrid assay between prey (AD; GAL4 activating domain) and bait (BD;GAL4 binding domain) pairs. LEUNIG HOMOLOG (LUH)-AD against SEU-BD served as a positive control (Sitaraman et al., 2008). SEU-BD contains a truncated SEU (residues 1-563) with its C-terminal domain removed to avoid self-activation (Sridhar et al., 2006). The plate on the right shows various negative controls. The selection medium was –Trp, –Leu, –His, –Ade (–TLHA), plus 3 mM 3-amino-1,2,4-triazole. (**B**) A BiFC assay showing interactions in planta. Fluorescent (top row) and bright-field (bottom row) images of onion epidermal peels bombarded with BiFC plasmids. N and C represent the N- and C-terminal fragments of YFP, respectively. White arrows indicate fluorescent nuclei and black arrows indicate the same nuclei in bright field. SEU-N and LUH-C, previously shown to interact via BiFC (Hollender and Liu, 2010), serve as the positive control. Scale bar:100 μm. (**C**) AP2-AD and LUG-BD were tested for interaction in the presence or absence of full-length SEU expressed from the p426 vector.1, AP2-AD + p426 vector + LUG-BD; 2, AP2-AD + p426-SEU + LUG-BD; 3, AP2delta-AD + p426-SEU + LUG-BD; 4, SEU-AD + p426 + LUG-BD (positive control). The '–TLU' medium, which lacks Trp, Leu and uracil, selects for all three plasmids. '–TLUH' selects for His3. '–TLUHA' selects for His3 and Ade2.

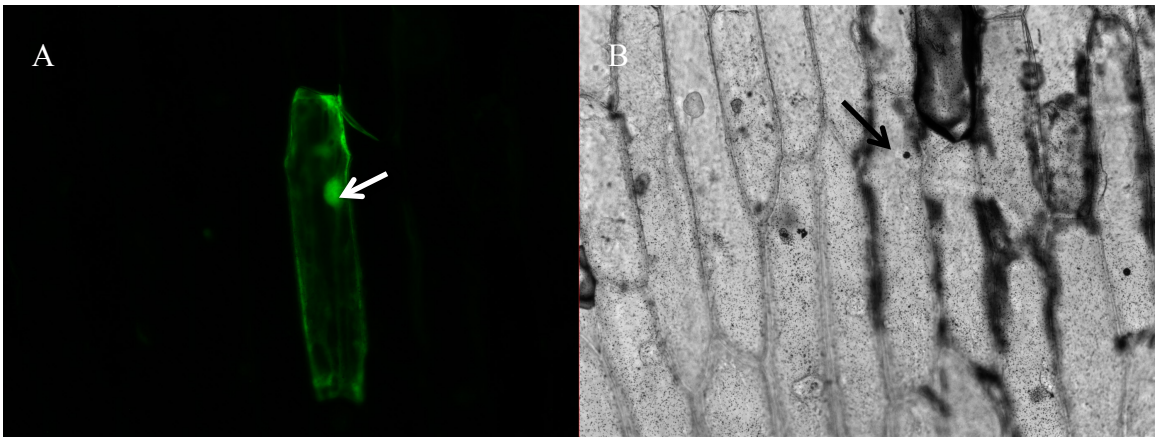

Figure 2-4. BiFC shows AP2 interacts with SEU in onion nucleus, where AP2 is fused to the N-terminal fragment of GFP in pUC-SPYNE (AP2-N) and SEU is fused to the C-terminal fragment of GFP in pUC-SPYCE (SEU-C). (A) Nuclear GFP fluorescence detected in dark field showing an interaction between AP2-N and SEU-C. (B) Bright field image of the same onion cell. Arrows indicate nucleus.

AP2 interacts with LUG through interactions with SEU

Since LUG was previously shown to interact with SEU and possesses the repressor activity (Sridhar et al., 2004), I tested if LUG could interact with AP2 indirectly via SEU using the yeast-three-hybrid assay (Fig 2-3C). LUG-BD interacted with AP2-AD only in the presence of SEU under the lesser stringent of the two selection media (–TLUH) (Fig. 3C, sector 2). Under this same selection stringency, AP2Δ -AD interacts weakly with LUG-BD in the presence of SEU (Fig. 2-3C, sector 3), even though AP2Δ is insufficient to interact with SEU alone. This result suggests that when all three proteins from the complex are present they can hold each other together despite the truncation. These results support the possibility that SEU/LUG could bind AP2 to repress target genes.

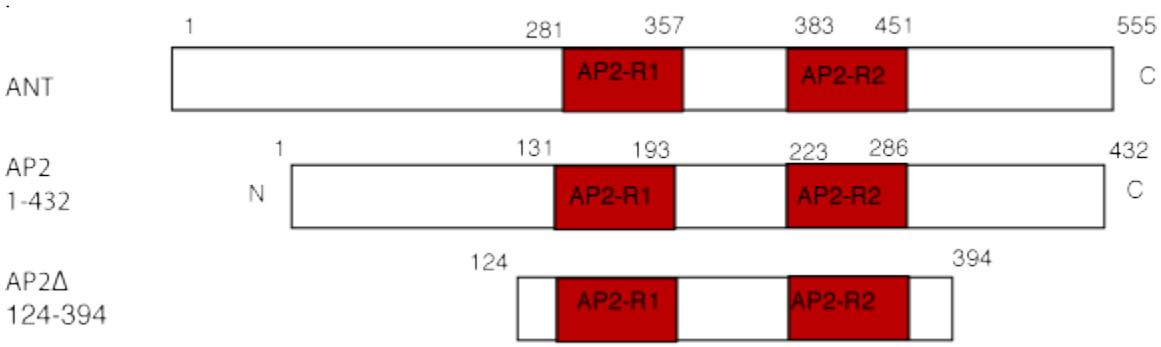

Fig 2-5. Cartoon comparing the protein sequences of ANT, AP2, and the truncated AP2 used for the Yeast-two- Hybrid assay (AP2Δ). AP2 domains are in red.

Genetic interactions between *SPT* and *SEU* and *LUG*

If the SEU/LUG complex represses *SPT* in the outer whorls, it's possible that any carpelloid outer whorl phenotypes observed in *seu* and *lug* mutants may be due in part to ectopic *SPT* expression. The removal of ectopic *SPT* function from *seu* and *lug* mutant flowers by constructing *seu; spt* and *lug spt* double mutants may reduce the degree of carpelloidy in these double mutants. To test this concept, the *spt-2* allele was crossed into *seu-1* and *lug-3* to generate *spt; seu* and *spt2; lug* double mutants and the outer whorl phenotypes were examined using scanning electron microscopy (Fig 2-6). Sepals of *seu-1* flowers exhibited a very weak carpelloid phenotype, primarily in the form of thicker edges in first whorl carpels (Fig. 2-6 A-B). The *spt-2; seu-1* double mutant exhibited a floral phenotype similar to *seu-1* (Fig 2-6 C-D); since there is very rarely any ectopic stigmatic tissue in the carpelloid sepals of *seu-1*, it may be difficult to observe the impact of *spt-2*. Likewise, the carpelloid phenotype of *lug-3* sepals, easily detectable by the

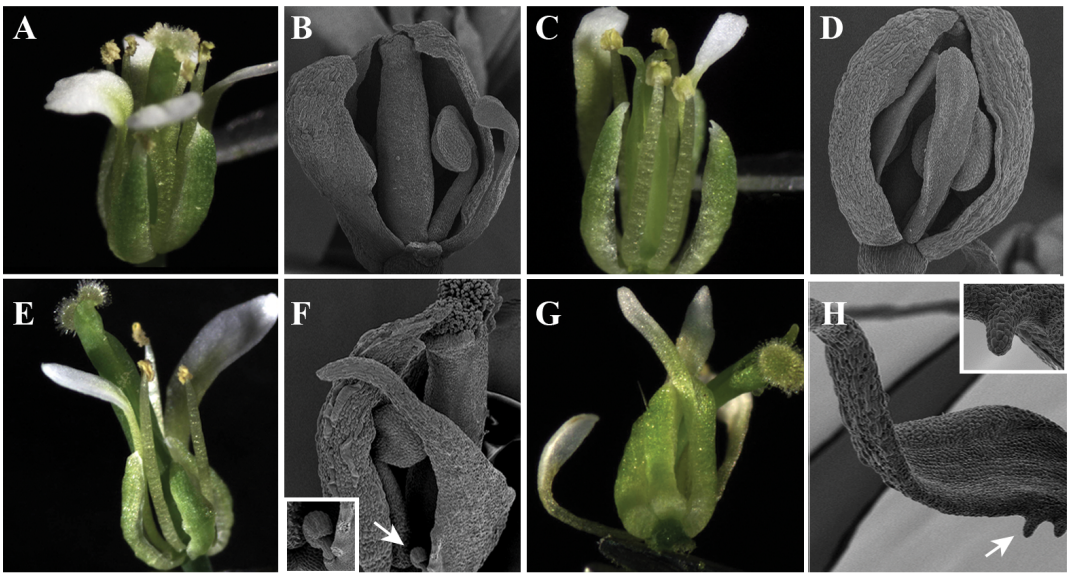

Figure 2-6. *spt-2* does not suppress carpelloid sepals in *seu-1* and *lug-3*. Stereo and SEM images of (A-B) *seu-1*, (C-D) *seu-1; spt-2*, (E-F) *lug-3*, and (G-H) *lug-3, spt-2*. Ovule primordia on *lug-3* and *lug-3, spt-2* sepals are indicated by arrows and in inset boxes.

presence of ectopic ovule primordia (Fig 2-6 E-F), did not exhibit any obvious reduction of carpelloidy in the *spt-2 lug-3* double mutant sepals (Fig 2-6 G-H).

During the time that the *seu-1* ;*spt-2* and *lug-3 spt-2* plants were being generated, pollen from *seu-1; lug-8/+* flowers was crossed into *spt-2* flowers to produce *seu; lug spt* triple mutants, however we failed to identify triple mutants due to poor fertility of single and a lack of fertility of double mutants as well as a linkage of *LUG* to *SPT* on chromosome 4. A much larger population of F2 would have to be screened to identify a *seu;lug spt* triple mutant. Nevertheless, now that *spt-2 lug-3/+ lug-3* and *spt-2 lug-3/spt* + lines are available, it will be possible in the future to generate a triple mutant by crossing these heterozygous lines with *seu-1*.

Discussion

The ectopic *SPT* expression observed in *seu* single*, lug* single*,* and *seu; lug* double mutant flowers indicates that these two proteins are necessary for the repression of *SPT* in the sepals and petals of flowers. Whether or not the SEU/LUG repressor complex directly represses *SPT* has yet to be determined. However, the physical interaction between AP2 and SEU (in both yeast and plants), the ability of SEU to bridge an interaction between AP2 and LUG (in yeast), and the similar function between AP2 and SEU/LUG in *SPT* repression strongly suggests that SEU/LUG may directly interact with AP2 to repress *SPT* (Fig. 2-7). In this model, the SEU/LUG complex acts to repress *SPT* by direct interacting with AP2, which binds the *SPT* promoter (Fig. 2-7). What remains to be tested is if the AP2/SEU/LUG complex I showed in yeast (Fig. 2-3C) exists *in planta*, and if AP2 can bind to the *SPT* promoter. Additionally, the ability of this potential binding to cause *SPT* repression would need to be tested as well.

Although the *in situ* hybridization data showed ectopic *SPT* expression in *seu* and *lug* single and *seu; lug* double mutants, the ectopic *SPT* expression in these mutants may be either too weak to cause ectopic stigmatic tissues or may require additional partners that are absent in the outer whorl (ie. the missing partner genes may not be repressed by LUG or SEU). My genetic analysis showed that the removal of *SPT* from *seu* or *lug* single mutants did not reduce outer whorl carpelloidy. This may not be surprising given that *SPT* is associated most strongly with stigmatic tissue development. Although *seu, lug,* and *seu; lug* flowers have carpelloid sepal phenotypes, they rarely have ectopic stigmatic

tissues on their sepals. The phenotypes of *spt; seu* and *spt lug* double mutants contrast with previous observation that the stigmatic tissues formed on the margins of *ap2-2* carpelloid sepals were drastically diminished in *spt-2; ap2* double mutants (Alvarez and Smyth, 1999). The stronger carpelloid phenotype of *ap2* could be attributed to a lack of redundancy in AP2 function whereas LUG and SEU may play redundant functions with other LUG-like (e.g. *LEUNIG HOMOLOG*, LUH) or *SEUSS-like* (e.g. *SEUSS-LIKE*, SLK) genes. Alternatively, AP2 may repress more carpel development genes than SEU/LUG.

CRC, like *SPT*, was also found to be an essential carpel development gene that works in parallel to *AG* (Alvarez and Smyth, 1999). While the addition of *spt-2* to *ap2-2* greatly reduced carpelloid phenotypes, it took the removal of both *AG* and *CRC* function in addition to *SPT* (in *crc-1 spt-2 ap2-2 pi-1 ag-1* flowers) to completely diminish any carpel identity in sepals due to the absence of AP2 (Alvarez and Smyth, 1999). It remains to be tested if *CRC* is the missing partner of *SPT* and if *CRC* is ectopically expressed in

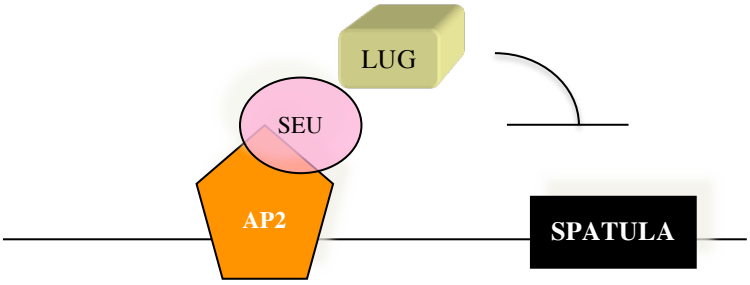

Figure 2-7. Cartoon illustrating hypothetical mechanism for C class gene *SPATULA* repression in sepals and petals by the SEU/LUG co-repressor complex via a physical interaction with the A class protein AP2

lug and *seu* mutants.

Materials and Methods

Plant materials

All plants were grown in growth chambers at 20^0C with 16-hour light. *spt-2* was described by Alvarez and Smyth (1999; 2002). *seu-1*, *lug-3*, and *seu-1; lug-8* were previously generated and described (Liu and Meyerowitz, 1995; Franks et al., 2002). To develop a genotyping marker for *lug-8,* the mutant DNA was amplified by PCR, sequenced and found to contain a C to T change at base 1612 causing a glutamate (CAA) to become a stop codon (TAA) (See Appendix C for details). *SPT* promoter::*B*-glucuronidase (*pSPT::GUS*) lines, *pSPT6271::GUS (in Col-0)* and pSPT1280::GUS (in Ler) were gifts of David Smyth (Groszmann et al., 2010). The *spt2,lug-3* and *spt-2;seu-1* double mutants were generated by crossing *spt-2* pollen into single *lug-3* and *seu-1* mutants. The genotyping method designed for *spt-2* is described in Appendix C, as are the methods for genotyping *lug-3*, *seu-1*, and *lug-8.*

Scanning Electron Microscopy

Flowers were fixed for SEM and imaged according to (Hollender et al., 2011).

GUS (β-glucuronidase) reporter gene staining and flower embedding

Tissues were harvested into cold 90% acetone and incubated at room temperate for 20 minutes. After a quick rinse with staining buffer (0.2% triton x-100; 50mM $NaHPO_4$ pH7.2; 2 mM potassium ferrocyanide; 2 mM potassium ferricyanide), tissue was placed under vacuum in a solution of 2 mM X-Gluc (x-glucuronide; 5-bromo-4-chloro-3-

indolyl-beta-D-glucuronic acid) in staining buffer on ice for 15 minutes and then left overnight at 37 degrees. The next day, the tissues were processed through an increasing ethanol series up to 50% at room temperature for 30 minutes each and then fixed with fresh FAA (50% ethanol, 5% formaldehyde, 10% acetic acid) for 30 minutes. After FAA fixation, the tissues were incubated in 70% ethanol for a minimum of 30 minutes before taking whole mount images under a dissecting microscope or being processed for wax embedding for tissue sectioning. GUS-stained flowers were embedded following the same protocol used for *in situ* hybridization (Hollender et al., 2011) beginning with the 70% ethanol dehydration step. 8μm thick flowers sections were prepared using a rotary microtome. After wax removal, tissues were imaged using dark field microscopy.

In situ hybridization and flower embedding

Tissue fixation and the hybridization in ler, *seu-1, lug-3,* and *seu-1; lug-3* flowers were carried on 8 μm sections according to Hollender et al. (2011). The *SPT* sense and antisense probes correspond to a 567 bp fragment of the *SPT* CDS were *in vitro* transcribed from PCRII TOPO vectors using the T7 polymerase and DIG labeling mix (Roche) after linearization with BamHI or HindIII. The PCRII TOPO vectors containing the *SPT* fragment were gifts from Dr. Robert Franks at North Carolina State University.

Yeast two- and three-hybrid assays

The Matchmaker System (Clontech, Mountain View, CA, USA) was used. *ANT-pGAD424* (Krizek and Sulli, 2006) and *AP2delta-pGAD424* were gifts of B. A. Krizek. *SEU (1-563)-pGBT9* and *LUH-pGAD424* were reported previously (Sridhar et al., 2004;

Sitaraman et al., 2008). To make *AP2-pGADT7*, *AP2* was excised from *pGG30* with *Nco*I and *Eco*RI and cloned into *pGADT7* at the same restrictions sites. For *P426-GAPD*, the *GAPD* promoter was excised with *Bam*HI and *Eco*RI, cloned into *pCR2.1-TOPO*, excised again with *Sac*I and *Eco*RI and cloned into *p426 GAL*, replacing the *GAL* promoter. For *P426-SEU*, *SEU* was excised from *pCRII-TOPO-SEU* (Franks et al., 2002) with *Hin*dIII and *Xho*I and cloned into *p426 GAPD* at *Hin*dIII-*Sal*I. Constructs were introduced one at a time into *Saccharomyces cerevisiae* strain PJ694A according to the Yeast Protocols Handbook (Clontech).

Bimolecular fluorescence complementation (BiFC)

AP2, *SEU* and *LUH* were cloned into *pUC-SPYNE* and *pUC-SPYCE* (Walter et al., 2004). Specifically, full-length *AP2*, *SEU* or *LUH* was amplified (for primers, see Table S1 in the supplementary material), cloned into *pGEM-T Easy* (Promega, Fitchburg, WI, USA) for *AP2* and *SEU* or into *pCR8/GW/TOPO* (Invitrogen) for *LUH*, excised with *Sal*I and *Xma*I, and then cloned into *pUC-SPYNE* and *pUC-SPYCE*. Helios Gene Gun (BioRad) was used according to a published procedure (Hollender and Liu, 2010). Results were imaged under a Zeiss Axio Observer.Z1 inverted microscope. The experiment was performed twice.

Chapter III: Regulation of *SPATULA* by *LEUNIG, SEUSS,* and *ETTIN* in gynoecium

Introduction

As introduced in the previous chapter, *SPT* is a critical regulator of carpel margin tissue development and its expression is highly regulated within the gynoecium. A *SPT* promoter driven *GUS* reporter showed that *SPT* expression is restricted to the marginal tissue regions and is overtly absent from the valves and style walls (Figure 3-1A-C). The work described in this chapter delves into the question of how *SPT* is regulated within the gynoecium. Could the SEU/LUG co-repressor complex also play a role in this regulation like it does in the outer floral whorls? And if so, how is it tethered to the *SPT* promoter in these tissues? The AP2 protein, which may bridge the interaction between SEU/LUG and *pSPT*, is not active in the gynoecium as *ap2* mutants develop wild type gynoecium (Bowman et al., 1991b), and AP2 is not expressed in gynoecium (Wollmann et al., 2010). Therefore, the SEU/LUG co-repressor may rely on other DNA-binding transcription factors to bind to *SPT* regulatory regions in the gynoecium.

ETTIN (ETT) is an auxin response factor (ARF) that is essential for the development of abaxial gynoecium tissues, such as the valves (Sessions and Zambryski, 1995). The *ett* mutants have a severe reduction in valve and ovary development as well as "abaxialization" of marginal tissues, as a result of the reduction of the valve. Marginal tissues, such as the transmitting tract and placentae, are exposed on the exterior (or abaxial portion) of *ett* gynoecium. In addition, *ett* gynoecium exhibit a "basalization of stigma and style cells (these tissues expanded toward the base of the gynoecium)

(Sessions and Zambryski, 1995). The application of auxin efflux carrier inhibitor NPA to the wild type gynoecium mimicked the *ett* phenotype, suggesting that ETT may mediate the auxin signal to promote valve and abaxial identity. In the absence of auxin due to NPA (which causes the auxin to pool at gynoecium apex and instead of being transported downward), *ETT* cannot specify valve and abaxial identity (Nemhauser et al., 2000) (Refer to Chapter I for information about the auxin gradient theory).

Genetic analysis indicated that the abnormal gynoecium phenotype of *ett* is due to the ectopic expression and activity of *SPT* (Heisler et al., 2001). Specifically, wild type *ETT* is needed to restrict *SPT* to the marginal tissues. Ectopic *SPT* expression in *ett* mutants is responsible for the valve-less phenotype as introducing the *spt-2* mutant allele into *ett* reversed the valve reduction and abaxialization phenotype seen in *ett* single mutants (Heisler et al., 2001). However, it is not known if this transcriptional repression of *SPT* by ETT is direct or indirect. ETT, being a member of the ARF family, encodes an amino-terminal DNA binding domain that binds AuxRe elements (TGTCTC) (Ulmasov et al., 1999b). I identified two such elements in the *SPT* promoter, one ~275 bp upstream of the start codon and another ~1275 bp upstream. This suggested that there could be direct binding of ETT to the *SPT* promoter.

Interestingly, a genetic screen for *ett* enhancer mutations identified the *seu-3* allele (Pfluger and Zambryski, 2004), suggesting that SEU may perform similar functions as ETT and may be involved in auxin signaling. Through a yeast two-hybrid assay, Pfleuger and Zambryski showed that SEU physically interacted with ETT in yeast, suggesting the

possibility that SEU (possibly with LUG) may aid ETT in the negative regulation of *SPT* in the gynoecium (2004). In other words, ETT may recruit the SEU/LUG co-repressor to repress *SPT* expression in the valve/ovary region of the gynoecium.

Using a combination of genetics, reporter gene expression, chromatin immunoprecipitation, and a protoplast transient expression assay, I investigated *SPT* regulation within the gynoecium and tested whether or not the SEU/LUG complex plays a role in it. Genetic and qRT-PCR analysis suggested SEU surprisingly has a positive role in regulating *SPT* within the gynoecium. In addition, preliminary Chromatin immunoprecipitation (ChIP) data are consistent with the speculation that SEU and LUG interact with the *SPT* promoter *in vivo*. A protoplast-based *in vivo* transient expression/repression assay was established and used to test the exact role of SEU and ETT in *SPT* regulation as well as the effect of auxin on this regulation. The assay revealed a positive role of ETT for *SPT* regulation. These somewhat conflicting results produced more questions than answers. My work reported here suggests that gynoecium development is complex and future research is needed to reveal the mechanisms dictating its development.

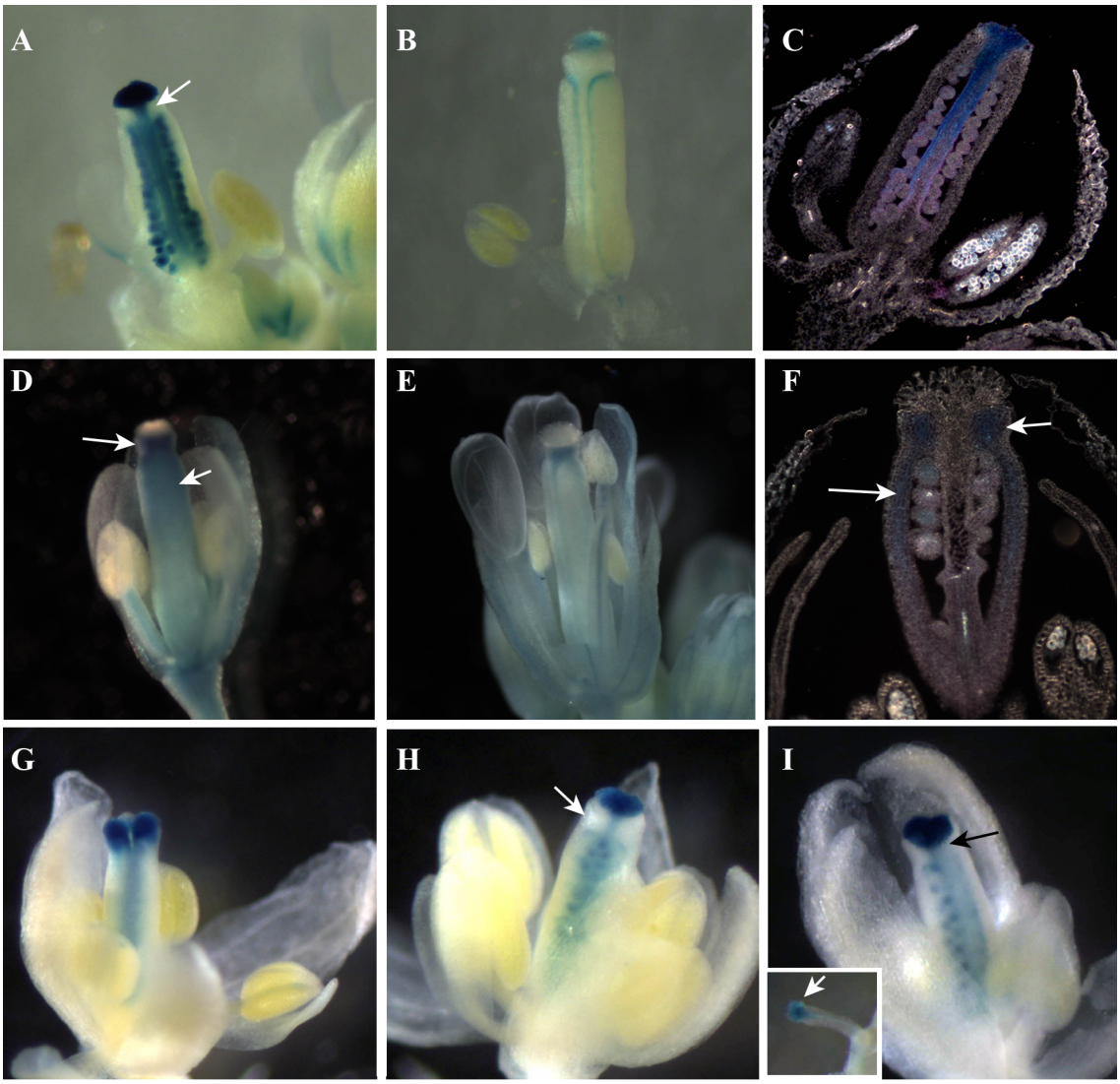

Figure 3-1 Complementary expression pattern of *SPT* and *LUG* in wild type gynoecium (A-C) *pSPT::GUS* in wild type flowers. Arrow in (A) indicates an absence of *SPT* in the style wall. (B) The same reporter shown in older gynoecium. (C) Dark field image of a longitudinal section illustrating high levels (blue) of *SPT* expression in stigma and transmitting tract. There appears to be a gradient of GUS expression from high (blue) in the apex to low (pink) in the base. (D-F) *pLUG::GUS* in wild type flowers. Arrows in (D) and (F) show *LUG* expression in style and apical region of the carpel valve. (G) *pSPT::GUS* expression in a stage 9-10 *seu-1* flower showing unfused carpels at the apex. (H) *pSPT::GUS* expression in a stage 12 *seu-1* flower. (I) *pSPT:GUS* in *lug-3*. Arrows in (H) and (I) indicate absence of *SPT* expression in areas of style. Inset in (I) shows a rare ectopic stigmatic tissue from a *lug-3* sepal, which showed strong *SPT* expression.

Results

pSPT::GUS and *pLUG::GUS* reporters exhibit complementary expression patterns in the gynoecium

A 5 kb *LUG* promoter driving a GUS reporter (*pLUG::*GUS) was used to examine LUG expression in the gynoecium. Similarly, a *pSPT::GUS* reporter (Groszmann et al., 2010) was used to examine *SPT* expression in the gynoecium (seeds were a gift from David Smyth). Interestingly, *SPT* and *LUG* appeared to be expressed in complementary domains in the gynoecium (Fig 3-1 A-F). LUG is expressed in the valve and style wall tissues (Fig 3-1 D-F), and not at all in the stigma, transmitting tract and ovules. In contrast, *SPT* is highly expressed in the apical stigmatic tissues, transmitting tract, septum and ovules (Fig 3-1A-C). This observation led to the hypothesis that the SEU/LUG complex may be involved in restricting *SPT* to the marginal regions of gynoecium.

SPT remains restricted to marginal tissues in *seu* and *lug* mutants

To test if LUG or SEU plays a role in the negative regulation of *SPT* within the gynoecium, I investigated whether the *SPT* expression domain would expand in *lug* or *seu* mutant gynoecium. Wild type plants containing the *pSPT6253::GUS* (Groszman et al 2010), were crossed into *seu-1* and *lug-3* mutants. In *seu-1* and *lug-3* mutant gynoecium, *SPT* was expressed in the same regions as it was in wild type (Fig. 3-1 A-C, G-I) and did not expand into the valve or style wall tissues of *lug* or *seu* mutants (Fig. 3-1 H, I). In one *lug-3* flower, an extremely rare ectopic stigma formation on sepal also expressed high levels of *SPT* (Fig3-1 I, inset). Contrary to our predictions, there appeared to be a slight reduction in *pSPT::GUS* expression in *seu* and *lug* mutants. This reduction was

initially thought to be indirect due to a reduction of marginal tissues in respective mutants.

Genetic interaction between *spt* and *lug* or *seu*

To investigate the genetic relationship between *SPT, SEU,* and *LUG*, double mutants were constructed by crossing *spt-2* into *seu-1* and *lug-3* flowers (Fig. 2-5, Fig. 3-2). The outer floral whorl phenotypes of the double mutants were no different than the single *seu-1* and *lug-3* phenotypes and were discussed in chapter 2 (Fig. 2-5). Analysis of the double mutant gynoecia, on the other hand, revealed an unexpected phenotype. Both *seu-1* and *lug-3* gynoecia lack complete carpel fusion at their apex, and thus develop a split stigma (Fig. 3-2 A-C). The *lug* phenotype is always much stronger than *seu*, and is often accompanied by horn-like projections as extensions of the valve tissue (Fig. 3-2C). The *spt-2* flower lacks apical carpel fusion, but also has a severe reduction of stigmatic tissue (Fig. 3-2D). In *spt-2 seu-1* double mutants, the gynoecia not only showed enhanced defects in carpel fusion, but also completely lost stigmatic tissues (Fig. 3-2 E). This synergistic genetic interaction implies that *SPT* and *SEU* are both required for the development of stigma and carpel fusion and they may act in parallel or partially overlapping pathways to promote gynoecium marginal tissue formation. In contrast, the *spt-2 lug-3* double mutant gynoecia looked nearly identical to the *lug-3* gynoecia (Fig 3-2F). This is not entirely surprising as *lug-3* has a more severe reduction of carpel fusion and it may mask the much milder defect of *spt-2*.

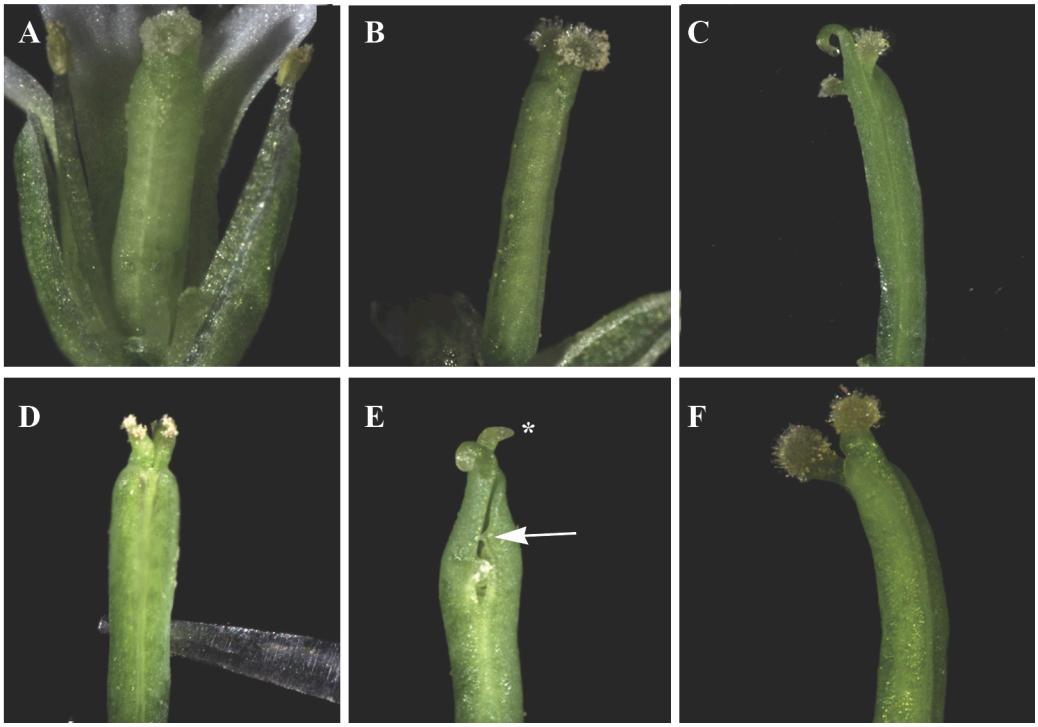

Figure 3-2. *Arabidopsis* gynoecium from (A) wild type, (B) *seu-1*, (C) *lug-3,* (D) *spt-2*, (E) *spt-2 seu-1,* and (F) *spt-2 lug-3*. Asterisk in (E) indicates absence of stigmatic tissue. Arrow in (E) indicates region lacking carpel fusion

***seu-1* carpels have reduced *SPT* expression**

The genetic analysis above indicated that *LUG*, *SEU*, and *SPT* may work together or separately to promote carpel marginal tissue development. One way *SEU* and *SPT* may work together is that SEU could positively stimulate *SPT* expression. This potential activation could occur directly, via SEU binding *pSPT* in the absence of the LUG repressor, or it could be indirect, where SEU/LUG may repress a repressor of *SPT*. To investigate if SEU was in anyway activating *SPT*, young (stages 6-9) wild type and *seu-1* gynoecia were isolated, and *SPT* levels were measured by qRT-PCR. At this early stage

of development, there are no significant differences in gynoecium tissues between wild type and *seu* or *lug* mutants, unlike in the late stage flowers observed in the *pSPT::GUS* study above, where there was a reduction of marginal tissue in the mutants. I found that *SPT* transcript levels in *seu-1* gynoecium had a 40% reduction compared to wild type *SPT* levels (Fig 3-3). This reduction suggests that SEU may be one of several proteins that positively regulate *SPT* expression, either directly or indirectly. SEU cannot be the only protein involved in *SPT* activation, as *seu-1* gynoecium still both expresses *SPT* transcripts at 60% wild type level, and develops stigmatic tissues.

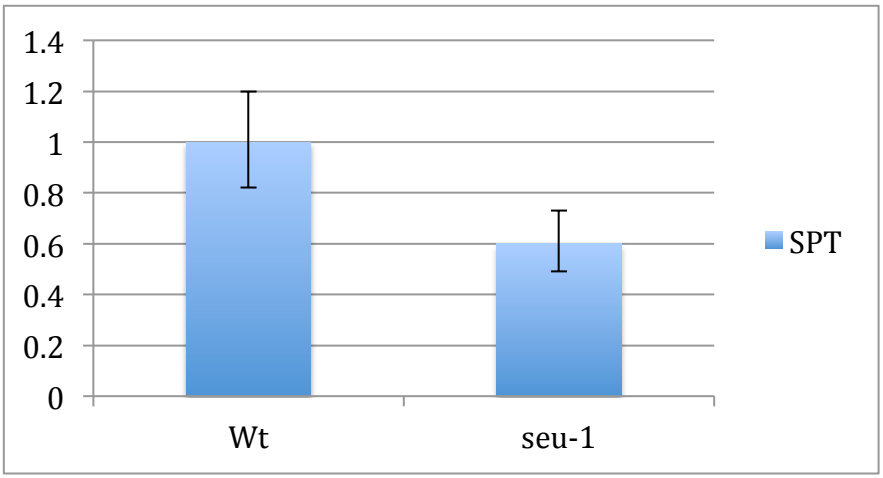

Figure 3- 3. Relative *SPT* expression in young *seu-1* carpels (stages 6-9) assessed by qRT-PCR. Error bars represent standard deviation from 3 biological replicates.

Enrichment of *SPT* promoter regions by ChIP using anti SEU-GFP and LUG-GFP antibodies

To test if SEU or LUG can bind directly to the *SPT* promoter region for direct regulation, a chromatin immunoprecipitation (ChIP) assay was performed on floral tissue from *seu-1*

plants rescued by *pSEU::SEU-GFP* and *lug-16* plants rescued by *35S::LUG-GFP.* Anti-GFP antibodies were used to pull down SEU and LUG, in the respective tissues. qPCR using primers designed for two different *SPT* promoter regions.was used to test for *pSPT* enrichment in the immunoprecipitated DNA. The first region tested, referred to as P3, lies at -395 to -251 bp upstream of the *SPT* start codon as defined by Heisler et al. (2001). This region contains a general enhancer E-Box, an Auxin Response Element (AuxRE), tissue-specific regulatory regions determined empirically by Groszman et al. (2010), and an AT-rich consensus sequence defined by the X. Chen lab that may serve as the binding site for the AP2 domain (X. Chen, UC Riverside, personal communication). The second region, P4, is about ~1000 bp upstream of the ATG and contains only a potential AP2 binding site.

Primers surrounding a CArG box in the 2nd intron of *AG* were used as a positive control (Fig. 3-4A). Previous work from our lab showed that SEU and LUG (by its association with SEU) can bind to this AG 2nd intron region through both MADS box proteins SEP3 and AP1 (Sridhar et al., 2006). Primers for a GAPC transcript were used as a negative (non-target) control (Fig. 3-4B). To determine enrichment values, ChIP assays can be normalized using several methods to eliminate technical variations, but each method has advantages and disadvantages (Haring et al., 2007). The normalization method should be carefully chosen. Although, if there is true enrichment of a target in a high quality ChIP experiment (one carried out with a reliable protocol and careful execution) most if not all normalization methods will show it, but the levels may vary. We chose to use normalize our data to the ChIP input (chromatin taken after the 'pre-clearing' step) (See Materials

and Methods Section). Specifically qRT-pCR was carried out for each primer pairs with both undiluted immunoprecipiated DNA and input DNA as templates. Ct value for the immunoprecipitated DNA was subtracted from the Ct value of the input DNA to yield ΔCt. After the normalization, enrichment value (ΔΔCt) was calculated by subtracting the ΔCt of test tissue described above from ΔCt derived from the negative control tissue (non-GFP wild type tissue). In other words, the ΔΔCt value was calculated by ΔCt (SEU-GFP or LUG-GFP) – ΔCt (Ler). Finally, fold enrichment was calculated using the Livaak formula, $2^{-\Delta\Delta Ct}$.

In two separate experiments using a GFP antibody, ChIP DNA from the SEU-GFP plants was enriched for the *SPT* P3 promoter region an average of 2.26 fold compared to ChIP DNA from Ler tissue (Fig 3-4). The P3 promoter region was enriched in the LUG-GFP tissue to a slightly lesser degree, 1.76 fold. P4 showed a very slight (1.33) fold enrichment with SEU-GFP tissue and no enrichment with LUG-GFP. The results suggest that both SEU and LUG bind *SPT* promoter region. LUG-GFP showed lesser enrichment than SEU-GFP, likely due to a more indirect attachment of LUG to *pSPT* than SEU.

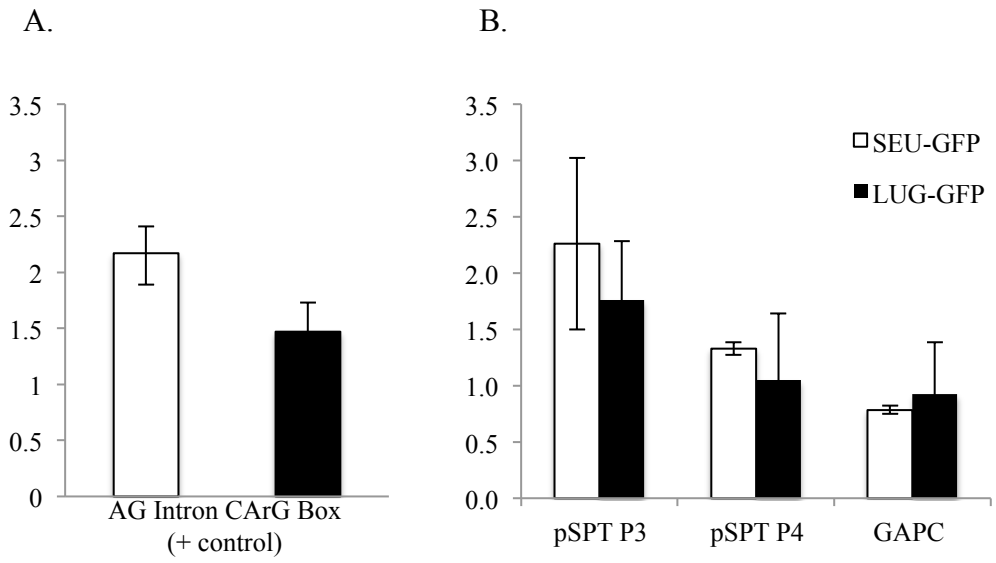

Figure 3-4. qPCR analysis showing enrichment of DNA from Chromatin Immunoprecipitation using anti-GFP antibodies against SEU-GFP or LUG-GFP proteins in the *pSEU::SEU-GFP; seu-1* or *35S::LUG-GFP; lug-16* flower meristem tissues (A) Enrichment of the CArG box regulatory element in the 2nd intron of *AG* served as a positive control. (B) Average fold enrichment from two biological replicates. *pSPT* P3 and *pSPT* P4 are two distinct regions of the *SPT* promoter. The GAPC exon region served as a non-target control. Bars in (A) are standard deviations from three technical replicates within one biological experiment, bars in (B) are standard deviations from two biological replicates.

Mechanism of *SPT* regulation by *ETT*

To investigate the possible direct role of ETT in *SPT* regulation, plants with a *35S::ETT-GFP* construct rescuing the *ett-2* phenotype were used for ChIP with GFP antibodies. Unfortunately, preliminary ChIP analysis failed to detect an enrichment of *SPT* promoter (data not shown). It's possible that the GFP antigen in the ETT-GFP fusion protein is inaccessible to the antibody, or that the ChIP experiment did not work due to technical issues. Alternatively, ETT may not be involved directly in mediating the *SPT* repression. Using an ETT specific antibody for ChIP would be more favorable to test if ETT can bind to the regulatory elements of *SPT*.

An additional approach used to investigate *SPT* regulation by ETT was a transient expression assay in protoplasts (Sheen, 2001). The results of this assay could also suggest that ETT binds to the *pSPT*. Protoplasts derived from leaves were transfected with a luciferase reporter construct driven by the *SPT* promoter (*pSPT::LUC*) in the presence or absence of constitutively expressed SEU (*pART7-35S::SEU*) and/or constitutively expressed ETT (*pART7-35S::ETT*). The *pSPT::LUC* reporter was created by inserting 1665 bp of the *SPT* promoter into pGREENII_0800_LUC vector (Hellens et al., 2005). This vector also contains a *35S::Renilla Luciferase* cassette that acts as an internal control for transformation efficiency (Hellens et al., 2005). The *pSPT::LUC* reporter expression was measured as the ratio of firefly luciferase emission to Renilla luciferase emission using the Promega Dual-Luciferase Reporter system.

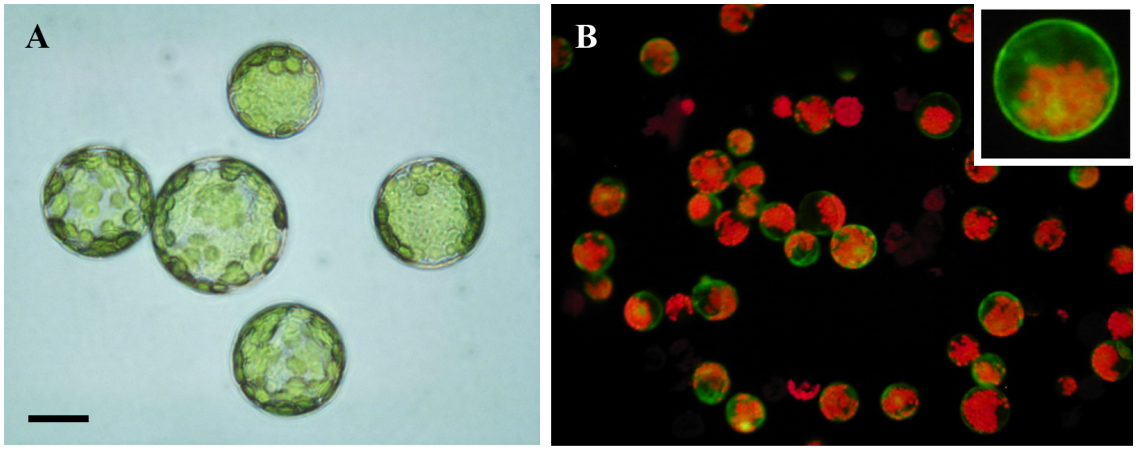

Figure 3-5. *Arabidopsis* leaf mesophyll protoplasts prepared for this study. (A) Protoplasts before transfections. (B) Protoplasts transformed with *35S::GFP*. Red color is autofluorescence from chlorophyll in the chloroplasts. Inset in (B) highlights a protoplast transformed with *35S::GFP*.

This assay relied on having a high transformation efficiency, as multiple plasmids would need to enter the same protoplasts. The protocol was first optimized using a *35S::GFP* construct (*35S::Glowbug*) (Hollender and Liu, 2010) that allowed for easy visualization of transformation efficiency (Fig 3-5B). In addition, *35S::GFP* was transformed alongside experimental constructs to ensure that reagents and conditions were optimal. Protoplasts from each experiment had a *35S::GFP* transformation efficiency of at least 65%.

Co-transformation of *35S::ETT* and *pSPT::LUC* in protoplasts consistently showed a significant increase (between 2 to 4 fold) in reporter activity compared with the *pSPT::LUC* plus empty pART7 vector control (Fig 3-6). The co-transformation of

35S::SEU and *pSPT::LUC*, on the other hand, produced no significant change in luciferase activity (Fig 3-6). This is not surprising given that SEU cannot directly bind to the *SPT* promoter in the absence of partner DNA-binding factors. When both *35S::SEU* and *35S::ETT* were co-transformed together with the *pSPT::LUC* reporter construct, the luciferase expression was decreased, suggesting that SEU represses *SPT* in the presence of ETT, which may be tethering SEU to the *SPT* promoter.

As mentioned earlier, *ETT* is an auxin response factor, known both to mediate auxin signaling and have an essential role in gynoecium valve development (Sessions and Zambryski, 1995; Sessions et al., 1997; Ulmasov et al., 1999b). Since gynoecium development is believed to be dependent on an auxin gradient (Nemhauser et al., 2000), ETT may play a crucial role in translating this auxin gradient to the developmental outcome. For this reason, it was of interest to test if presence of auxin could enhance or decrease ETT's regulatory role on *SPT* expression. After protoplast transfection, NAA, a stable and commonly used synthetic form of auxin, was added to the protoplast growth media and then incubated overnight alongside transfected protoplasts in media without auxin. The addition of auxin with *35S:ETT* produced a statistically significant ($P<0.0001$) increase of luciferase reporter activity by 27% (Fig 3-6B). Auxin had no effect on the ability of SEU to decrease reporter activity produced by ETT, nor did it affect reporter activity levels from SEU alone (Fig. 3-6B).

A.

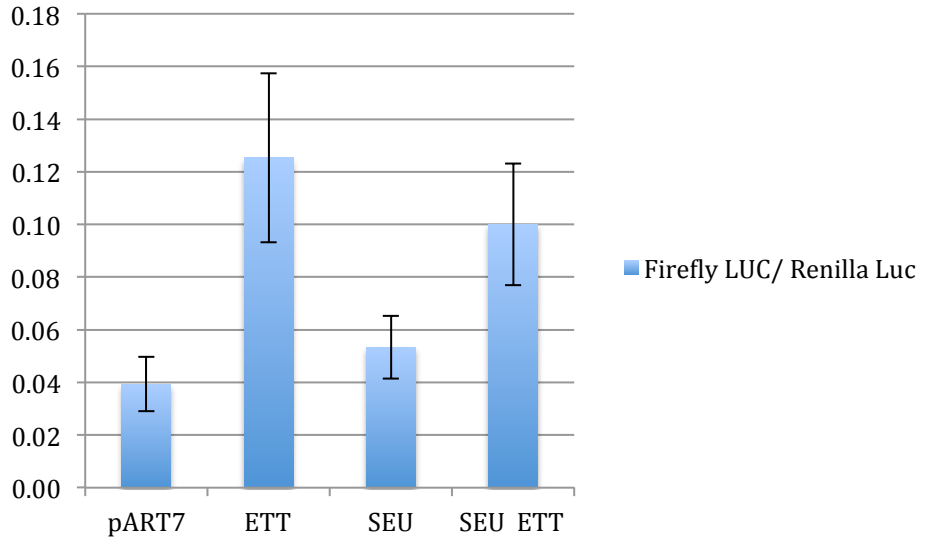

B.

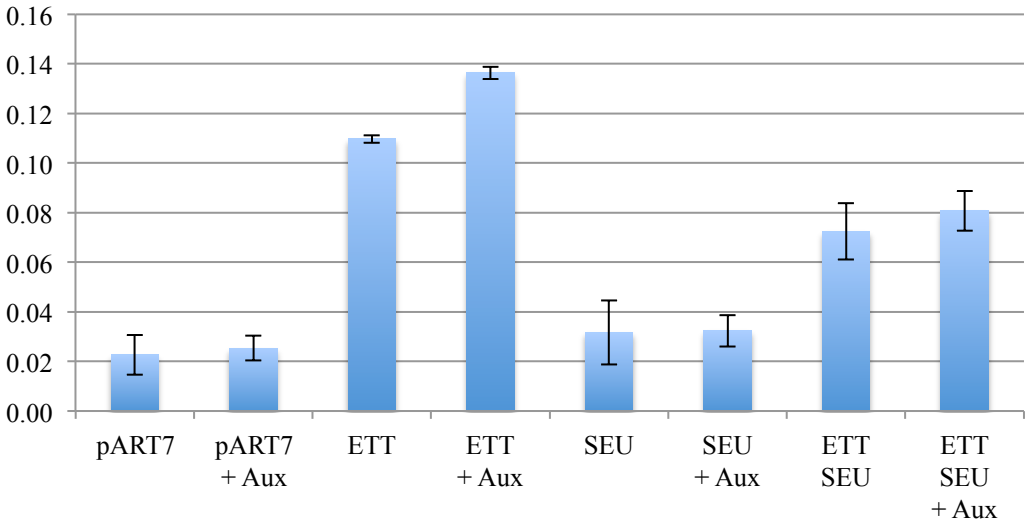

Figure 3-6. *pSPT::LUC* transient expression in protoplasts. Y-axis indicates the relative expression level (fireflyLUC/RenillaLUC ratio). Bars represent standard deviations from three biological replicates. *35S::ETT* and/or *35S::SEU* were transformed into protoplasts in addition to the *pSPT::LUC* /*35S::Renilla Luciferase* plasmid The empty 35S vector pART7 was used as a negative control. In (B), auxin (Aux) was added in the form of 1 µm NAA to the overnight growth media.

Discussion

If the SEU/LUG protein complex were solely responsible for restricting *SPT* expression in the gynoecium then the absence of these repressors would have led to an expansion of *SPT* expression into the valve and style tissues. However I found that in *seu-1* and *lug-3* mutants, the domain of *pSPT::GUS* reporter expression remained unchanged, suggesting that the SEU/LUG complex may not repress *SPT* expression in regions of the valve and style regions of gynoecium. This contrasts with SEU/LUG's role in *SPT* repression in sepals and petals (see Chapter 2). Either the regulation of *SPT* expression in the gynoecium may involve a different mechanism or the *Arabidopsis* homologs of both SEU and LUG may have overlapping roles for this regulation (Sitaraman et al., 2008; Bao et al., 2010). The two SEUSS-LIKE (SLK) proteins and one LEUNIG HOMOLOG (LUH) may help repress *SPT* in the gynoecium valves or style region in *seu-1* and *lug-3* mutants.

SEUSS may act to promote stigma development

I showed that double mutants of *SPT* and *SEU* exhibited strong synergistic genetic interactions, as the *spt-2 seu-1* double mutant gynoecium had a complete loss of stigmatic tissue (Fig 3-2). This suggests that both SEU and SPT are essential for stigma development. However, the exact mechanism of how SEU and SPT regulate stigma development is not easy to deduce. Their roles in stigma development may be completely independent of one another, in parallel pathways, and/or they may overlap in the same pathway. SEU could play a role in directly activating *SPT* through its binding to the *SPT* promoter region, which was shown as enrichment among the DNA precipitated by ChIP (Fig. 3-4). Yet, SEU cannot be the sole upstream activator of *SPT*. If it was,

seu-1 gynoecium should not be plush with stigma. Additionally, the 40% reduction of *SPT* transcript seen in young *seu-1* gynoecium suggests SEU could be an activator of *SPT* expression (directly or indirectly). However, the fact that 60% of the wildtype level of *SPT* transcript still remained in *seu-1* indicates that SEU is not alone in this role (Fig 3-3).

Other genes, such as *CRABSCLAW (CRC),* have also been implicated in stigma development (Alvarez and Smyth, 1999). As mentioned in chapter 2, the ectopic stigma in *ap2-2* mutants could not be completely removed until the function of *AG*, *SPT* and *CRC* were also removed (Alvarez and Smyth, 1999). Double mutants of *spt-2 crc-1* also lack stigmatic papillae (Alvarez and Smyth, 1999). It is possible that SEU may act as a direct transcriptional activator for both *SPT* and *CRC* (as well as other unknown essential stigma development genes) by binding via other factors to their promoter regions and recruiting transcriptional machinery in an as of yet unknown mechanism. If this were the case, it would make sense that neither *seu* nor *spt* single mutants lose all stigma, but when both genes are not functional, then stigma will not develop.

If SEU has an activating function, there still lies the question of what adapter protein it interacts with to bind to DNA. Initially, when I believed the SEU/LUG complex had a main role in repressing *SPT* in the gynoecium, ETT was thought to be this adapter protein both because of its known repression of *SPT* and its physical interaction with SEU. Could ETT, a known repressor of *SPT*, work with SEU to activate it in the marginal tissues?

Consistent with the above hypothesis, my protoplast transient expression data indicated a repressor function of SEU in *SPT* reporter expression. The protoplast assay also supports a binding of SEU to the *SPT* promoter via ETT. Further the ChIP experiment showed *in vivo* binding of SEU to the *SPT* promoter, consistent with a direct association of SEU to the *SPT* promoter to affect *SPT* expression. However, my qRT-PCR and genetic data indicated a positive rather than a negative role for SEU in SPT expression, complicating the ability to understand the genetic and molecular connections between SEU and SPT in the realm of gynoecium development.

One scenario to explain SEU's positive role in *SPT* activation, is that the binding of SEU to ETT in the marginal tissues physically blocks ETT's ability to repress *SPT*, thereby causing activation. A scenario to explain SEU's negative role, could be that the binding of SEU to ETT would lead to SEU's recruitment of other co-repressors such as LUG or LUH to help repress *SPT*. Alternatively, both scenarios could be possible in the context of different tissue types within the gynoecium and their tissue-specific co-factors.

Implications of SEU and LUG binding to the *SPT* promoter

ChIP revealed that the SEU protein binds the *SPT* promoter ~300 bp upstream of the start codon, and to a lesser extent farther upstream, at -1000 bp. The -1000 bp region may lack the necessary regulatory elements to support the binding. ChIP data also shows that LUG binds to the *pSPT*, but to a lesser degree. It is likely that LUG's interaction with the promoter is not as direct as SEU and is mediated by SEU.

This binding of SEU to *pSPT* supports the possibility that SEU can directly activate *SPT* in the gynoecium. However, this result, combined with the association of LUG-GFP to the *SPT* promoter, mostly strengthens the hypothesized SEU/LUG repression of *SPT* in the outer whorls (Fig 2-6). The ChIP data cannot distinguish between SEU binding to the p*SPT* in the outer floral whorls versus in the gynoecium, as entire flower buds were used for the chromatin isolation. Further experimentation is needed to accurately determine if SEU can directly activate *SPT* in the gynoecium.

The roles of ETT and SEU in SPT regulation within the gynoecium

Using protoplasts as a model *in vivo* system, I investigated *SPT* regulation by ETT and SEU using a *pSPT::LUC* reporter. ETT lacks the 'Q' (glutamine) – rich activation domains associated with activating ARFs (Tiwari et al., 2003), and published data indicated that ETT acts as a repressor (Heisler et al., 2001). When ETT was transfected into carrot protoplasts alongside an auxin responsive GUS reporter it produced little to no reporter activity in the presence or absence of auxin (Ulmasov et al., 1999a). Further, no reporter activity was observed when *ETT* was fused a GAL4 DNA binding domain and co-transfected into protoplasts with *GAL4(4x)::GUS* (Ulmasov et al., 1999a). In addition, the addition of ETT to auxin responsive reporter *DR5(7x)::GUS* in protoplasts caused reduced reporter expression (Tiwari et al., 2003), and genetic and molecular evidence show that ETT represses *SPT* in the gynoecium valves (Heisler et al., 2001). Contrary to these studies, I found ETT to have an activating ability in the *Arabidopsis* leaf protoplast assay. In the presence of *35S::ETT*, *pSPT::LUC* reporter expression was significantly upregulated (Fig 3-6). This result was not only highly reproducible, but it was also slightly enhanced by the addition of auxin. Further, the combination both of

35S::SEU and *35S::ETT* produced a decrease in reporter activity, suggesting SEU represses the ability of ETT to activate *SPT* (Fig 3-6). This also brings back the initial idea that an ETT/SEU (or ETT/SEU/LUG) complex could mediate *SPT* repression in valves.

An alternative explanation for the ETT/SEU repression of *SPT* shown in protoplast assay is that perhaps SEU works through ETT, in addition to AP2, in the outer whorls to help repress *SPT*. Along with the severe gynoecium phenotype exhibited in *ett* mutant flowers, *ett-2* flowers occasionally produce one or two additional petals (Sessions et al., 1997), suggesting *ETT* has a subtle role in outer whorl development. Further, plants containing *pETT::GUS* exhibited slight reporter expression in young petals (Charles Hawkins, University of Maryland, personal communication). It is possible that SEU works with ETT to both repress and activate *SPT*, and the regulatory role that these proteins play depends on both spatial and temporal factors. The activating function of ETT/SEU in one tissue may have been masked by its repressor role in other tissues.

It is essential to point out that there are several drawbacks to using leaf mesophyll protoplasts to transiently test gene regulatory mechanisms that occur in gynoecia. Genetic data showing interactions between genes is always more trustworthy than expression data from non-native conditions. This protoplast assay relies on the assumption that all the necessary regulatory proteins and cofactors associated with the mechanism are both present and at sufficient levels in the protoplasts. In addition, *Tas3* Ta-siRNA negatively regulates *ETT* in young leaves (Fahlgren et al., 2006). Thus, *ETT*

expression in protoplasts may be subjected to post-transcriptional regulations by small RNAs.

Conclusions

In sum, the relationship between the LUG, SEU, and ETT proteins, and their role in the regulation of the C-class gene *SPT* in the gynoecium is not yet clear. As the gynoecium is a complex organ essential to the reproductive success of the plant, a clear understanding of how LUG, SEU, and ETT function together in the gynoecium is likely being complicated by many factors. Such factors include genetic redundancy, the dual or opposing roles of ETT, LUG, and SEU in the *SPT* regulation occurring in distinct gynoecium and floral tissues.

Materials and Methods

Plant material

All plants were grown in growth chambers at 20^0C with 16 hour light. *spt-2, ap2-2, ett-1,* and *ett-2* have all been previously described by Alvarez and Smyth (1999, 2002). *seu-1*, *lug-3*, and *seu-1; lug-8* were previously generated in our lab using EMS mutagenesis and crossing (Liu and Meyerowitz, 1995; Franks et al., 2002). *lug-8* was sequenced and found to be a transition mutation of a C to a T at base 1612, causing a glutamate (CAA) codon to change into a stop codon (TAA). To construct *seu-1; spt-2* double mutants, *spt-2* pollen was crossed into *seu-1* stigma. To construct *lug-3 spt-2* double mutants, *spt-2* pollen was crossed into *lug-3* stigma.

SPT promoter::GUS lines, *pSPT6253::GUS* (in Col-0*)* and *pSPT1262::GUS* (in Ler) were gifts of David Smyth (Groszmann et al., 2010). *pSPT6253::GUS; lug-3*, and *pSPT6253::GUS; seu-1* were created by crossing the *GUS* lines into the mutant lines. *pLUG::GUS* plants were created in our lab by Joann Conner (Conner and Liu, unpublished). The full LUG promoter sequence, the entire first exon and intron, and most of the second exon (5.77kb total) were fused to GUS in the pCambia vector p1381Za.

The *pSEU::SEU-GFP* (GFP C), rescuing *seu-1*, was a gift of Bob Franks at North Carolina State University. The *ap2-2; pSEU::*SEU-GFP lines were created by crossing *pSEU::SEU-GFP* into *ap2-2/ant-9* (Grigorova et al., 2011*)*. The *35S::LUG-GFP* rescued *lug-16* and was been previously described (Grigorova et al., 2011*)*. *35S::LUG-GFP* in *ap2-2* was created by crossing *35S::LUG-GFP* into *ap2-2/ant-9*. *35S::ETT-GFP-HIS* in *ett-2* background was created by amplifying the ETT CDS from clone U09387 (ABRC) using ETT forward Primer ETT_F_pEG103 (5' ATG GGT GGT TTA ATC GAT CTG AA) and ETT reverse primer ETT_R_pEG103 (5' GAG AGC AAT GTC TAG CAA CAT GTC T), ligated into pCR8/GW/TOPO (Invitrogen), sequenced, and then cloned into pEARLEYgate103 (Earley et al., 2006). The *35S::ETT-GFP* construct was transformed into *Agrobacteria tumefaciens* and subsequently into *ett-2* mutant plants. 18 *35S::ETT-GFP* lines were generated. Of those 18, 16 lines had complete rescue and no additional phenotypes. Plants from those 16 lines were used for ChIP.

GUS reporter gene staining and flower embedding

GUS staining of flowers, wax imbedding, and sectioning was done as described in Chapter II.

Construction of transient expression assay vectors

For the protoplast luciferase reporter assay, the reporter construct *pSPT*::*LUC* was created by PCR amplification of a 1665 bp region upstream of the ATG start codon using Col-0 gDNA with the following primers with an engineered KpnI site on the forward primer and an XhoI site on the reverse primer: SPTprm_KpnI_F2 (5' ATG GTA CCC AAC CAT CGT TTC ATT AAT ATC TTT) and SPTprm_XhoI_R2 (5' ATC TCG AGT CAT TAC ACC AAC AAC AAA AAA A). This PCR fragment was cloned into pCR8/GW/TOPO (Invitrogen), sequenced, and then excised using KpnI and XhoI. A gel purified fragment was inserted into pGreenII_0800_LUC (Helens et al 2005) at the KpnI and XhoI restriction sites. ETT and AP2 were cloned into pART7 to create the 35S::ETT and 35S::AP2 constructs for the protoplast assay. The ETT CDS was amplified from clone U09387 (ABRC) using a forward primer with a KpnI site (ETT_KpnI_Fwd: 5' AT GGT ACC ATG GGT GGT TTA ATC GAT CTG AAC) and a reverse primer with an XbaI site immediately following a stop codon (ETT_XbaI_rev 5' AT TCT AGA CTA GAG AGC AAT GTC TAG CAA CAT GTC). This amplicon was cloned into pCR8/GW/TOPO (Invitrogen), sequenced, excised with KpnI and XbaI, gel purified, and then ligated into pART7 at the KpnI and XbaI sites. For 35S::AP2, the AP2 CDS was amplified from the yeast two-hybrid vector *pGADT7-AP2* (Grigorova et al., 2011) using a forward primer that introduced a HindIII site (AP2-F-HindIII: 5' AT AAG CTT ATG ATG TGG GAT CTA AAC GAC GC) and a reverse primer that introduced a stop codon

and an XbaI site (AP2-R-Stp-XbaI: 5' AT TCT AGA TCA AGA AGG TCT CAT GAG AGG AG) and cloned into pCR8/GW/TOPO (Invitrogen) and sequenced. Due to HindIII/XbaI digestion difficulties, the AP2 CDS + stop codon was excised from PCR8/GW/TOPO using EcoRI, gel purified, and then ligated into pART7 at the EcoRI site. The forward orientation of the insert was confirmed using a BamHI digestion. The *35S::SEU* was previously cloned into pART7 (Sridhar et al., 2006).

RNA analysis

For each biological replicate, approximately ten stage 6-9 carpels were dissected from *Ler* and *seu-1* flowers and placed in the extraction buffer from the Arcturus® PicoPure® RNA isolation kit (Applied Biosystems, Foster City, CA) and then ground with an RNAse-free plastic pestle. Plants were grown at the same time under identical conditions, and tissues were collected at the same time. RNA was isolated using the Arcturus® PicoPure® RNA isolation kit from 3 biological replicates. For all samples, first strand synthesis was carried out using 120ng of total RNA and the iScript^{TM} cDNA synthesis kit (BioRad, Hercules CA).

For qRT-PCR analysis, a 126 base pair amplicon spanning the first and second exon of the *SPATULA* gene (At4g36930) was amplified with the following primers: SPTqRT_1_Fwd (ATAGCTCTGGGACTCGAGTATCGT) and SPTqRT_1_Rev (5'-CTGACTTGGAAGAGGGAGCTTCAT) with a 58^0 C annealing temperature and 40 cycles in the BioRad CFX96^{TM} Real-Time System using SsoFast^{TM} EvaGreen® Supermix (BioRad, Hercules, CA). GAPC amplification used the following primers:

GAPC1qRTgene Fwd (5'CCC GTC ACT GTT TTC GGC AT) and GAPC1qRTgene Rev (5' AGC TGC AGC CTT GTC TTT GT) using an annealing temperature of 60^0C. *SPT* Ct values were normalized to those of GAPC to yield ΔCt values. *SPT* expression in Δ Ct from *seu-1* tissue was compared to Ler using the Livak method, $2^{-(seu\Delta Ct - Ler\Delta Ct)}$. The average from three technical replicates for each qPCR reaction was used to get an average of the three biological replicates. Standard deviations are based on three biological replicates.

Chromatin Immunoprecipitation

The ChIP protocol was done essentially according to the Wagner Lab Simplified ChIP protocol (https://www.plant-epigenome.org/protocols/wagner-lab-simplified-chromatin-immunoprecipitation-chip), but with the modifications described below. Approximately 1 g of stage 12 and younger flowers was collected for each genotype and fixed for 20 minutes total (with two 10 minute vacuum steps) in 1% formaldehyde in MC buffer (10 mM potassium phosphate pH7, 50 mM NaCl, 0.1M sucrose). Fixation was stopped by addition of glycine to a final concentration of 0.125M. After inverting several times with fixative + glycine, tissues were washed three times with MC buffer, blotted dry on paper towels, frozen in liquid nitrogen, and then stored at -80°C. 55µl of Dynal-Protein A beads (Invitrogen/Life technologies, Grand Island NY) was used for each sample for both preclearing and the immunoprecipitation (IP), and 2.5µl of AbCam rabbit polyclonal GFP antibody (cat no ab290) was used per sample for IP. Additional chromatin extraction steps were used and the extraction buffers differed slightly from the Wagner protocol. After grinding tissues in liquid nitrogen, it was resuspended in 10 ml of Extraction Buffer

1 (0.04M Sucrose, 10 mM Tris-HCl pH 8, 5 mM β-mercaptoethanol, 0.1mM PMSF, 0.6ml/100ml Protease Inhibitor Cocktail (Sigma p9599)) before centrifugation for 20 minutes at 4,000 rpm and 4°C. The pellet was resuspended in 1 ml of Extraction Buffer 2 (0.25M Sucrose, 10 mM Tris-HCl pH 8, 10 mM $MgCl_2$, 1% Triton X-100, 5 mM β-mercaptoethanol, 0.1 mM PMSF, 0.6ml/100ml Protease Inhibitor Cocktail) and centrifuged for 10 minutes at 12,000g in 4°C. Nuclei were resuspended in 300μl Extraction Buffer 3 (1.7 M Sucrose, 10 mM Tris-HCL pH 8, 0.15% Triton X-100, 2mM $MgCl_2$, 5 mM β-mercaptoethanol, 0.1 mM PMSF, 0.6ml/100ml Protease Inhibitor Cocktail) and then dripped over an additional 300 μl Extraction buffer 3. Nuclei were purified through a sucrose gradient by centrifugation for 1 hour at 16,000g and 4°C. The resulting pellet was resuspended in 300μl of Nuclear Lysis Buffer (50 mM Tris pH 8, 10mM EDTA, 1% SDS, 0.1 mM PMSF, 0.6ml/100ml Protease Inhibitor Cocktail) and then brought to a final volume of 2.5 mls with ChIP Dilution buffer (1.1% Triton X-100, 1.2 mM EDTA, 16.7 mM Tris pH 8, 167mM NaCl, 0.1mM PMSF, 0.6ml/100ml Protease Inhibitor Cocktail). To produce DNA with an average size of ~500 bp, chromatin was sheared by sonication with a Microson Ultrasonic Cell Disruptor XL (Misonix Incorporated, Farmingdale, NY) set to 50% power. 6 ten-second sonications were done, with 20-second breaks in between each sonication. Samples sat in an ethanol/ice water bath during sonication. On day 2 of the ChIP, three ten minute washes were done for each of the buffers (Low Salt, High Salt, LiCl, and TE). DNA was eluted from beads twice with 150μl of Elution Buffer each time (1% SDS, 0.1M $NaHCO_3$). The Qiagen PCR Purification kit was used to clean the resulting 300 μl of eluted ChIP DNA prior to analysis. qPCR was done using the primers and annealing temperatures listed below.

qPCR primers for Chromatin Immunoprecipitation				
Description	Primer name	Sequence	Annealing temp (^{o}C)	Efficiency
AGAMOUS 2nd Intron CArG box 1	AG_2ndInt_CaRG1_F	TCTCTCCATCGAGAAGGTTG	53	98%
	AG_2ndInt_CaRG1_R	GTAACTAAATGACTTGTCCGAGTAAC		
SPATULA promoter primer pair 3 (P3)	AP2_qPCR_pSPT_p3F	CGATTTCATCCGTAGCAGATTTCCA	53	100.5%
	AP2_qPCR_pSPT_p3R	ACTTTTCCTCGTCGCACGTGA		
SPATULA promoter primer pair 4 (P4)	AP2_qPCR_pSPT_p4F	ACGCTGCGAACGATCAAA	54	99.5%
	AP2_qPCR_pSPT_p4R	CGGCGAACAAAGTGAATGCACA		
GAPC transcript	GAPC1-qRTgene-F	CCAGTCACTGTTTTCGGCAT	60	>95%
	GAPC1-qRTgene-R	AGCTGCAGCCTTGTCTTTGT		

Protoplast isolation and luciferase reporter assay

Protoplast isolation and transfection was performed essentially according to Sheen (2002). 20 to 40 young rosette leaves taken from unbolted wildtype plants (Ler or Col-0) grown in short day photoperiod for 4-6 weeks were harvested and sliced widthwise to 0.5-1 mm slivers, excluding the leaf tip and the petiole. Leaf slivers were transferred to a petri dish containing enzyme solution (1.5 % cellulase R10, 0.4% macerozyme R1, 0.4 M Mannitol, 20 mM KCl, and 20 mM MES, pH 5.7, 10 mM $CaCl_2$, 0.1 % BSA), vacuumed for 5 minutes, and then incubated for 3 hours at room temperature in the dark. After incubation, the petri dish was gently swirled for two minutes, 10 ml of W5 (154 mM NaCl, 125 mM CaCl2, 5 mM KCl, 2 mM MES pH 5.7) was added, and then protoplasts were swirled for an additional two minutes. Protoplast solution was then filtered through two layers of MiraCloth (Calbiochem, San Diego, CA) and then spun at 2,000 rpm (500g) in a fixed angle centrifuge. Supernatant was immediately replaced with ~20 mls of W5 and cells were left to settle on ice for 30-60 minutes. After settling, supernatant was removed and protoplasts were resuspended in MMg (0.4 mM mannitol, 15 mM

$MgCl_2$, 4 mM MES, pH 5.7) to a final concentration of 2 x 10^5 cells / ml. 10 μg of each plasmid in a final volume of 5μl was mixed with 50μl of protoplasts and 60μl of a PEG solution (40% PEG 4000, 0.24M mannitol, 100 mM $CaCl_2$) and incubated at room temperature for 8 minutes. Transfection was stopped with the addition of 200μl W5, protoplasts were pelleted by 1 minute of centrifugation at 1,000 rpm, and then enough supernatant was removed so that 25 μl remained. The 25 μl of transfected protoplasts were added to a well in a 24 well plate that had been coated with 5% fetal bovine serum (FBS) and contained 250 μl WI solution (0.5M mannitol, 4mM MES pH 5.7, 20 mM KCl). If 1-NAA was added to the assay, it was added as a WI/1-NAA solution in place of the normal WI solution so that the final concentration with the protoplasts was 1 μM. Cells were incubated at room temperature in dim light for 20-24 hours.

After incubation, protoplasts were pelleted by centrifugation for 1 minute at 5,000 rpm and suspended in 100μl of 1X passive lysis (Promega, Madison, WI) vortexed, freeze/thawed twice in liquid nitrogen, and shaken at 300 rpm for 15 minutes. Cell debris was pelleted by centrifugation at 10,000 rpm for 1 minute, and then the cleared lysate was transferred into a fresh 1.5 ml tube. The Promega dual luciferase assay (Promega, Madison, WI) was used according to manufacturers instructions with 20 μl of cleared lysate. Firefly and renilla luciferase readings were taken with the Turner Designs TD-20/20 (Turner Designs, Sunnyvale, CA) at a sensitivity of ~25%. For each experimental condition, three biological replicates for each type of transformation (combination of plasmids) were done using protoplasts from the same preparation.

Chapter IV: Flower and early fruit development in a diploid strawberry, *Fragaria vesca*[1]

Introduction

The diploid woodland strawberry, *Fragaria vesca*, is being recognized as a model for the more complex octoploid commercial strawberry, *Fragaria* × *ananassa*. *F. vesca* exhibits a short seed to seed cycle, can be easily transformed by *Agrobacteria*, and a draft genome sequence has been published. These features, together with its similar flower structure, potentially make *F. vesca* a good model for studying the flower development of other members of the Rosaceae family, which contains many economically important fruit trees and ornamental plants. To propel *F. vesca*'s role in genetic and genomic research and to facilitate the study of its reproductive development, we have investigated in detail *F. vesca* flower and early fruit development using a seventh generation inbred diploid line, Yellow Wonder 5AF7. We present here standardized developmental staging and detailed descriptions of morphological changes associated with flower and early fruit development based on images of hand dissected flowers, histological sections, and scanning electron microscopy. In situ hybridization with the *F. vesca AGAMOUS* homolog, *FvAG,* showed expression in young stamen and carpel primordia. This work lays the essential groundwork and standardization for future molecular, genetic, and genomic studies of *F. vesca*.

[1] Text and figures for this chapter are the author's original work taken from Hollender et al. (2011).

Results

Fragaria vesca shoot structure

The biology of the shoot meristem has economic relevance in crop plants. Runners and branch crowns, which are shoots capable of developing into new plants, arise as buds from leaf axils. In two different inbred *F. vesca* lines, YW5AF7 and Ruegen F7, only branch crowns, and no runners, are formed, while in H4 × 4, both branch crowns and runners are produced (Slovin and Rabinowicz, 2007; Slovin et al., 2009). The choice between developing a branch crown or runner is environmentally and hormonally regulated. Factors such as the phytohormone gibberellin, day length, and temperature influence this choice (Hartmann, 1947; Durner and Poling, 1988; Serçe and Hancock, 2005; Hytönen et al., 2009).

Like the octoploid commercial strawberry and other *F. vesca* cultivars, YW5AF7 has a determinate dichasial cyme inflorescence (Anderson and Guttridge, 1982; Galletta and Himelrick, 1990; Hancock, 1999). The primary shoot terminates in a single flower which gives rise to the first fruit (Fig. 4-1B–D). Subtending the primary flower are two secondary shoots that arise simultaneously at opposite sides of the peduncle, ending in secondary terminal flowers (Figs. 4-1C–D, 4-2P). The secondary terminal flowers are about three to five stages younger than (and 5–8 days behind) the primary flower. Figure 4-2P illustrates two stage 7 secondary flower buds subtending a stage 10 primary flower

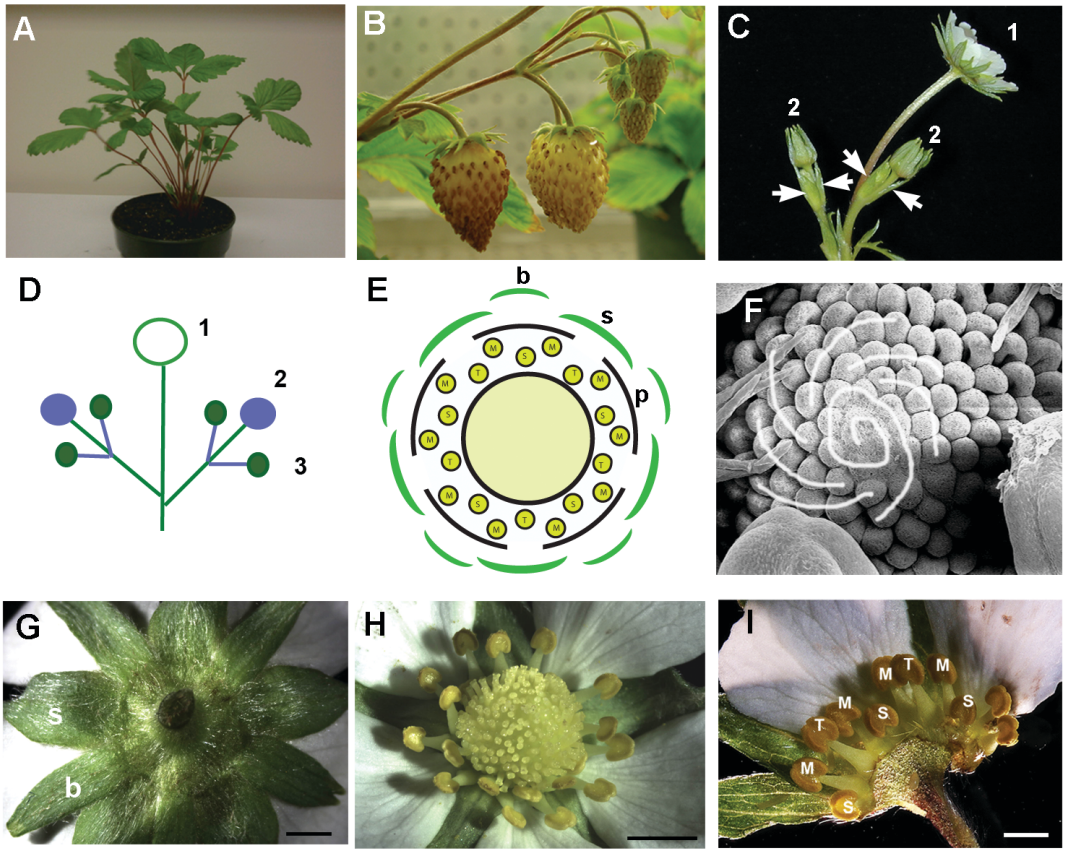

Figure 4-1 *Fragaria vesca* shoot and flower development. **(A)** *F. vesca* YW5AF7 grown in a 10.2 cm pot. **(B)** YW5AF7 dichasial cyme bearing yellow berries. **(C)** Inflorescence with primary flower *1* and two developing secondary flowers *2*. Young tertiary buds (*arrows*) are present beneath the secondary flower buds. **(D)** Diagram of shoot architecture. Numbers indicate primary, secondary and tertiary flower buds. **(E)** Diagram illustrating floral organ arrangement. The two outer whorls are concentric rings of 5 bracts *b* alternating with 5 sepals *s*. The third whorl consists of five white petals *p*. Interior to the petals are 5 tall (T) and 5 short (S) stamen in the inner whorl and 10 medium length (M) stamen in the outer whorl. The center circle indicates a receptacle topped with numerous, spirally arranged carpels. **(F)** Scanning electron micrograph (SEM) of a developing floral bud, illustrating spirally arranged carpel primordia. **(G)** Abaxial view of a typical *F. vesca* flower with 5 narrow bracts *b* alternating with 5 wider sepals *s*. **(H)** Adaxial view of typical *F. vesca* flower illustrating a whorl of 5 white petals, two whorls of 10 stamens each, and an apocarpous gynoecium with ~160 pistils. **(I)** Dissected flower illustrating the "S, M, T, M, S" stamen pattern. Scale bars: 1 mm

bud. Each secondary shoot adopts the branching pattern of the primary shoot (Fig. 4-1 B–D). Depending on environmental conditions, this pattern can repeat itself. In contrast to *Arabidopsis*, flowers show basipetal succession, as the oldest flower is at the apex, and the youngest flowers are towards the base.

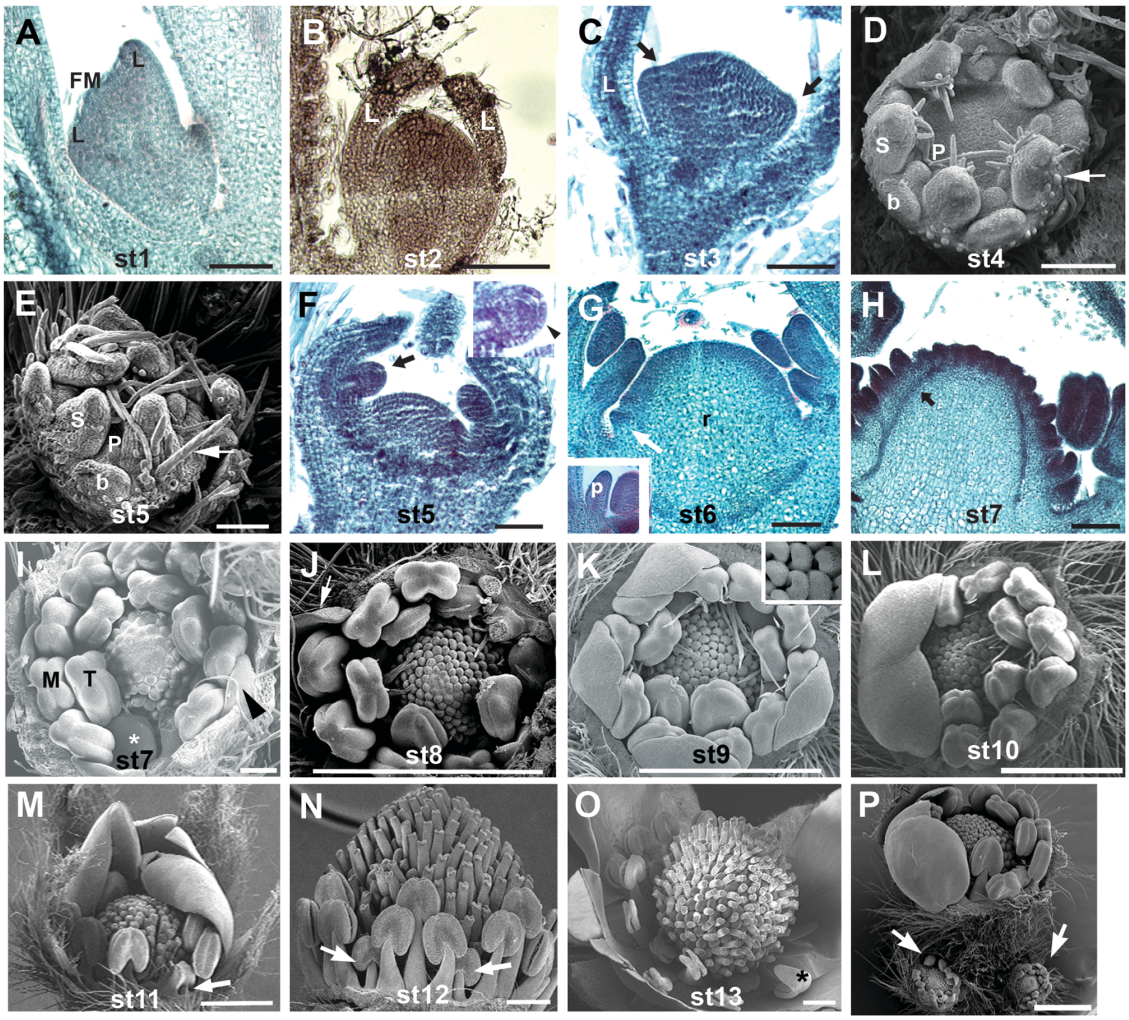

Fig. 4-2 *Fragaria vesca* flower developmental stages (stages 1–13) SEM images

Fig. 4-2 *Fragaria vesca* flower developmental stages (stages 1–13) SEM images (I–P) depict floral buds with bracts and sepals removed. Histological sections (**A**–**C**, **F**–**H**) are stained with Safranin-O/Fast Green. (**A)** Stage 1 floral meristem (*FM*) flanked by leaf *L* primordia. **(B)** Stage 2 floral meristem flanked by two developing leaves *L*. **(C)** Stage 3 flower bud with emerging sepal primordia (*arrows*). **(D)** Stage 4 bud with flat central region surrounded by sepal *s* and petal *p* primordia. Petal primordia are aligned in radial axis with bracts *b*. Spike-like trichomes are seen on the adaxial surface of sepals with trichome primordia on the lower abaxial surface. **(E)** SEM of stage 5 flower bud. Sepals meet at flower center and trichomes have elongated (*arrow*). **(F)** *Longitudinal section* of stage 5 flower bud, illustrating a pronounced central dome. Stamen primordia (*arrow*) have a distinct epidermal layer enclosing archesporial cells (*arrowhead* in inset). **(G)** Stage 6 bud characterized by emerging carpel primordia (*white arrow*) at the base of the receptacle *r*. *Inset* shows a petal primordium *p* to the left of a developing anther. **(H)** Stage 7 floral bud with carpel primordia emerging acropetally to the receptacle apex, with a gradient of increasing maturity from apex to base. Vasculature runs parallel to the receptacle dome surface (*black arrow*). **(I)** SEM of a stage 7 floral bud, illustrating carpel primordia initiation at the apex, with *M* and *T* type stamens and petals (*black arrowhead*) visible. *Asterisk* indicates one of two anthers broken off during analysis. **(J)** Stage 8 floral bud containing thumb-like developing carpels (see Fig. 4-5). Petals (*arrow*) reach the top of the M stamens. **(K)** Stage 9 floral bud with indented carpel primordia (inset) and expanding petals. **(L)** Stage 10 flower with expanded and overlapping petals. **(M)** Stage 11 floral bud with visible short "S" stamens (*arrow*). **(N)** The Stage 12 mature floral bud (petals removed) is closed, with fully developed organs. The repeating unit of "S, M, T, M, S" stamens is visible between *arrows*. (**O)** Late stage 13 is the open flower with dehisced anthers. *Asterisk* indicates a petaloid anther **(P)** SEM of the basic shoot unit. A stage 10 floral bud is flanked by two stage 7 buds (*arrows*). *Scale bars* in **A**–**G**: 100 μm; **H**–**P**: 1 mm

Fragaria vesca flower

The outer two whorls of the *F. vesca* flower consist of a whorl of five narrow bracts alternating in alignment with an inner whorl of five wider sepals (Fig. 4-1E, G). Interior to the sepals is a whorl of 5 white petals (Fig. 4-1E, H). Two whorls of 10 stamens each (Fig. 4-1E, H–I) surround the central receptacle dome. Stamens can be classified into three types based on their height: short (S), medium (M), and tall (T). Ten M stamens occupy the outer whorl (just interior to petals), while five T and five S stamens are alternately arranged in the interior whorl (Fig. 4-1E, H–I). Along the outer to inner whorl concentric axis, the S stamens always align with petals, and the T stamens align with sepals (Fig. 4-1E, H). In the innermost whorl, the domed receptacle is topped with pistils embedded in a spiral pattern on the epidermis of the receptacle (Fig. 4-1F, H). The number of pistils is approximately 160, but this can vary depending on plant variety and age, as well as the position of the flower on the inflorescence. Primary flowers have more pistils than flowers that develop later on the same inflorescence. Each pistil, an individual carpel with one ovary and one ovule, can remain fertile and receptive to pollen for several days after flower opening. Occasionally four or six petals were observed in wild type flowers. In addition, petal tissue occasionally develops from a stamen, forming petaloid stamens, and resulting in supernumerary petals.

Table 4-1 Summary of key landmark events during flower development

***F. vesca* Floral Stage**	**Floral Meristem**	**Leaf/Bract/Sepal**	**Petal**	**Stamen**	**Carpel**
1	Slightly rounded dome of dense cells	Leaf primordia buttress flanks bud			
2	Larger, rounder dome				
3		Bract and sepal primordia appear			
4			Petal primordia initiate		Flat flower center
5				Stamen primordia initiate (see Table 2)	Receptacle dome appears
6				See Table 2	Carpel primordia initiate from the receptacle base.
7				See Table 2	Round carpel primordia reach the receptacle apex
8				See Table 2	Thumb-like carpel primordial at the receptacle apex
9			Translucent petals	Translucent stamen	Bowling pin shaped carpel primordia Indented carpel walls and MMC visible
10			Translucent petals	Yellowing of anthers	Central carpel constriction divides organ into two almost equal apical and basal parts. Indentation is not yet fused
11			Petals show white finger-like regions		Style has narrowed and elongated to be twice or more in length than the ovary base Fully formed embryo sac Complete fusion of carpel walls
12			Petals are completely white and opaque		Music-note-like carpels Styles are further apart from each other. Birefringent layer appearing in the carpel wall
13	Fully developed open flower				

Fragaria vesca flower development

Using scanning electron microscopy, histological sections, and stereomicroscopy, we categorized *F. vesca* flower development into 13 stages based on significant structural and/or cytological events (Table 4-1). These flower developmental stages are described in three separate segments: early flower development (stages 1–4), reproductive organ initiation and development (stages 5–7), and floral organ differentiation (stages 8–13). Male gametophyte development, which occurs during stages 6–12, and female gametophyte development, which occurs during stages 8–12, are described in detail in later sections.

Early flower development: stages 1–4

Stages 1–4 include the development of the perianth. At stage 1, the floral meristem (FM), approximately 100 μm wide, consists of a slightly rounded dome of densely packed cells surrounded by leaf primordia (Fig. 4-2A). By stage 2, the FM has grown rounder and has a higher dome than the stage 1 bud, with leaf primordia meeting above the center (Fig. 4-2B). The main event characterizing stage 3 is the emergence of bract and sepal primordia (Fig. 4-2C) and the leaves have surpassed the height of the developing flower.

Stage 4 occurs with the emergence of petal primordia spaced between sepals (Fig. 4-2D). The enlarging sepal primordia are characterized by elongating trichomes on their adaxial surface and trichome primordia on the abaxial surface. The central dome, interior to the perianth, appears relatively flat (Fig. 4-2D).

Reproductive organ initiation and development, stages 5–7

Strawberry flower bud stages 5 through 7 encompass the initiation and development of stamen (microsporophyll) and carpel (megasporophyll) primordia. Key features of the stage 5 bud are increased sepal length (Fig. 4-2E), the emergence of oval-shaped stamen primordia (Fig. 4-2F), and protrusion of the receptacle dome (Fig. 4-2F). The developmental events occurring in the stage 5 floral bud anther are comparable to those in *Arabidopsis* anther stages 1–2, where a distinct epidermal cell layer surrounds archesporial cells (Table 4-2; Fig. 4-2F inset) (Sanders et al., 1999). At floral stage 5, petal primordia remain small (Fig. 4-2E).

One or two rings of early carpel primordia have emerged at the base of the receptacle dome when the bud reaches floral stage 6 (Fig. 4-2G). The stage 6 bud is also wider than and approximately twice as high as in stage 5. Short petal primordia are present (Fig. 4-2G inset) and anthers exhibit a lobed structure (Figs. 4-2G, 4-4A).

During stage 7, additional carpel primordia initiate acropetally from the receptacle dome and are arranged in a spiral pattern, with the more mature carpels at the receptacle base, as previously described for Rosoidea, a subfamily of Rosaceae that includes *Fragaria* (Kania, 1973; Weberling, 1989) (Figs. 4-1F, 4-2H–I). Vascular bundles run both parallel to and branch into the carpels on the surface of the receptacle (Fig. 4-2H). Petals extend upward, slightly curving around adjacent anthers, and are approximately three fourths of the anther height (Fig. 4-2I).

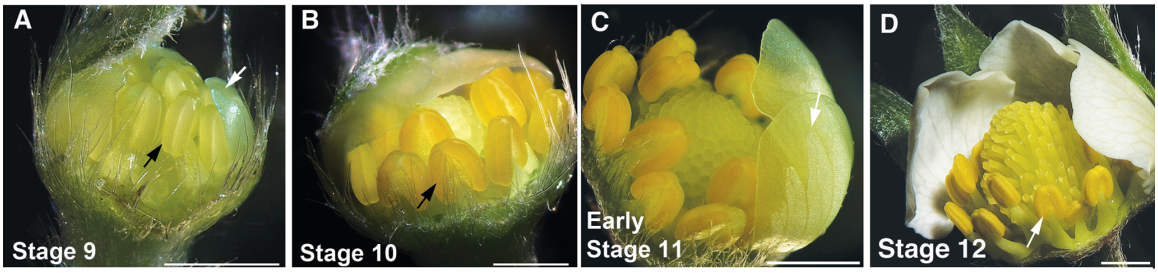

Fig. 4-3 Stereo images of dissected *F. vesca* floral buds from stages 9 to 12, showing color changes in developing organs. **a** Stage 9 floral bud with translucent petals (*white arrow*) and translucent pale yellow anthers (*black arrow*). **b** Stage 10 bud with opaque yellow anthers (*arrow*). **c** An early stage 11 bud with petals developing opaque white finger-like regions (*arrow*). **d** A stage 12 bud with fully opaque white petals and yellow-orange anthers (*arrow*). *Scale bars* 1 mm [Images courtesy of JP Slovin]

Floral organ differentiation, stages 8–13

From stages 8 to 13, petals increase in size and differentiate from translucent to opaque white organs. Specifically, at stage 8, petal width spans the midlines of two adjacent anthers, and petal height reaches the top of the outer whorl stamens (Fig 4-2J). At stage 9, the translucent petals, each covering two adjacent M stamens, do not yet overlap with each other (Figs. 4-2K, 4-3A). At stage 10, petals remain translucent, with neighboring petals overlapping and covering both whorls of stamens (Figs. 4-2L, 4-3B). Stage 11 petals have opaque white finger-like regions associated with the vasculature, and overlap above the center of the flower (Figs. 4-2M, 4-3C). By stage 12, petals are completely white and opaque, and appear fully differentiated (Fig. 4-3D).

On the surface, stages 8–11 stamens appear similar in morphology except that anther color changes dramatically from translucent and colorless to yellow between stages 9 and 10 (Fig. 4-3A–B). At stage 9, the filaments of the M and T stamens elongate so that their

anthers are above the apex of the receptacle dome (Figs. 4-2K, 4-3A). By stage 11, the filaments of the S stamens, which previously could be observed only in histological sections, have elongated. These stamens can now be seen in micrographs of partially dissected buds (Fig. 4-2M), forming the S, M, T, M, S units of the mature flower (Fig. 4-2N). At stage 12, the filaments of the small inner whorl stamens reach their final height (Fig. 4-2N) and anthers are opaque yellow and appear fully differentiated (Fig. 4-3D). By late stage 12, also referred to as balloon stage, buds begin to open, partially exposing the opaque white petals (Fig. 4-3D). Flower opening at stage 13 (Figs. 4-1C, 4-2O, 4-6 column A) is followed within 24 h by anther dehiscence. The anthers asynchronously dehisce with the S anthers dehiscing last.

Cellular activities occurring in stages 8 through 12, such as microsporogenesis in the anthers and female gametophyte development, are described in detail in a later section, as are details of developing carpel morphology. Between stages 7 and 9, carpel primordia undergo rapid morphological changes, transitioning from small bumps on the receptacle (stage 7), to a thumb-like organ (stage 8), and then into bowling pin-like structures (stage 9) (Figs. 4-2H–K, 4-5A–H). Stages 10–12 are accompanied by rapid elongation of the style and ovary expansion to attain the final musical quarter note shaped carpel with a fully developed ovule inside (Fig. 4-5I–T).

Male gametophyte development, floral bud stages 6–12

Figure 4 summarizes *F. vesca* male gametophyte development. An effort was made to correlate specific anther developmental events in *F. vesca* with anther developmental stages defined for *Arabidopsis* (Table 4-2) (Sanders et al.1999). At floral stage 6, *F.*

vesca anther cells have differentiated into distinct epidermal and parietal layers surrounding sporogenous cells exhibiting mitotic activity (Fig. 4-4A, E), comparable to events in *Arabidopsis* stage 3 anthers (Table 4-2).

Further differentiation of the anther in stage 7 *F. vesca* buds includes the development of the endothecium, middle layer, and tapetum from the parietal cells as well as the microspore mother cells (MMC) (Fig. 4-4B, F). With the development of the stomium (not shown), a clearly defined four-lobed structure is formed (Fig. 4-4B). Early vasculature is also present in the anther (Fig. 4-4B). At this stage, all *F. vesca* anthers (M, T, and S) appear to be at the same stage of development, although their filaments are of different lengths. The anthers of stage 7 flowers correlate with *Arabidopsis* anthers at stages 4–5 (Table 4-2) (Sanders et al., 1999).

Anther development of flower stage 8 is comparable to stages 5–6 of the *Arabidopsis* anther, when the MMCs enter meiosis (Table 4-2; Fig 4-4C, G) (Sanders et al., 1999). Stage 9 strawberry flower buds can be divided into early and late phases. In early stage 9, tetrads of four haploid spores (the product of meiosis of the MMCs) are held together by a thick callose wall and are tightly packed within the anther locules (Fig 4-4D, H). By late stage 9, each locule has expanded, allowing individual tetrads to separate from one other (Fig 4-4I, M). Tetrad development, as well as the middle layer degradation in stage 9 bud anthers, is comparable with development in *Arabidopsis* anthers at stages 6–7 (Table 4-2).

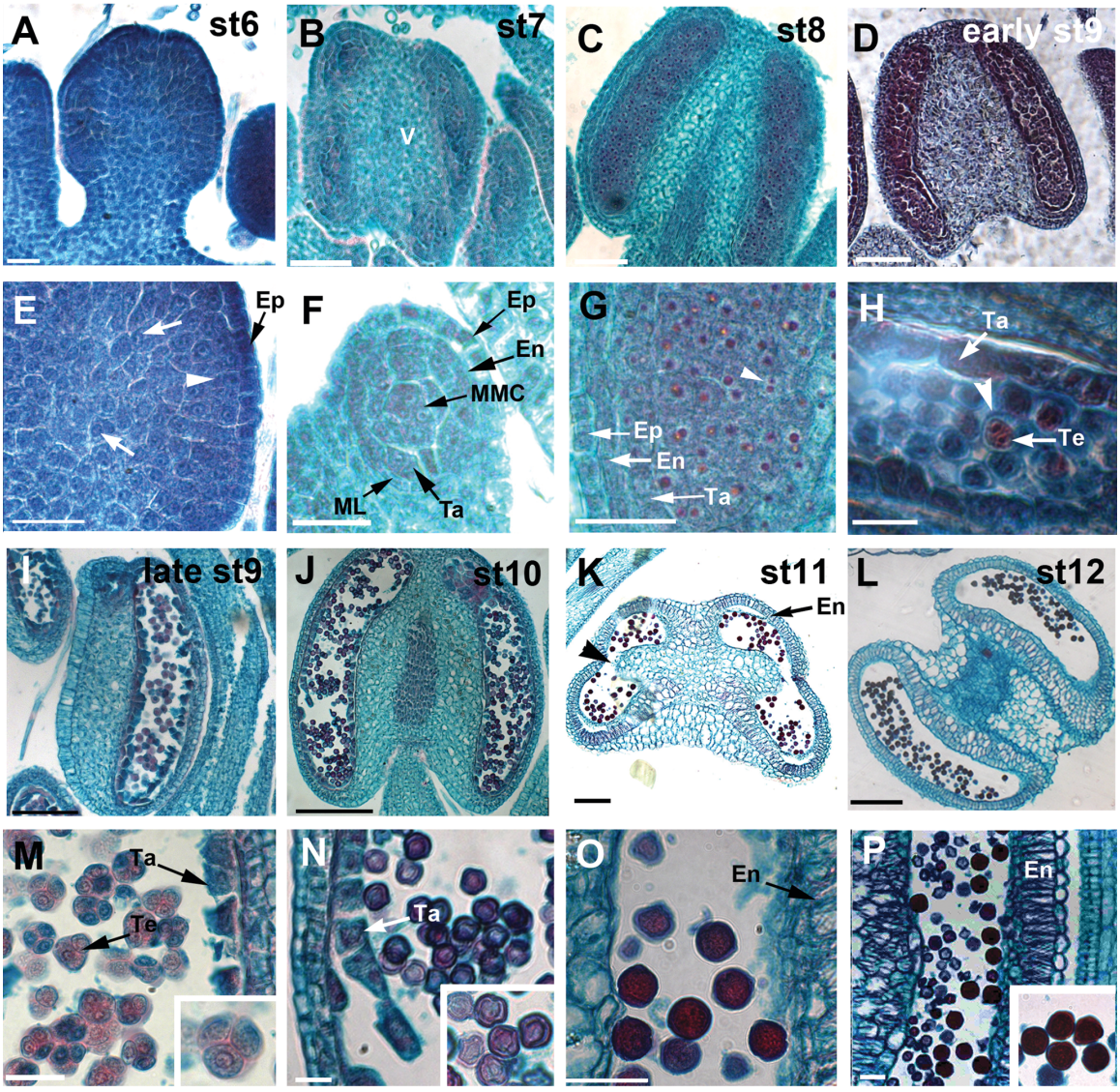

Fig. 4-4 *Fragaria vesca* anther development

Fig. 4-4 *Fragaria vesca* anther development. **A** and **E** Stamen of stage 6 floral bud showing a bi-lobed anther with defined epidermal and parietal layers (*arrowhead*). Sporogenous cells exhibit active mitotic activity (*white arrows*). **B** and **F** Stage 7 bud anther with developing vasculature *v*. Endothecium, middle layer, and tapetal cells surround the microspore mother cells. **C** and **G** Stage 8 floral bud anther filled with tightly packed MMCs undergoing meiosis (*arrowhead*). **D** and **H** Early stage 9 bud anther showing locules filled with tetrads of microspores bound by callose (*arrowhead*). **I** and **M** Anther of late stage 9 floral bud with tetrads loosely packed within the locule. **J** and **N** Longitudinal section of a stage 10 bud anther with individual microspores visible in the locules and degrading tapetum (*arrow*). **K** and **O** Cross section through a stage 11 floral bud anther showing four locules containing tricellular pollen grains. Tapetum and the septum between locules (*arrowhead*) are degraded. Endothecium cells (*arrows*) have increased in size and contain fibrous bands. **L** and **P** *Longitudinal sections* showing anthers of stage 12 floral buds, which are highly similar to anthers from stage 11 buds. *Ep* epidermal layer, *En* endothecium, *ML* middle layer, *MMC* microspore mother cells, *Ta* tapetum, *Te* tetrad, *V* vasculature. *Scale bars* in **A**, **E**–**H**, and **M**–**P**: 20 μm; **B**–**D**: 50 μm; **I**–**L**: 100 μm

Table 4-2. Key developmental events in the *F. vesca* anther. Corresponding *Arabidopsis thaliana* anther stages are based on (Sanders et al., 1999). As they continue to develop, most floral bud stages exhibit a progression through different anther stages.

F. vesca Floral bud stage	**Anther Stages in *Arabidopsis***	**Description**
5	1	Bi-lobed and round anther primordia and short filament form.
	2	Epidermal cells are distinguishable. Archesporial cells arise.
6	3	Archesporial cells have divided, producing inner 1^o sporogenous layers, outer 1^o parietal and subsequent 2^o parietal layers. Regions of mitotic activity in the sporogenous tissue are visible
7	4	Stomium develops, producing a preliminary lobed structure. Endothecium, middle layer and tapetum arise from parietal cells. Vasculature begins to develop.
	5	Microspore mother cells appear. Four locules are clearly distinct. Vasculature is larger and more distinct.
8		
	6	Microspore mother cells enter meiosis, but resulting tetrads are tightly confined in locules. Middle layer has degenerated.
9		
	7	Meiosis is complete and the tetrads of microspores are loose in each locule. All anthers (M, T,and S) are all at the same stage.
10	8	Microspores are loose in the locule after callose wall holding tetrads together disintegrates.
	9	Microspore exine wall develops. The microspores also become vacuolated (not obvious).
	10	Tapetum degeneration is initiated
11	11	Pollen mitotic division occurs. Tapetum is completely degraded. Filaments of short stamens elongate and all anthers reach final height. Endothecium cells elongate and thicken from the addition of fibrous bands.
	12	Septum is degraded. Anthers become bilocular and contain round tricellular pollen grains.
12		No visible change in anther development
13	13	Dehiscence.

In the stage 10 *F. vesca* flower bud, haploid microspores have been released from tetrads in the anthers, and tapetum degeneration is initiated (Fig 4-4J, N). Anthers from stage 10 floral buds are comparable to anther stages 8–10 in *Arabidopsis* (Table 4-2).

In *F. vesca* floral bud stage 11, as in *Arabidopsis* anther stages 11–12, the tapetum and septum are fully degraded, endothecium cells increase in size and are thicken due to the formation of fibrous bands, and trinuclear pollen grains are present (Table 4-2, Fig. 4-4K, O). Morphologically, *F. vesca* flower stage 12 anthers and pollen appear similar to those of stage 11 flowers (Fig. 4-4L, P).

Female gametophyte development, floral bud stages 8–12

Figure 5 summarizes carpel and female gametophyte development. *Fragaria* have uniovular peltate-ascidiate carpels (tubular carpels attached to the receptacle at their base) that exhibit anacrostyly, whereby the style and stigma appear near the base of the ovary as opposed to being an apical continuation (Weberling, 1989). At the beginning of floral stage 8, the receptacle is entirely covered with carpel primordia. The youngest primordia, at the apex, appear as rounded protrusions, while the more mature primordia at the base are thumb-like projections (Figs. 4-2J, 4-5A–D). Longitudinal sections of stage 8 bud carpels reveal an epidermal layer encasing undifferentiated cells (Fig. 4-5A–B).

At stage 9, individual carpels are shaped like a bowling pin with an indentation along their adaxial side from which the ovule develops in a downward direction (Fig. 4-5E–H).

Ovary wall margins fold inward to envelop the single ovule and fuse post genitally at their points of contact. At stage 9, the ovule primordium contains the megasporocyte (megaspore mother cell) (Fig 4-5E-F).

At floral stage 10, the top of the bowling pin structure, the future style, has enlarged so that the carpel has almost two equal parts separated by a horizontal constriction (Fig. 4-5L). The margins of the style walls bend towards each other on their adaxial side (Fig. 4-5K), and the ovule has increased in size (Fig. 4-5I–J).

Floral bud stage 11 carpels are tightly packed and have styles that have elongated to over twice the length of the ovary (Fig. 4-5O-P). The curled-in margins of the style wall have fused postgenitally (Fig. 4-5O), with the line of fusion facing the receptacle center. A mature 7 cell/8 nuclei embryo sac is present in the ovule which is surrounded by integuments (Fig. 4-5N). The ovary wall exhibits distinct layers (Fig. 4-5M–N).

In the stage 12 floral bud, the carpel possesses an enlarged, ovoid, ovary attached to a tall and thin style, resembling a musical quarter note (Fig. 4-5T). Due to the expansion of the ovary, styles are no longer tightly packed (Fig. 4-5S–T). Longitudinal carpel sections show the stigma to be composed of upright rectangular cells (Fig. 4-5Q inset), and the stigma surface has a puckered appearance (Fig. 4-5S–T). There are now three distinct tissues in the ovary wall, which has pulled away from the ovule (Fig. 4-5Q–R), and one of the ovary wall layers is highly birefringent (Fig. 4-5R).

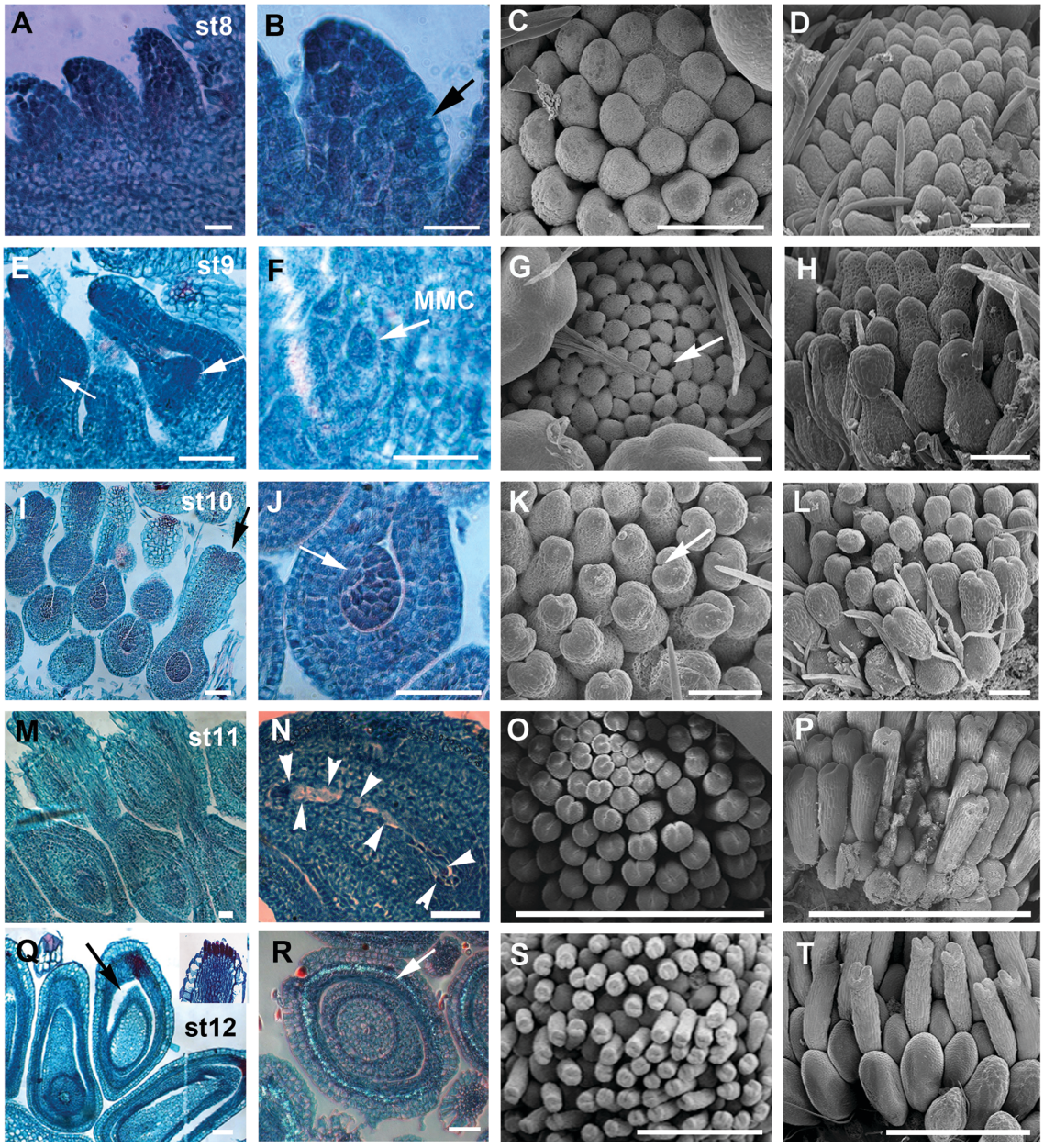

Fig. 4-5 *Fragaria vesca* carpel development

Fig. 4-5 *Fragaria vesca* carpel development. **A**–**D** Thumb-like carpel primordia protrude from the apical receptacle surface in a stage 8 floral bud. A distinct epidermal layer is visible (*arrow* in **B**). **E**–**H** Carpels of stage 9 floral buds have bowling pin shape (**H**) and an adaxial indentation (*arrow* in **G**). The developing ovary at the base of each carpel contains a single ovule primordium protruding from its inner wall (*arrows* in **E**) with a distinct megaspore mother cell (MMC) (*arrow* in **F**). **I**–**L** Carpels in stage 10 floral buds have a more pronounced apical half, and are constricted in their central region. The indentation started in stage 9 results in a narrow apical to basal furrow (*arrow* in **I** and **K**) that will close by Stage 11. *Arrow* in **J** indicates developing ovule. **M**–**P** Stage 11 carpels with a fully formed embryo sac (*arrowheads* in **N**). The indentation at the style apex has completely fused (**O**). The styles have further narrowed and become considerably elongated (**P**). **Q**–**T** Stage 12 carpels have distinct separation (*arrow* in **Q**) of the ovary wall and the ovule. Stigmatic cells stain darkly red (inset in **Q**) and birefringent deposits form in the carpel wall (*arrow* in **R**). Carpels now resemble music notes (**T**). Ovary expansion causes neighboring styles to spread further apart from each other (**S**). Histological sections stained with Safranin-O and fast green: A–B, E–F, I–J, M–N, Q–R. SEM: C–D, G–H, K–L, O–P, S–T. *Scale bars* A–B, and F: 20 μm. C–D, G–H, and K–L: 100 μm. E, I–J, M–N, and Q–R: 50 μm

Early fruit development, from floral bud stage 13 onwards

As the flower ages post fertilization, noticeable changes occur (Fig. 4-6). At anthesis, or soon thereafter, the anthers, particularly those at T and M positions, begin to brown at the edges. Between 2 and 4 days post anthesis (DPA), the petals dry up and fall off, and the stigmas become brownish-pink (Fig. 4-6B, row 1). Individual achenes were dissected to reveal the developing seed (Fig. 4-6B, row 4). Embryos were visualized in seeds cleared with Hoyers solution (Liu and Meinke, 1998; Stangeland and Salehian, 2002). At 2–4 DPA, embryos range from too small to be visible in our magnification range to 8-cell and globular stage (Fig. 4-6B, row 5). This variability may be due simply to pollen landing on individual stigmas at different times.

At 6–7 DPA, the stigma and style turn brown and start to dry. Anthers senesce and fall of the filaments. Fertilized achenes increase noticeably in size (Fig 4-6C, row 1) and the ovary changes from translucent to opaque (Fig 4-6C, row 3). At this stage, heart stage embryos could readily be dissected manually from the developing seed (Fig. 4-6C, rows 5–6). At 8–10 DPA, although styles have completely dried and are brown, they remain attached to the ovary and often remain so in the mature fruit. Torpedo stage embryos are easily visible (Fig. 4-6D, rows 5–6).

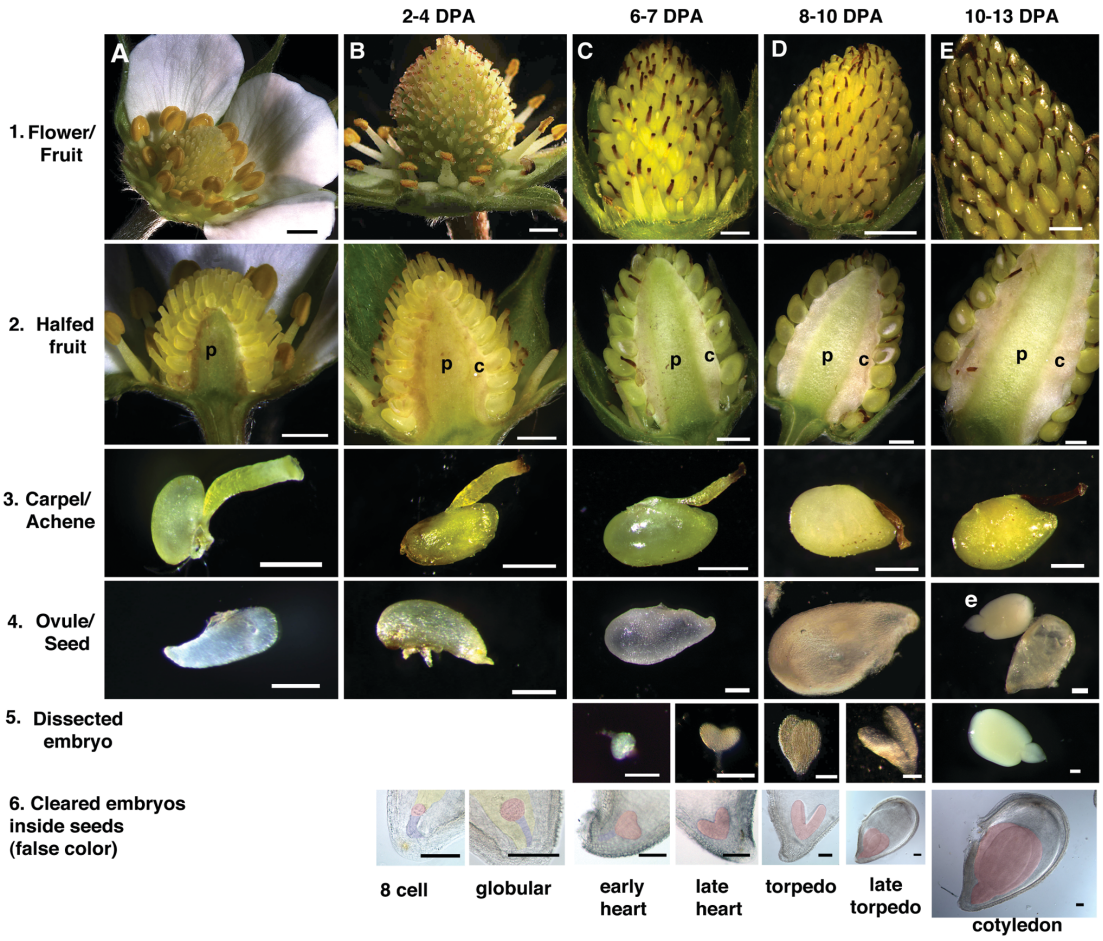

Fig. 4-6 *Fragaria vesca* early fruit development . *Columns* **A-E** Increasing maturity of the fruit, from day of anthesis to 13 days post anthesis (DPA). Rows focus on specific flower or fruit parts along the post anthesis time axis. *Row 1* shows the transition from an open flower to an early stage fruit. Most notable is the enlargement of ovaries/achenes along the time axis. *Row 2 longitudinal sections* through the center of the developing fruit show a gradual enlargement of the pith *p* and thickening of the cortex *c*. *Row 3* focuses on the individual carpel as it develops into an achene. Each carpel consists of a single ovary and a slender style. Its fertilization and subsequent maturation is accompanied by browning of the stigma followed by browning and drying of the style. The ovary wall changes progressively from translucent to opaque as the achene matures. *Row 4* Developing seeds dissected from the ovary (before fertilization) or achene (after fertilization). The opaque white seed fills the interior space of the carpel or achene. *Row 5* Embryos dissected from the developing seeds. *Row 6* Embryos inside cleared developing seeds imaged with DIC optics. Images are falsely colored: embryos are *pink*; the embryo sac is *yellow*; and the hypophysis is *purple*. *Scale bars* 1 mm (Rows 1–2); 500 μm (Row 3); 200 μm (Row 4); 100 μm (Rows 5–6)

At 8–10 DPA, although styles have completely dried and are brown, they remain attached to the ovary and often remain so in the mature fruit. Torpedo stage embryos are easily visible (Fig. 4-6D, rows 5–6). By 10 DPA, the two cotyledons of an embryo have grown in size and are in the same vertical axis as the hypocotyl, resembling two hands pressed together. Unlike the *Arabidopsis* embryo, the *Fragaria* embryo is spatulate, with the cotyledons remaining upright as they continue to enlarge and eventually fill the entire seed (Fig. 4-6E, rows 5–6).

The most dramatic visual changes during early fruit development are the increasing size of achenes and receptacle, whose cortex region is increasingly thickened (Fig. 4-6, row 2). Berry size varies according to flower position, number of carpels, and number of fertilized achenes. Primary fruit are larger than secondary fruit, and flowers with greater pollination success produce larger berries (Kronenberg, 1959). During early fruit development, a more accurate determinate of fruit developmental stage is the embryo morphology within the seeds on the berry, and not berry size.

FvAG expression is detected in stamen and carpel primordia in _F. vesca_

AGAMOUS (*AG*) encodes a class C MADS box transcription factor that is expressed specifically in the stamen and carpel primordia in *Arabidopsis*. Its domain-specific expression correlates with its function in specifying stamen and carpel identity (Yanofsky et al., 1990; Bowman et al., 1991b; Drews et al., 1991). We identified a single gene model in the *F. vesca* H4 × 4 genome that is likely the *AG* homolog (see "Materials and methods"). This gene, Hybrid Gene Model #24852, was named *FvAG*.

To test if expression of *FvAG* mirrors that of *Arabidopsis AG* in early flower development, we performed an in situ hybridization with *F. vesca* floral buds. Antisense *FvAG* probe did not detect any signal in an emerging floral bud (Fig. 4-7A). Signal is first detected in the central region of stage 4 flowers interior to sepal primordia. No signal is present in the sepal primordia themselves (Fig. 4-7B). In the early stage 5 floral bud, stamen primordia showed *FvAG* expression, the sepal and petal primordia do not (Fig. 4-7C). *FvAG* expression was seen in developing carpels in stage 7 buds (Fig. 4-7D). At the receptacle apex, where primordia are absent, *FvAG* was not detected. At stage 9, intense *FvAG* signal was detected in developing carpels as well as in the vasculature connecting the receptacle and individual carpels (Fig. 4-7E). At all stages, *FvAG* was detected in the stamen and carpel primordia but was absent from sepal and petal primordia, mirroring expression of its homolog in *Arabidopsis*. Expression signal was absent in negative control hybridizations using sense probes (Fig 4-7F).

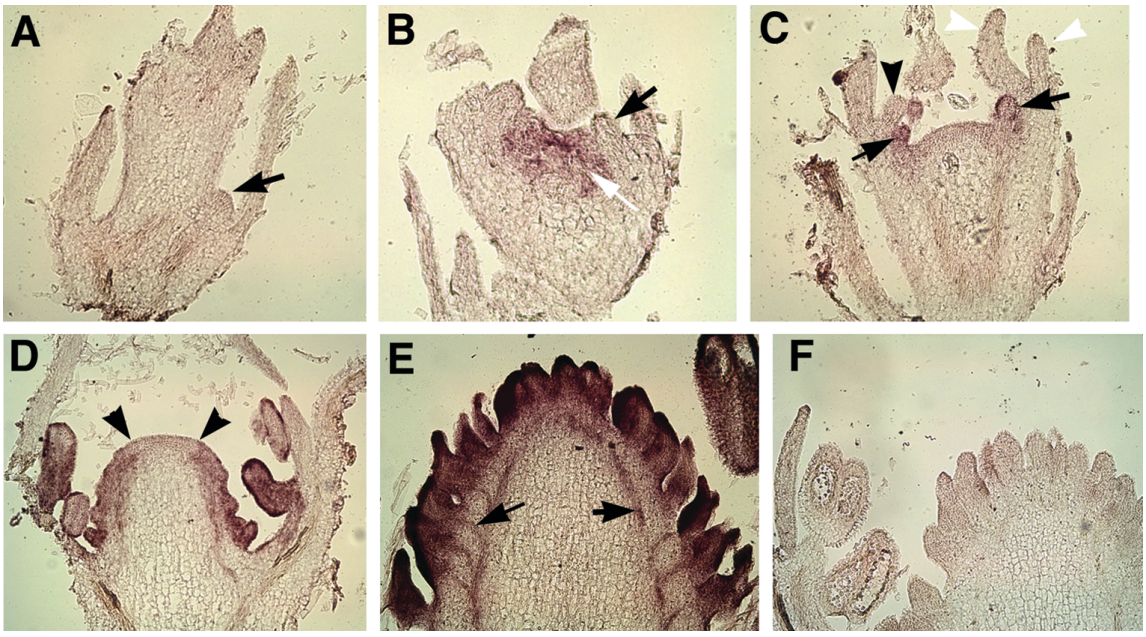

Fig. 4-7 In situ hybridization with an *FvAG* probe shows stamen and carpel-specific expression**.** *Longitudinal sections* of *F. vesca* YW5AF7 flowers were hybridized with antisense (**A–E**) and sense (**F**) *FvAG* probes. **A** The emerging floral bud (*arrow*) did not express *FvAG*. **B** *FvAG* signal detected in the center of this stage 4 young bud (*white arrow*). The sepal primordium (*black arrow*) did not express *FvAG*. **C** Early stage 5 flower showing relatively flat central dome without carpel primordia. Emerging stamen primordia expressed *FvAG* (*arrow*). The petal primordium (*black arrowhead*) and sepals (*white arrow-heads*) did not express *FvAG*. **D** Stage 7 flower showing *FvAG* expression in developing stamens and carpels. Indicated between the two *arrowheads*, the apex has yet to initiate carpel primordia and does not express *FvAG*, suggesting that *FvAG* expression correlates with carpel primordia formation. **E** Stage 9 flower showing intense *FvAG* signal in developing carpels as well as in the vasculature (*arrows*). **F** Sense control showing the lack of signal in a stage 9 bud.

Discussion

Comparisons of shoot, flower and fruit development between Fragaria and Arabidopsis

Our current knowledge of flower development is largely based on the initial molecular

genetic analysis of floral mutants in *Arabidopsis thaliana* and *Antirrhinum majus* (snapdragon) (Coen and Meyerowitz, 1991; Krizek and Fletcher, 2005). The success of flower research would not be possible were there not a detailed description of morphological events during floral organ development in *Arabidopsis* (Smyth et al., 1990). Such detailed morphological and temporal description facilitated the characterization of floral mutants and the establishment of the ABCE model of flower development (Coen and Meyerowitz, 1991; Krizek and Fletcher, 2005). Compared with *Arabidopsis*, *Fragaria* develops different shoot architecture. In *Arabidopsis*, the shoot apical meristem (SAM) is an indeterminate structure that is situated at the tip of the *Arabidopsis* shoot and gives rise to lateral organs spirally and acropetally. In contrast, the primary SAM in *Fragaria* terminates in a single flower. Before its termination, it gives rise to secondary SAMs basipetally, and these secondary SAMs repeat the fate and pattern of the primary SAM. It will be interesting to compare the expression patterns of stem cell markers such as *WUSCHEL* and to monitor the meristem activities in primary, secondary, and higher order SAMs of *Fragaria*.

In flowers, *Arabidopsis* and *Fragaria* differ in the number of whorls. While each floral organ type (sepals, petals, stamens, or carpels) only occupies a single whorl in *Arabidopsis*, stamens of *Fragaria* occupy two adjacent whorls and develop into short, medium, or tall heights (Fig. 4-1E, H–I). The large number and different height of *Fragaria* stamens may serve to maximize fertilization of hundreds of apocarpous pistils at different positions of the receptacle. In addition, *Fragaria* has a whorl of five bracts, which are absent in *Arabidopsis*. The most striking distinction lies in the carpel. In

Arabidopsis, two congenitally fused carpels form the gynoecium with two rows of ovules aligning the fused margins within each carpel (Smyth et al., 1990; Liu et al., 2000). In contrast, *Fragaria*, as well as other *Rosoideae* species (the rose subfamily), have aggregate fruits, which develop from the apocarpous gynoecium. We show that about 160 single and free carpels are initiated acropetally and spirally from the apex of the receptacle, where floral meristem cells may reside. Within each carpel, a single ovule initiates from the indented carpel wall. Upon fertilization, the *Arabidopsis* gynoecium elongates to form the two-chambered fruit, the silique, containing rows of seeds. In contrast, fertilized individual carpels of *Fragaria* become the achenes that dot the surface of the receptacle and produce auxin to stimulate the growth of the underlying receptacle. Future molecular genetic studies of *F. vesca* may identify the regulatory genes and mechanisms controlling the unique aspects of *Fragaria* flower and fruit development.

Comparisons between Fragaria and rose flower development and AG expression

As a member of the *Rosaceae* family, *Fragaria* develops flowers highly similar to those of other *Rosaceae* family members including rose, apple, and peach. Since *F. vesca* only takes 3.5 months to develop from seed to flower, it offers significant advantage in genetic studies over other *Rosaceae* species, particularly the fruit trees. Up to now, many studies of flower development in *Rosaceae* have been in rose due to rose's significant economical value and the long history of cultivation and selection. Both wild rose and *Fragaria* flowers develop five petals, a large number of stamens and apocarpous gynoecium. However, rose flowers are perigynous meaning that the multiple apocarpous pistils are initiated from a flat receptacle base buried within a cuplike hypanthium

(Dubois et al., 2010). The multiple free fruits (seeds) of rose are buried within the enclosed fleshy hip. In contrast, *Fragaria* flowers are hypogynous with apocarpous pistils forming on the surface of a raised receptacle.

Despite this difference in gynoecium, the developmental staging and *AG* expression are similar between *F. vesca* and rose. The early stages of rose flower development are divided into five stages (Dubois et al., 2010), which mirror stages 3–7 of *F. vesca* flower development. (Fig. 4-2C–H). Further, the rose *AG* ortholog (*Rose hybrida AG*) was specifically expressed in the stamen and carpel primordia (Dubois et al., 2010), similar to the expression of *FvAG* in *F. vesca* (Fig. 4-7). *AG* encodes a member of the MADS box family of transcription factors and acts with other MADS box proteins to specify stamen and carpel identity in *Arabidopsis* (Yanofsky et al., 1990; Bowman et al., 1991b; Drews et al., 1991). The stamen and carpel-specific expression pattern of *RhAG* and *FvAG* suggests that *RhAG* and *FvAG* likely function similarly to *Arabidopsis AG* in specifying stamen and carpel identity despite differences in stamen and carpel numbers and arrangements. The function of *RhAG* in stamen and carpel identity specification was further supported by the study of two existing rose cultivars, Malmaison that develops an average of 116 petals and St Anne's that develops an average of 12 petals but more stamens (Dubois et al., 2010). In the cultivar with a high petal number, the *RhAG* expression domain was found to be more restricted to the floral meristem center, leaving more outer whorls free of *RhAG* and thus the development of petals. In the low petal number cultivars, *RhAG* expression is more expanded to the outer whorls, leading to increased number of stamens and reduced number of petals. The study suggests that the

RhAG expression boundary was labile and served as the target of selection (Dubois et al. 2010). A somewhat labile *FvAG* expression boundary is consistent with our observation of petaloid anthers in *F. vesca* flowers.

Previously, the expression of the octoploid *F.* × *ananassa AG*, *STAG1*, was studied by RNA blot analysis, in situ hybridization, and promoter-driven reporter expression with primary focus on the late stage flower and fruit development (Rosin et al., 2003). This study showed that *STAG1* RNA accumulated in late stage stamens, carpels, receptacles, and green to red fruits, and the *STAG* signal was specifically found in achenes, seeds, and vasculature from green fruits. Our study also found *FvAG* expression in the vasculature connecting achene and the subtending receptacle and vasculature aligned parallel to the receptacle surface. The functional significance of the *FvAG* expression in the vasculature is unknown and may underlie the specific fruit development of *Fragaria*. Further functional analyses including generation of *FvAG* knockout or over-expression transformants are needed to confirm *FvAG* function in flower and fruit development.

Basic description is necessary for future studies and data comparison.

Until now, there has been a lack of both detailed descriptions of diploid strawberry flower and early fruit development, as well as a lack of a standardized staging of such development. Without these, it would be difficult to undertake meaningful subsequent studies including transcriptome analysis of floral and fruit development and mutant characterization and description. More significantly, it would be difficult to compare molecular, genomic, or genetic data pertaining to flower and fruit development across

research groups. To take advantage of the promise *F. vesca* has in being a model organism, further tools and background knowledge need to be developed in a timely manner. Our work presented here fulfills one such need.

There are many basic and applied questions related to flower and early fruit development that can now be addressed using *F. vesca*. The longstanding question of what triggers auxin production by the achenes upon fertilization is now approachable using transcriptome analysis and mass spectrometry. The answers to basic questions such as floral organ positioning, including the spiral arrangement of carpels on the receptacle, are dependent on being able to accurately describe spatial and temporal gene expression in flower and early fruit development. Another important basic question that can be addressed is what modification of the stem tip enables the receptacle to develop into a fleshy fruit. The answer to this question relates to how fruit type is determined. Why does raspberry form aggregate druplets while the true fruit of its close relative, strawberry, is an achene? Similarly, addressing questions of agricultural importance, such as how carpel number and thus fruit size potential are regulated, and how temperature affects fertility, will benefit from having an accurate developmental staging, which may ultimately lead to improvement in strawberry fruit size, shape, and yield.

Materials and Methods

Plant materials

Fragaria vesca inbred line Yellow Wonder 5AF7 (YW5AF7) (Slovin et al. 2009) was grown in growth chambers (Conviron, Winnepeg, Manitoba, Canada) under a 12 h

daylength essentially as described (Slovin and Rabinowicz, 2007). After sowing seeds in Metromix 360® (SunGro Horticulture) in plant bedding containers, trays were watered, covered with plastic wrap, and treated at 4°C in the dark for 5 weeks to synchronize germination before they were transferred to the growth chamber. The temperature was maintained at 20°C during the night, and 25°C during daytime. Light was supplied by a mixture of cool white fluorescent bulbs and incandescent bulbs. After the appearance of the first trifoliate leaf, seedlings were transplanted into 10.2 cm pots. For maintenance, every 3–5 weeks, older shoots, leaves and sometimes crowns were trimmed off. Safer brand insect killing soap (SaferSoap®, Lititz, PA) and BioNEEM (SaferSoap®, Lititz, PA) were used to treat spider mites, aphids, and thrips. Miracle Grow® Tomato Plant Food (Scott's Miracle-Grow Products, Inc. Marysville, OH) was used according to manufacturer's recommendation. To ensure effective self-fertilization, small paintbrushes were used to facilitate self-pollination after anthesis.

Visualizing embryo development

Individual carpels were removed from fertilized flowers at the indicated times. The developing seed was dissected out of the ovary under a dissecting microscope, fixed for 10 min in 1:1 acetic acid:ethanol, and then transferred to Hoyers solution for clearing (Liu and Meinke, 1998; Stangeland and Salehian, 2002). Hoyers solution contains 7.5 g gum arabic, 100 g chloral hydrate, 5 ml glycerol, and 30 ml water. After 10 min in Hoyers solution, samples were examined with a Nikon ECL1PSE E600 W microscope using bright Weld and DIC optics and photographed with a DXM1200 digital still camera. About 20 seeds from 2 berries at each developmental stage were examined.

Scanning electron microscopy (SEM)

Scanning electron microscopy of developing flowers was performed essentially as described for *Arabidopsis* (Bowman et al., 1991b). Primary through quaternary floral buds of different sizes were dissected under a stereomicroscope to remove stipules, sepals, and to shave off trichomes from stems before fixation in 3% glutaraldehyde in 25 mM sodium phosphate buffer pH 7.0. After two 15-min vacuum infiltrations, samples were incubated overnight at 4°C. Samples were then incubated with 1% osmium tetroxide in 25 mM sodium phosphate buffer at 4°C overnight before dehydration through an ethanol series. Critical point drying with liquid CO2 was done with a Denton DCP-1 critical point dryer, venting slowly at each step, to avoid cellular collapse. Samples were coated with gold palladium (AuPd) in a Denton DV 502 vacuum evaporator, and visualized with an AMRAY 1820D electron microscope. Two to three developing floral buds at each stage were observed except stage 4, where only one floral bud was observed.

Tissue Fixation for histological staining and in situ hybridization

For histological staining, tissue was fixed in Farmer's fixative (75% ethanol and 25% acetic acid) for 15 min under vacuum. Then the fixative was replaced with 90% ethanol with 0.5% Eosin Y (Sigma, St. Louis, MO), and the samples placed on a rocker at 4°C overnight. For in situ hybridization, flowers were fixed at room temperature for 2–4 h in FAA (3.7% formaldehyde, 5% acetic acid, and 50% ethanol) after stipules and sepals were removed and stems sliced. Two or more vacuum infiltrations were applied to facilitate fixative infiltration. Tissues were then dehydrated in an ethanol series and left

overnight in 95% ethanol with 1% Eosin Y (Sigma). After two or more 100% ethanol changes, the Eosin Y stained tissue was gradually transitioned into 100% xylene. After 4 changes of 100% xylene, Paraplast Plus® wax chips (McCormick Scientific/Leica Microsystems, St. Louis, MO, USA) were added to the sample in 100% xylene at 42°C gradually until the wax reached 50%. Half of the wax/xylene solution was replaced with liquid Paraplast and the sample/wax was incubated at 60°C for a minimum 4 h before the entire solution was replaced with 100% liquid Paraplast. After 7 more 100% wax changes over the course of 4–7 days, the sample/wax was poured into boats. Wax blocks were sectioned at 10 μm.

Histological staining

Safranin-O/Fast Green staining was done according to (Jensen 1962). Following dewaxing in 100% xylene, tissues went through a decreasing ethanol series to 30% ethanol, two washes with water, staining in 0.5% Safranin-O in 43% ethanol for 1 h, another water rinse, and an increasing ethanol series (acidified ethanol at 70, then 95, and 100%). Subsequently, tissues were stained with 0.5% (w/v) Fast Green (in 50% clove oil and 50% ethanol) for 5–10 s. Slides were quickly passed through 100% ethanol and two 10 min changes of clove oil:ethanol:xylene (50:25:25). Slides went through three 15-min xylene changes before mounting with Permount (Fisher Scientific). Sections from four or more flowers per stage were observed.

In situ hybridization

FvAG was identified in the strawberry genome (http://www.rosaceae.org/) as Hybrid

Gene Model #24852 using BLAST searches with *Arabidopsis AG* (At4g18960), *F.* × *ananassa AG* (AF168468), and other known homologs in other species, as well as with intron/exon structure, protein domain, and known *cis*-element analysis. A high degree of conservation at the protein level was observed both among members of the Rosoideae and with *Arabidopsis*. Sense and antisense probes were created by amplifying a 534 base region from the cDNA that spans from the end of the first exon through the last exon. For the antisense probe, the reverse primer (5_GAA ATT AAT ACG ACT CAC TAT AGG GCT AAC TGA AGG GAA ACT TGG TCA TGG 3_) containing the T7 RNA polymerase recognition sequence was paired with the forward primer (5_GTG GCC GCC TCT ATG AGT ATT CC). For the sense probe, the forward primer (5_GAA ATT AAT ACG ACT CAC TAT AGG GGT GGC CGC CTC TAT GAG TAT TCC) containing the T7 RNA polymerase recognition sequence was paired with the *FvAG* sense reverse primer (5_CTA ACT GAA GGG AAA CTT GGT CAT GG). PCR products were purified with the QIAquick Gel Extraction Kit (Qiagen, Hilden, Germany) prior to transcription with T7 RNA polymerase and DIG RNA labeling Mix (Roche, Mannheim, Germany). Approximately 150 ng of PCR product was used as template per transcription reaction. After DNase I treatment and phenol/chloroform extraction, the resulting RNA probe was precipitated with lithium acetate. Sections from seven flowers were probed with the *FvAG* sense probe and sections from nine flowers were probed with the *FvAG* antisense probe. In situ hybridization was performed as described for *Arabidopsis* with minimal modification (Long et al. 1996). Sections (10 μm) were mounted on Probe On Plus slides (Fisher Scientific). After dewaxing in 100% xylene and hydration, slides were passed through 2£ SSC, incubated with 1 μg/ml proteinase K

(in 100 μM Tris pH 8, 50 μM EDTA) at 37°C for 30 min, rinsed in 2 mg/ml glycine in 1x PBS, washed twice in 1X PBS, and fixed in 4% paraformaldehyde in 1X PBS for 10 min, followed by two changes of 1X PBS, and an ethanol dehydration series to 100% ethanol. Slides were then air dried briefly before hybridization with approximately 200 ng of Digoxigenin-labeled probe in 150 μl hybridization solution in a humid airtight container for 20 h. Following hybridization, slides were washed two times in 0.1X SSC. Both hybridization and washes were at 60°C. Slides were then rinsed in 1X PBS and incubated in Blocking Reagent (Roche) for 45 min at room temperature followed by a wash in TBNT (0.3% Triton, 1% BSA, 150 mM NaCl, and 100 mM Tris 7.5) for 45 min at room temperature before antibody application. The Anti-Digoxigenin-AP Fab fragments antibody (Roche) was diluted 1:1,250 with TBNT and applied to two slides at a time using capillary action. After a 2 hour incubation with antibody, slides were washed 4 times in TBNT and once in a Tris/NaCl/MgCl2 solution (100 mM Tris pH 9.5, 150 mM NaCl, and 50 mM MgCl2) before application of NBT/BCIP Western Blue® substrate (Promega, Madison WI), also by capillary action. Slides were developed in a dark humid container for 20–24 h and development was stopped with 1X TE before mounting a coverslip with Crystal Mount (Biomeda Corp., Foster City, CA).

Chapter V: Generation and analysis of the *Fragaria vesca* flower transcriptome

Introduction

With the recent completion of the *Fragaria vesca* genome sequencing (Shulaev et al 2011) and the detailed description of *F. vesca* flower development and staging (Chapter IV; Hollender et al 2011), the time is ripe for the development of additional genomic resources to study important developmental questions in this new model plant. Using RNA isolated from different flower tissues at different developmental stages, I have generated *F. vesca* floral transcriptomes using the next-generation sequencing technology. This data set can be mined to investigate gene regulatory networks as well give a molecular description of strawberry flower development. Since proper flower development preludes fruit development, this work is a foundation for future discoveries both in basic research and agricultural applications. This work was part of a larger transcriptome project aimed at generating stage and tissue-specific transcriptomes for both flower and early fruit development. My contribution to this project is the generation of RNA-Seq data for 10 different floral tissues with 2 biological replicates (twenty samples in total). These include transcriptomes from young flower primordia and male and female reproductive organ primordia from different stages of development.

To isolate tissues from the youngest stage flowers, laser capture microscopy (LCM) was employed. The process of tissue fixation, wax embedding, sectioning, and the laser capture itself, all presented obstacles to the isolation of high quality RNA needed for RNA-sequencing. Optimization was necessary and achieved through testing alternative

fixation and sectioning protocols. Another obstacle was the minute amount of total RNA isolated from LCM samples, which required linear amplification before sequencing. A summary of the optimization and the amplification strategy is provided here to facilitate future work requiring LCM. Since the LCM tissue and hand-dissected tissues are processed differently before RNA-Seq, a comparison between stage 10 carpel transcriptomes generated using hand-dissected and LCM-derived tissue was performed. This was done to investigate both the reliability of the LCM transcriptomes and reveal the contribution of tissue processing differences to the transcriptome profiles, such as read counts and percent coverage of genes in the genome.

To test the reliability and utility of the transcriptome data as well as to gain insight into the regulatory genes for *F. vesca* flower development, I mined the newly generated transcriptome data for the *F. vesca* homologs of the *ABCE* classes of genes previously known to regulate flower development in *Arabidopsis* and other angiosperms. As described in Chapter I, these four classes of genes are expressed in very predictable organ-specific patterns during early stage flower development. A-class genes are active in developing sepals and petals, B-class genes are expressed in developing petals and stamen, C-class genes are expressed in developing anthers and carpels, and E-class genes are expressed in all flower four whorls. *ABCE* gene expression was used to both validate the transcriptomes and identify possible novel expression pattern and potential novel genes or gene function in *F. vesca* flower development.

The entire transcriptome data from this project will eventually be made available to the research community through our website: http://bioinformatics.towson.edu/Strawberry.

Results

Transcriptomes generated from hand-dissected anthers and carpels

In *Fragaria* vesca, anther and carpel development spans several stages of flower development (Chapter IV, Fig 4-4 and 4-5), and the tissues are distinctly different in each stage in terms of structure, morphology, and stage of gamete development. The creation of carpel and anther transcriptomes as they progress through development will allow for a more in-depth understanding of the gene expression behind significant events such as the formation of megaspores and microspore mother cells and their respective ovules and pollen.

RNA-Seq libraries were generated from hand-dissected (HD) anthers (stages 7-8) and carpels (stages 7-8, 9, 10-11, and 12). For each tissue type, two biological replicates–each prepared from RNA isolated from 2 to 6 flowers– were sequenced. Total RNA was isolated using the Arcturus® PicoPure® RNA isolation kit (Applied Biosystems, Foster City, CA) and then sent to the Cornell Weil Medical Genomics Resources Core. After poly-A selection for mRNA, barcoded Next-Generation (NGS) Illumina® RNA-Seq libraries were made by the sequencing facility. Four to five samples were pooled and sequenced in one lane of an Illumina HiSeq 2000. Bioinformatic analysis, including filtering and alignment of reads to the strawberry genes and genome, was carried out in

Nadim Alkharouf's lab at Towson University. A summary of the sequencing reads for each of the floral tissues is shown in Table 5-1. After filtering out non-barcoded sequences, ~70% of the reads aligned to the annotated *F. vesca* genes, covering on average 72% of the 34,390 currently annotated genes in the genome (see % Reads aligned to genes and % Genes covered in Table 5-1). Most of the reads that did not map to genes but mapped to the genome likely represent expression of genes that are not yet annotated or improperly annotated in the newly sequenced draft genome. However, it is possible that some of the sequences also represent non-coding RNA or 5' or 3' UTRs.

Table 5-1. Summary of RNA-Sequencing data from hand-dissected flower tissues

Flower Stage	Tissue Type	Rep.	Total Reads	Reads after Filtering	% Reads aligned to genes	# Reads aligned to genes	# Genes with at least one read	% Genes covered
7-8	Anther	A	47,403,443	40,070,895	71.2	28,530,477	25,797	74.11
		B	38,488,498	32,376,422	67.21	21,760,193	25,362	72.86
7-8	Carpel	A	37,479,936	31,624,418	70.72	22,364,788	24,832	71.34
		B	39,448,525	33,439,768	70.27	23,498,124	25,029	71.90
9	Carpel	A	31,495,838	26,524,086	69.99	18,564,207	23,953	68.81
		B	39,009,005	32,956,527	71.7	23,629,829	24,520	70.44
10-11	Carpel	A	45,391,242	37,703,697	70.08	26,422,750	25,106	72.13
		B	32,532,046	26,995,535	71.51	19,304,507	24,157	69.40
12	Carpel	A	60,705,678	50,033,561	68.65	34,348,039	26,753	76.86
		B	37,851,326	31,191,265	68.12	21,247,489	26,008	74.72
Averages			40,980,554	34,291,617	70	23,967,040	25,152	72

Optimization of laser capture for early stage tissues

To capture the expression profile of anther and carpel tissues from their inception, as well the earliest stage flowers (which lack anther and carpel primordia), Laser Capture Microscopy (LCM) is needed to be able to precisely carve out the specific tissue or organ primordia at the early floral developmental stages. These tissue or organ primordia are too small to isolate by hand-dissection. The LCM process entails fixation of flower

tissues, wax embedding, tissue sectioning by a microtome, and finally isolation of the desired cells/tissues under a microscope with a laser. Initial attempts with LCM-harvested tissues produced poor quality RNA. As shown in Figure 5-1 B, total RNA extracted from the LCM-tissues produced a large bell shaped curve on a BioRad® Experion electrophoretic graph, indicative of high levels of RNA degradation. This is in contrast to a high quality RNA sample that exhibits two distinct ribosomal RNA subunit peaks (Fig 5-1 A). To improve RNA quality, I tested a variety of relevant parameters that are summarized below.

First, I tested an alternative fixation solution as well as several of the post-fixation steps. I found that tissue fixation using acetone provided higher quality RNA than the initial Farmers protocol (compare Fig. 5-1 B with C). Second, I found that RNA quality increases as the amount of time the freshly sectioned tissues remained on the slide warmer decreases. RNA from tissues dried on the slide warmer for 30 minutes total (Fig. 5-1 C) was less degraded than tissues that sat on slide warmer for 90 minutes (Fig. 5-1 D). In addition, the collection of the LCM-tissues into the caps of PCR-tubes containing RNA extraction buffer (Fig. 5-1 F) produced higher quality RNA than buffer-free caps of PCR-tubes (Fig. 5-1 E). Finally, slides containing the sectioned tissues should be dewaxed and then LCM dissected right away. As shown in Fig. 5-1G, using tissues from a dewaxed slide (already used once for LCM) that was stored overnight at 4 degrees yielded lower quality RNA. Slides not yet dewaxed can be stored at 4 degree for at ~1 week with only a minimal decrease in RNA quality, as is shown in Fig. 5-1 H.

The optimized LCM pipeline used to generate tissue for RNA-seq libraries for the youngest stage floral transcriptomes is as follows. The tissues were fixed with acetone, sectioned into 10μm thick ribbons the day of the laser capture. The ribbons were expanded on RNAse-free water and dried on specialized LCM PEN-membrane slides placed on the slide warmer for only 15-30 minutes. The slides were then immediately dewaxed and used within several hours for laser microdissection on a Leica ASLMD microscope in Ben Matthew's lab at the USDA Beltsville Agricultural Research Center. All dissected tissues were collected in caps of tubes containing RNA extraction buffer.

RNA-sequencing library preparation for laser captured tissues

To generate transcriptomes of very young flower tissues (stage 1- 6), LCM was used to isolate the tissues. Details of the optimized methods for isolation are described above. An average of ~2 x 10^6 μm^2 of tissue was collected for each sample over several three hour LCM sessions. Both the amount of time needed for dissection and the amount of tissue needed depended on the size, availability, and cell density of the desired tissues. RNA was isolated using Arcturus® PicoPure® RNA isolation kit. RNA yield varied depending on tissue types and quantity of the dissected tissues. For example, approximately 1x10^6 μm^2 of dense stage 5 or 6 flower tissue yielded ~30 ng total RNA, while 8.7x10^6 μm^2 of microspores yielded only 10 ng of RNA.

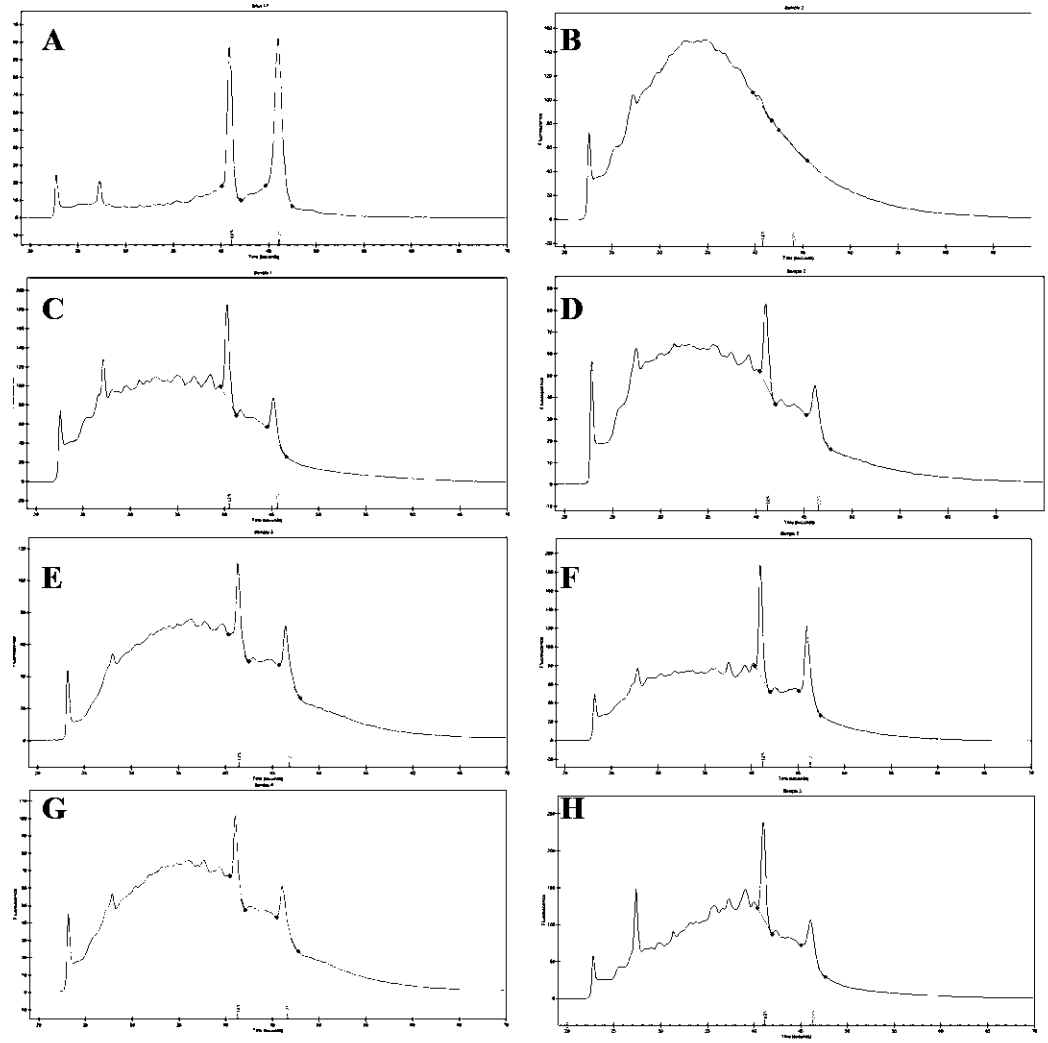

Figure 5-1. BioRad Experion electrophoresis histograms of RNA extracted from tissues from various conditions before or after LCM. (A) RNA from hand-dissected stage 7 anthers. (B) RNA from LCM-tissue fixed with Farmers fixative. (C) RNA from LCM-tissue fixed with acetone. Tissues dried on slide warmer for 30 minutes before dewaxing and laser capture. (D) RNA from LCM-tissue fixed with acetone whose slide sat on the slide warmer for 90 minutes. (E) RNA from LCM-tissues that were collected in an empty PCR tube lid. (F) RNA from LCM-tissue that were collected in a lid containing RNA extraction buffer. (G) RNA from LCM-tissues. The slide containing the sections was dewaxed 1 day prior to the LCM dissection. (H) RNA from LCM-tissue from a slide that was stored for 1 week at 4^{o}C prior to dewaxing. In both H and G, the LCM sections were collected into the RNA extraction buffer inside the caps of a PCR tube.

For standardized RNA-seq, 100 ng to 1 μg of total RNA is needed. The RNA isolated with LCM was often too low in quantity and also too poor in quality to be acceptable for library preparation by sequencing facilities (see Fig 5-1 A and F for comparison of quality). For that reason, I prepared RNA-Seq libraries myself before sending them to the sequencing facility. Total RNA was amplified using the NuGen Ovation® RNA-Seq System V2 kit without poly-A selection. Barcoded libraries were prepared from the amplified total RNA using the NuGEN's Encore® NGS Multiplex Library System I. Four different barcodes were used allowing four different libraries pooled and sequenced in the same lane at the Cornell Weill genomics core.

Key steps of RNA-Seq library preparation are illustrated in Fig. 5-2. Using stage 5 anther and receptacle LCM RNA (Fig. 5-2 A), cDNA was prepared (Fig. 5-2 B) and then sonicated so that the majority of sequences were ~150 bp long (Fig. 5-2 C). After sonication, the sheared cDNA was used to make a sequencing library (Fig. 5-2 D) with a unique four nucleotide barcoding sequence attached to each cDNA. Bioinformatic analysis of the LCM RNA-Seq data was also performed by Dr. Alkharouf's lab. The number of sequencing reads and the percentage that mapped to the genes is summarized in Table 5-2.

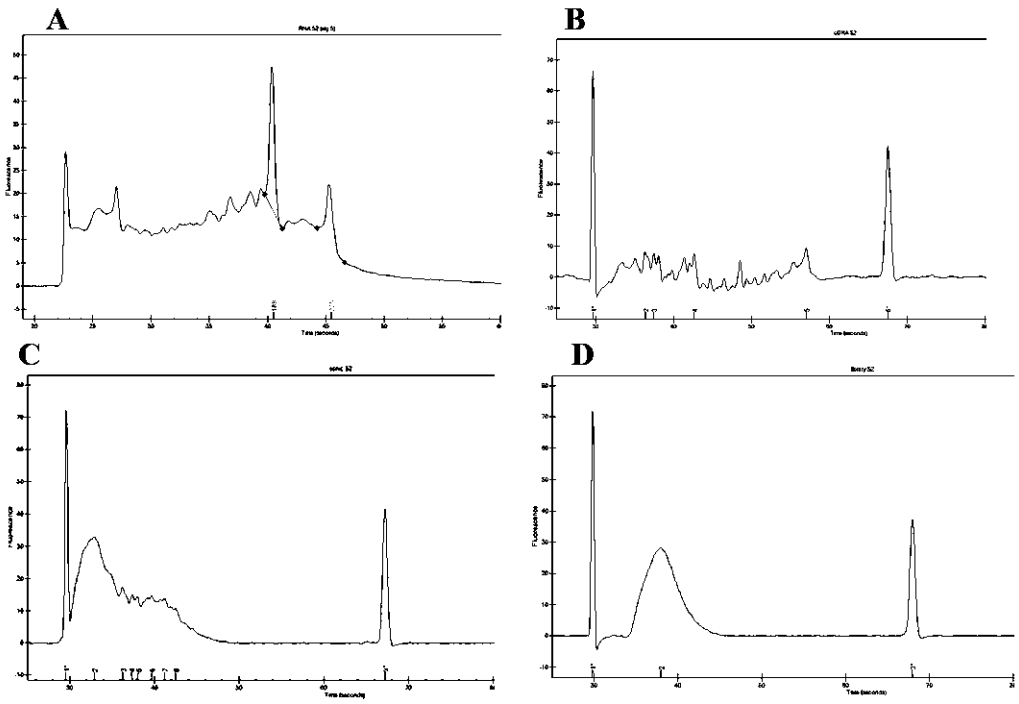

Figure 5-2. Next generation RNA-Seq library preparation for stage 5 anther & receptacle tissue. Electrophoretograms of (A) RNA from LCM tissue, (B) cDNA, (C) sonicated cDNA, (D) NGS library.

Table 5-2. Summary of RNA-Sequencing data for LCM samples (All missing values should be available by May 2012.)

Flower Stage	Tissue Type	Rep.	Total Reads	Reads after Filtering	% Reads aligned to genes	# Reads aligned to genes	# of genes aligned	% Genes covered
1-4	Flower	A	31,087,701	24,285,002	7.56	1,835,946	30,197	86.75
		B	-	-	-			
5	Anther + Receptacle	A	-	-	-			
		B	-	-	-			
6	Anther	A	-	-	-			
		B	-	-	-			
6-7	Receptacle	A	21997718	14708758	5.79	851,637	27,222	78.20
		B	-	-	-			
10	Microspores	A	30788482	23878432	5.39	1,287,047	30,135	86.57
		B	-	-	-			
10	Carpel	A	30395791	23685579	10.29	2,437,246	29,372	84.38
Averages			28,567,423	21,639,443	7	1,602,969	29,232	84

Comparative analysis between Hand-Dissected and LCM transcriptomes

The percentage of reads from the LCM libraries that aligned to genes was significantly lower than those from the hand-dissected (HD) samples (~7% compared to ~70%) (Table 5-2 compared to Table 5-1). This difference may result from the filtering of ribosomal RNA from the LCM reads. Due to the low total RNA starting amount, ribosomal-RNA removal or poly-A enrichment was not performed before the amplification and library preparation processes. Thus the ribosomal RNA was included in the sequencing libraries along with the mRNA and could only be eliminated with bioinformatics. Interestingly, although LCM derived data had fewer reads that aligned to genes (1.6 million compared to 24 million), those that did align covered more genes than the non-LCM samples. Specifically, for LCM samples 84% of the genes in the genome have at least 1 read, whereas with the hand-dissected samples 72% of the genes in the genome have at least 1 read (Tables 5-1 and 5-2). Additionally, when comparing HD and LCM transcriptomes of stage 10 carpels, there are similar numbers of genes with reads ≥ 5, and the LCM library had over twice as many genes with just one read (Table 5-3).

To gain insight into how the RNA-seq data could be affected by two different isolation and processing methods, I prepared transcriptomes from stage 10 carpels isolated by both

Table 5-3 Comparison between LCM vs. Hand-dissected (HD) samples, showing number of genes with minimum reads of 0 to 10.

	0 reads	1 read	< 5 reads	≥ 5 reads	≥ 10 reads
LCM stage 10	5,017	3,366	13,745	20,645	16787
HD stage 10 carpel A (HD1)	9,283	1,617	12,811	21,579	20,022
HD stage 10 B (HD2)	10,232	1,651	13,870	20,520	19,081

LCM as well as hand dissection. The resulting data were normalized and then compared. The RPKM (Reads Per Kilobase of exon model per Million mapped reads) is the normalized value for each gene. The total number of mapped reads is significantly lower for the LCM stage 10 carpel sample (2.4 million compared to 34 and 21 million), yet the average RPKM values for all genes in LCM, HD1, and HD2 are highly similar, at 22, 24, and 26 respectively. This suggested that the normalized RPKM might allow for comparisons between transcriptomes prepared by these two very different methods. However, a global analysis of the most highly expressed genes in these three transcriptomes showed that the different processing methods might have contributed to certain differences in transcriptome outcome. The two HD stage 10 carpel transcriptomes had almost twice as many genes with an RPKM ≥ 300 compared to the LCM transcriptome (Fig. 5-3). The numbers of genes with an RPKM ≥ 1000 in each other samples were more comparable, however few genes were shared between the HD and LCM transcriptomes. Only 7 of the 41 genes with RPKM >1000 from the LCM transcriptomes were also expressed at an equally high level in the HD transcriptomes.

Interestingly, my analysis showed that the two hand dissected samples also exhibited differences both in the number of genes in these high expression categories and in the level gene overlap between these biological replicates (Fig. 5-3). These differences could be the result of the replicates having disproportionate number of carpels that were at a slightly more or less mature point in development (e.g. HD1 may have a had more carpels at early stage 10, while HD2 may have had more carpels that were late stage 10 or early stage 11).

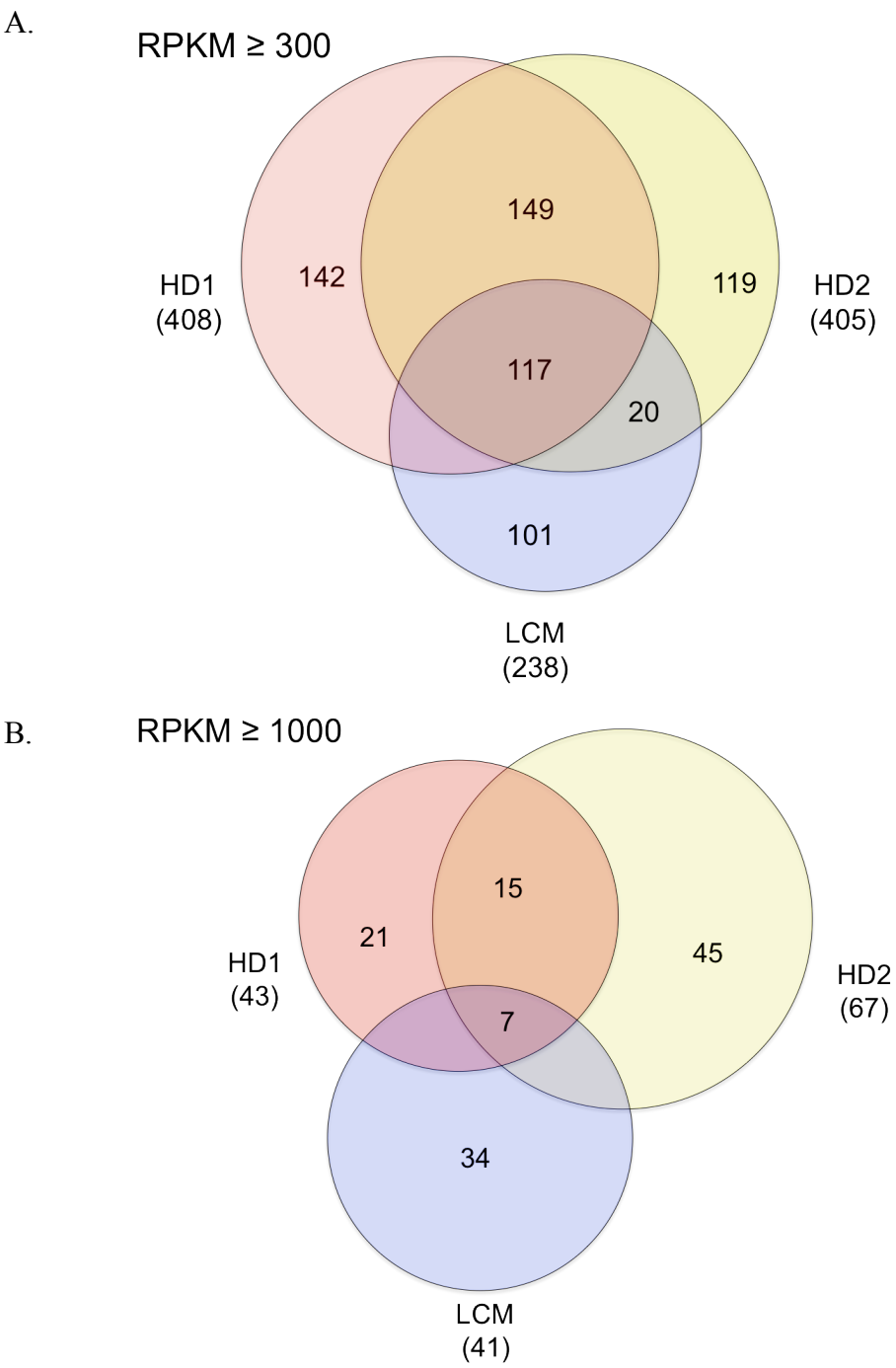

Figure 5-3. Comparison between numbers of highly expressed genes in HD and LCM stage 10 carpel transcriptomes. RPKM values (Reads Per Kilobase of exon model per Million mapped reads) were used for comparison of gene expression between the different transcriptomes. The average RPKM values for each transcriptome is ~20. Genes with (A) an RPKM ≥ 300 and (B) RPKM ≥ 1000 are considered to be highly and very highly expressed, respectively. The total number of genes from each library is in parenthesis.

Identification of *F. vesca ABCE* homologs

The *ABCE* model of flower development provides predictable gene expression patterns of the *ABCE* classes of genes in each of the floral organs. Since the model was built based on research in *Arabidopsis*, how these genes are expressed and function in *F. vesca* flower development is presently unknown, although my *in situ* analysis with *FvAG* showed that *FvAG* is expressed in the carpel and stamens (Chapter IV, Figure 4-7). Mining these floral transcriptomes for *ABCE* genes not only serves a means of validating the RNA-Seq data, but also reveals where the *ABCE* genes are expressed and regulated in strawberry flowers. Bioinformatic approaches were used to identify probable *F. vesca* homologs of the *Arabidopsis ABCE* genes (Table 5-4, Fig. 5-4). Protein sequences of the *Arabidopsis ABCE* genes were BLASTed against translated protein sequences of the strawberry genome hybrid gene models version 2.0 (hosted at strawberrygenome.org) with filtering for low complexity regions. Initial BLAST results were then BLASTed against the flowering plant protein database in NCBI to ensure that the *ABCE* genes could be retrieved from other species. Additional validations included the identification of conserved protein structures (i.e. MADS and AP2 domains), and most importantly, the grouping of each gene in phylogenetic distance trees (as in Fig. 5-4). Single genes with sequence homology to *Arabidopsis thaliana* A-genes *APETALA1* (*AP1*) and *APETALA 2* (*AP2*), B-class genes *APETALA3* (*AP3*) and *PISTILLATA* (*PI*), and C-class gene *AGAMOUS* (*AG*) were identified (Table 5-4 and Fig 5-3). In *Arabidopsis,* there are four *SEPALLATA* genes*, SEP1-4* (Ditta et al. 2004). *F. vesca* appears to have homologs of *SEP1, SEP3*, and *SEP4*. An additional gene, which I named *SEPLIKE1,* is also highly homologous to the SEP genes but does not group with any of the *SEP1-4* genes (Table 5-

4, Fig. 5-3). Final validation of an orthologous relationship requires functional as well as expression analysis.

Table 5-4. *F. vesca* homologs of *ABCE* flower development genes. Asterisk (*) indicates novel gene

A Genes	*APETALA1*	*(FvAP1)*	gene04562
	APETALA2	*(FvAP2*	gene23876
B Genes	*APETALA3*	*(FvAP3)*	gene14896
	PISTILATA	*(FvPI)*	gene11267
C Gene	*AGAMOUS*	*(FvAG)*	gene24852
E Genes	*SEPALLATA1*	*(FvSEP1)*	gene04229
	SEPALLATA3	*(FvSEP3)*	gene07201
	SEPALLATA4	*(FvSEP4)*	gene26118
	*SEPLIKE1**		gene04563

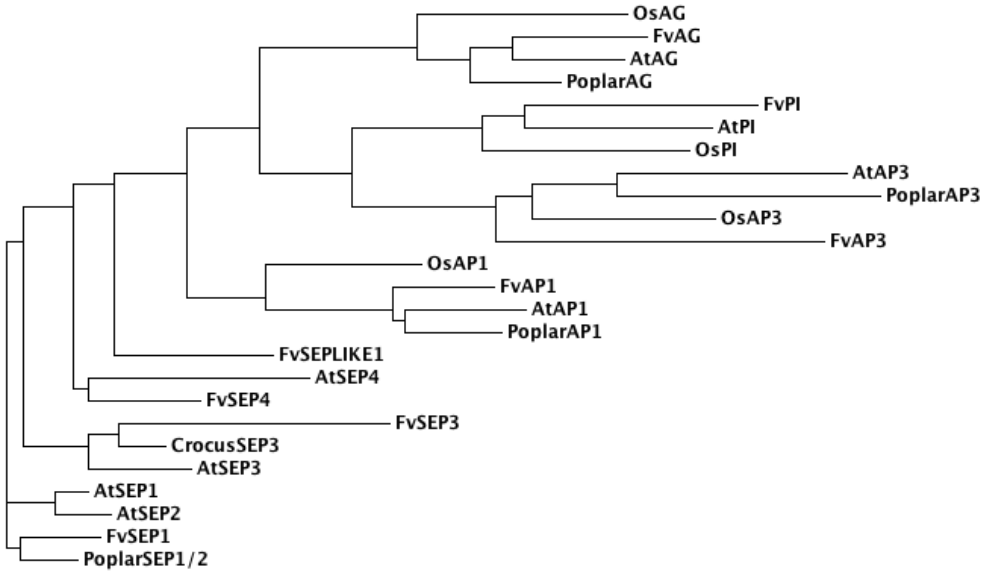

Figure 5-4. Phylogram of annotated ABCE proteins in *Arabidopsis* (At), Rice (Os; *Oryza sativa*), Poplar (*Populus trichocarpa* for AP1, AG, SEP1/2; *Populus tomentosa* for AP3), and Crocus (*Croscus sativus*) alongside probable *F. vesca* homologs. Entire protein sequences were aligned using MUSCLE, and the tree was generated using ClustalW2 Phylogeny. Protein accession numbers are listed under materials and methods.

A.

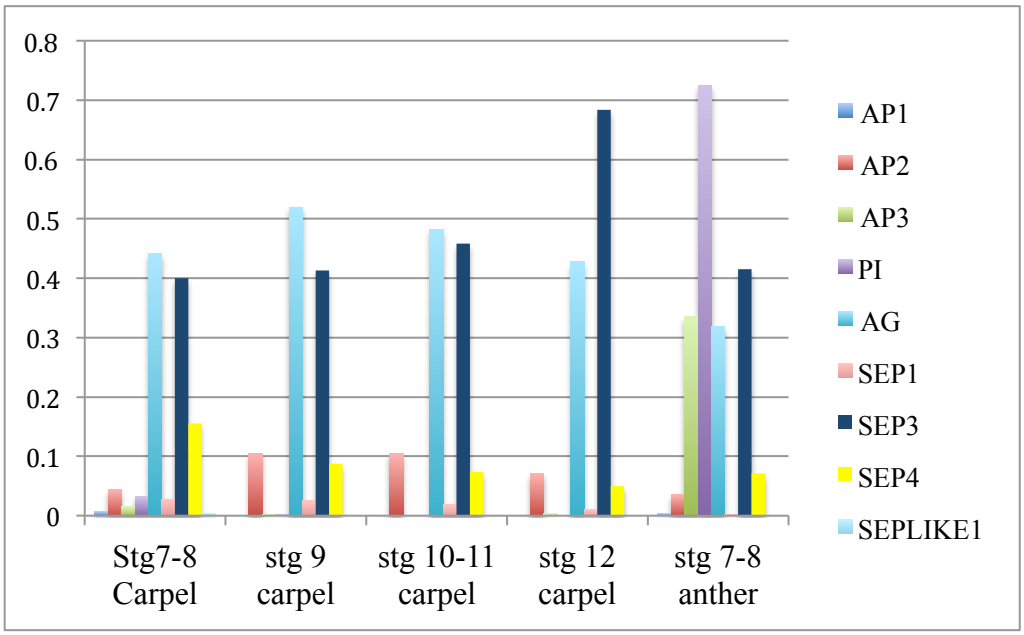

B.

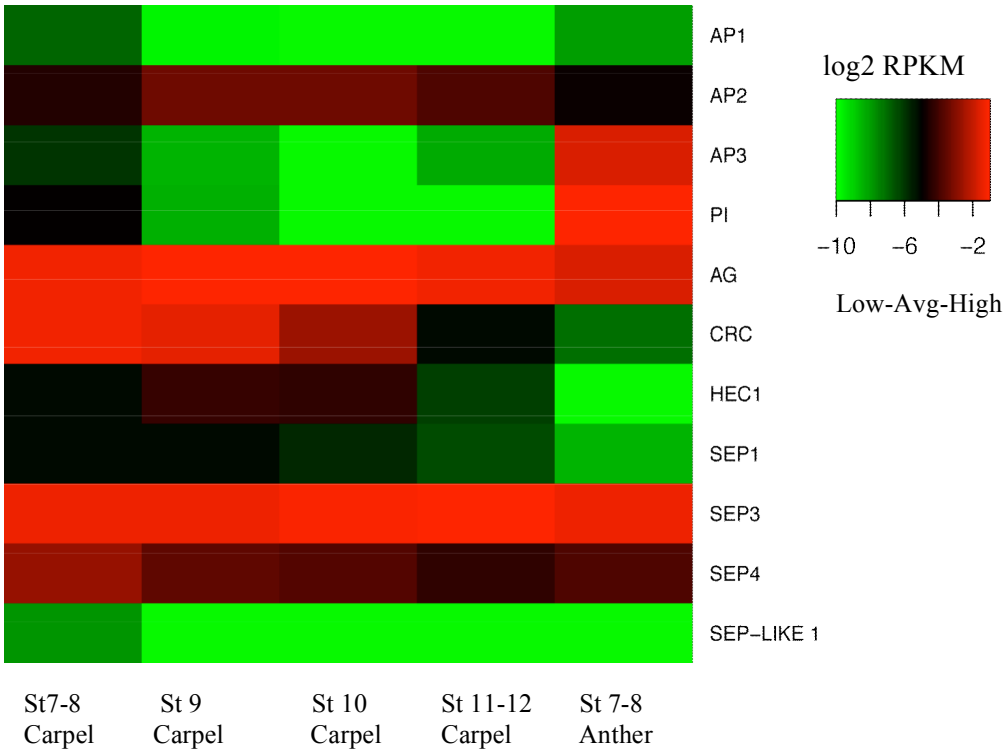

Figure 5-5. Expression of *F. vesca* homologs of *ABCE* genes in developing carpels and anthers. (A) Graphical view with Y-axis showing RPKM values. (B) Heat map based on log2 RPKM values compared to average log2 RPKM value for each tissue; black color represents average expression, green is below average, and red is above average. *FvCRC* (gene04566) and *FvHEC1* (gene23830) are probable homologs of two *Arabidopsis* carpel specific genes.

FvABCE expression in carpel and anthers based on hand-dissected transcriptomes

Stages 7 to 12 carpel and stage 7-8 anther transcriptomes were analyzed for the expression of probable *FvABCE* homologs (Fig. 5-5). Similar to *Arabidopsis*, the A-class gene *FvAP1* was not expressed in carpel or anther tissue, the B-class gene *FvPI* was only expressed in anthers, and the C-class gene *FvAG* was highly expressed in both carpels and anther. Further, *FvSEP3* and *FvSEP4* were expressed in anther as well as carpel tissues at all stages with *FvSEP3* at a much higher level. *FvSEP1* was expressed at very low levels in the carpel tissues, and the *FvSEPLIKE1* was not expressed at all in carpels or anthers. There is no significant change of expression levels across different carpel stages for all genes tested except for *FvSEP3*, whose expression increases in stage 12 carpels. *FvAP2* had a low level of expression in all tissues.

Expression of _FvABCE_ genes based on transcriptomes from LCM tissues

Thus far, only four of the eventual 11 LCM transcriptomes are available for analysis: young flower primordia (stages 1-4 pooled), receptacles from stage 6-7 flowers, stage 10 microspores, and stage 10 carpels (Table 5-2). Out of the remaining seven samples, four are being sequenced and 3 have not yet been laser dissected. Nonetheless, analysis of the four available LCM transcriptomes revealed the predicted expression patterns based on the ABCE model of flower development (Fig. 5-6). *FvAP1* was highly expressed in the young flowers while absent from the inner whorl tissues (the stamen and carpels) (Fig 5-6). *FvAG* was highly expressed in stage 10 carpels as well as receptacles at stage 6-7, when carpel primordia are emerging on the surface of the receptacle (Fig 5-6). This receptacle expression is consistent with my *in situ* hybridization showing *FvAG* expression in the vasculatures of the receptacles (Chapter IV, Fig 4-7). All three *FvSEP*

genes are expressed in the three floral stages: stage 1-4 floral primordia, stages 6-7 receptacle, and stage 10 carpels with SEP3 expression at the highest level (Fig. 5-6). *SEPLIKE1* on the other hand was expressed at very low levels in the stage 1-4 flowers and receptacle (Fig 5-6). Expression of the ABCE genes in microspores was very low if at all (Fig 5-6). The flower development genes, primarily involved in flower organ identity, may not have a significant role in microspore and pollen development.

Interestingly, Fig. 5-6 shows a temporal progressive activation of the A, B, and C genes; A gene *FvAP1* is highly expressed in stage 1-4 floral buds, corresponding to the development of sepals and petals. The class B genes *FvAP3* and *FvPI* are also expressed in stage 1-4 buds, but to a slightly lesser degree, as these genes are associated with the emergence of petal primordia at stage 4. The C gene *FvAG* is not activated in stage 1-4 flowers but is expressed by stage 6-7 in the receptacle, the stage at which carpel primordia begin to emerge. *FvAG* is expressed to a greater degree in the more developed stage 10 carpels. Additionally, homologs of two *Arabidopsis* carpel specific genes, *FvHEC* and *FvCRC,* showed expression in the developing carpel primordia, and not stage 1-4 flowers (Fig. 5-6).

FvABCE **expression in stage 10 carpel transcriptomes prepared from hand-dissected and laser captured tissues**

The differences in LCM vs. HD transcriptomes described earlier indicated that caution should be exercised in comparing data sets generated by the two approaches. However, to determine if the LCM transcriptomes are at least reliable in showing similar gene

expression trends compared to HD transcriptomes of the same tissues, *ABCE* expression profiles from the stage 10 carpel LCM transcriptome and the stage 10-11 carpel HD transcriptome were compared (Fig. 5-7). Qualitatively, expression trends of *ABCE* genes in the two data sets were quite similar (Fig. 5-7).

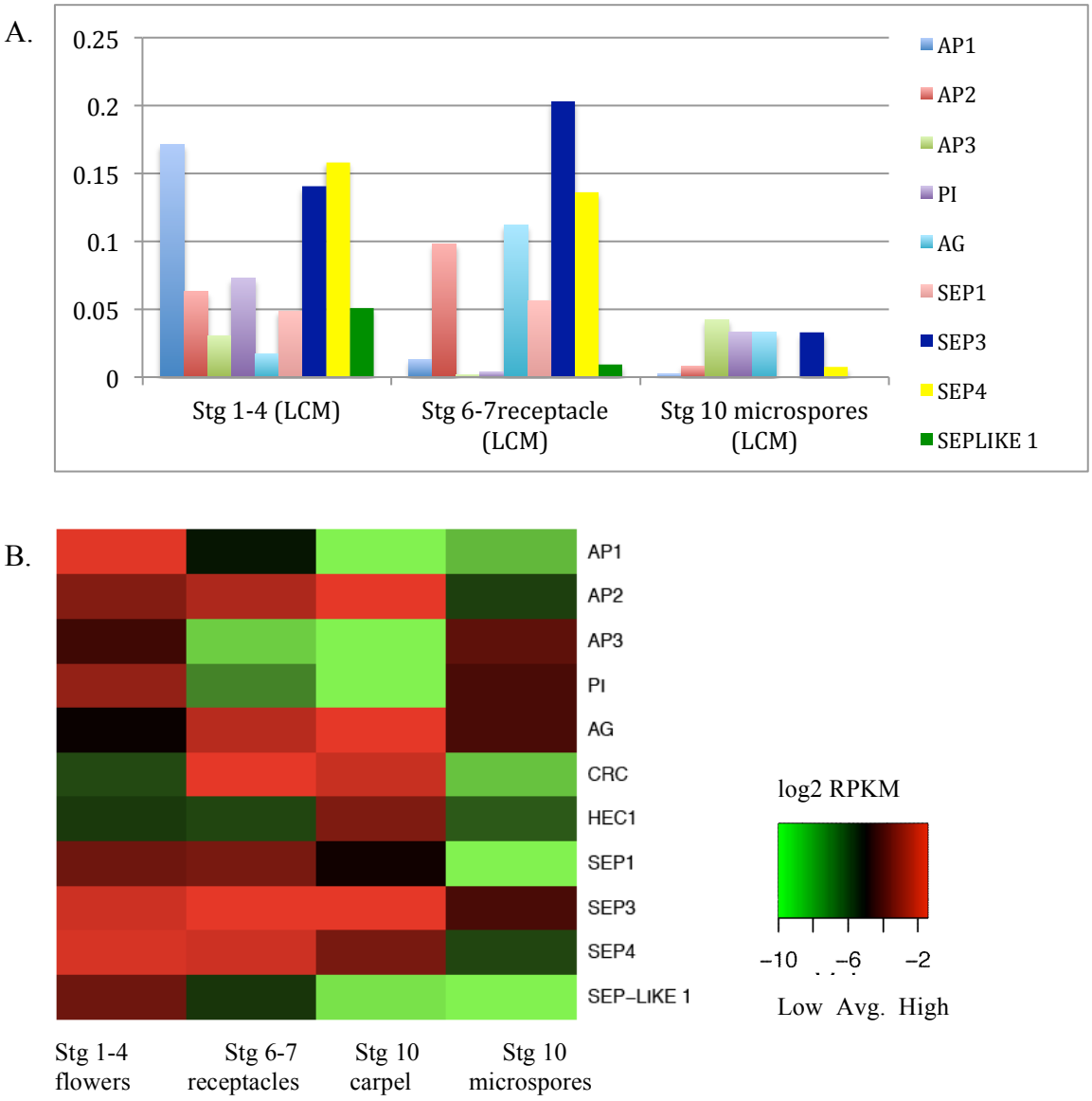

Figure 5-6. *ABCE* gene expression from four LCM transcriptomes: stage 1-4 flowers, stage 6-7 receptacle, stage 10 microspores, and stage 10 carpels. (A) Graph of RPKM values. (B) Heat map of log2 RPKM.

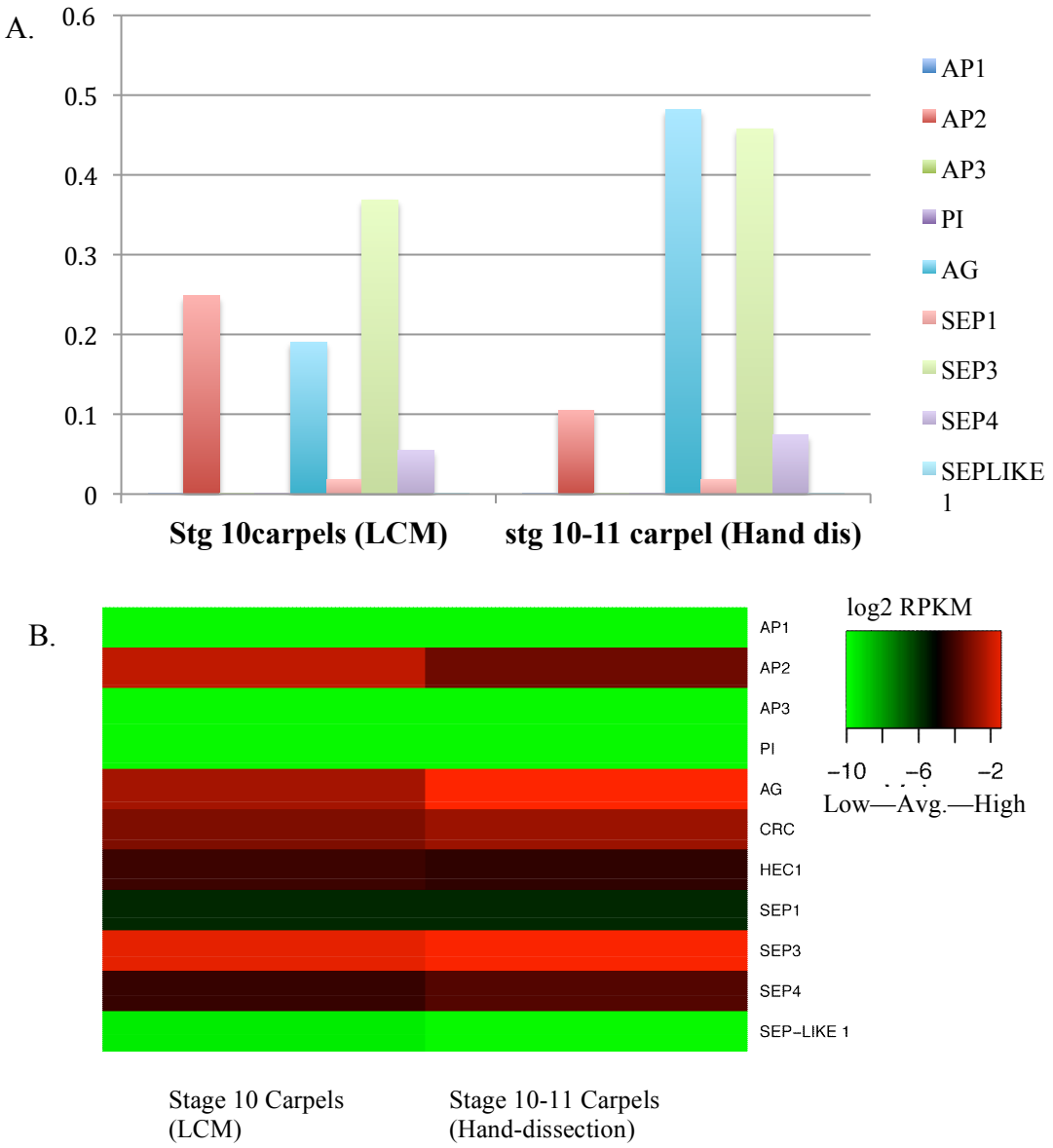

Figure 5-7. Comparison between LCM and HD carpel tissues. Expression data from hand-dissected tissues is an average of two biological replicates. (A) Graph of RPKM values. (B) Heat map of log2 RPKM.

Identification of differentially expressed genes in floral stages and organs

The analysis of the transcriptomes described here is at its early stage. To begin this analysis I first identified tissue type-specific genes by comparing carpel and anther tissues at similar stages 7-8. 896 genes with differential expression between stage 7-8 anthers and stage 7-8 carpels with a cut off of 2 fold and an adjusted p-value <0.01 have been identified. Of the 896 genes, 434 were induced in the anther, while 462 were induced in the carpel. Tables 5-5 and 5-6 list the top twenty most induced genes in each tissue.

Second, pairwise comparisons between adjacent stages of stage 7 to stage 12 carpels were performed. Specifically, the transcriptome of stages 7-8 carpels was compared with that of stage 9, the stage 9 transcriptome was compared with stages 10-11, and the stage 10-11 transcriptome was compared with that of stage 12 carpels (Fig. 5-8). Overall, the transition of carpels in stages 10-11 to carpels in stage 12 showed the greatest change in gene expression; 510 genes were upregulated in stage 12 carpels and 65 genes were downregulated compared to stages 10-11 (Fig 5-8). The high number of differentially expressed genes between these transcriptomes may reflect the significant physical changes occurring at this point in development. The carpels from stage 10 through stage 12 undergo significant changes in external appearance (the style elongates, the ovary widens, stigma develop) as well as tissue development (ovule primordia develops into highly differentiated tissues including the embryo sac and integuments) (Hollender et al., 2011).

Table 5-5. Top twenty highly induced genes in stage 7-8 carpels compared to stage 7-8 anthers. (Adj. P-value>0.01)

***F. vesca* Gene**	**Gene annotation from GDR (Genome Database for Rosaceae)**	**Fold Change (compared to anther)**	**Adjusted P-value**
gene15603	Transcriptional regulator STERILE APETALA	213	9.57E-18
gene13363	Arginine-glutamic acid dipeptide repeats protein	150	5.73E-50
gene16657	UvrABC system protein C (Protein uvrC)	108	2.20E-16
gene13423	Glutamyl aminopeptidase (AP-A)	105	1.58E-04
gene28757	B3 domain-containing transcription factor VRN1	101	2.42E-40
gene04547	Secologanin synthase (SLS)	94	5.06E-04
gene13480	Transcription factor bHLH140 (bHLH 140)	89	7.76E-04
gene14133	WUSCHEL-related homeobox 2	86	2.15E-17
gene08934	Centromere-associated protein E (CENP-E)	79	1.10E-30
gene02647	Homeobox protein knotted-1-like 2	74	1.95E-05
gene23334	DNA repair and recombination protein RAD54B	64	1.22E-06
gene08126	Probable LRR receptor-like serine/threonine-protein kinase At1g34110, Precursor	61	1.88E-08
gene04566	Adenosine 3'-phospho 5'-phosphosulfate transporter 2	61	5.73E-50
gene30749	Protein CUP-SHAPED COTYLEDON 2 (ANAC098)	61	1.28E-04
gene05720	Scarecrow-like protein 32 (AtSCL32)	58	1.64E-09
gene16221	Transcription factor bHLH94 (bHLH 94)	55	3.18E-06
gene05020	Gibberellin 2-beta-dioxygenase 2	55	7.02E-22
gene09459	Trinucleotide repeat-containing gene 6A protein	51	2.56E-49
gene06880	Copper-exporting P-type ATPase A	50	5.58E-36
gene31529	Protein UNUSUAL FLORAL ORGANS (AtFBX1)	48	2.24E-09

Table 5-6. Top twenty highly induced differentially expressed genes in stage 7-8 anthers compared to stage 7-8 carpels (adj. P-value>0.01). Inf refers to infinite, as these genes were not expressed at all in carpel.

***F. vesca* Gene**	**Gene annotation from Genome Database for Rosaceae**	**Fold Change (compared to carpel)**	**Adjusted P-value**
gene21160	Gamma-phospholipase A2 inhibitor LNF2, Precursor	Inf	5.35E-03
gene19023	1-aminocyclopropane-1-carboxylate synthase 1 (ACC synthase 1)	Inf	5.12E-03
gene08264	Putative F-box protein At1g47390	Inf	2.38E-03
gene06347	Elongation factor 1-delta (EF-1-delta)	Inf	2.11E-03
gene13347	Glutamyl-tRNA reductase (GluTR)	Inf	1.69E-03
gene05036	Vacuolar-processing enzyme (VPE), Precursor	Inf	1.31E-03
gene13599	(R)-mandelonitrile lyase 1 ((R)-oxynitrilase 1), Precursor	Inf	1.17E-03
gene28220	Phosphate import ATP-binding protein pstB	Inf	9.63E-04
gene29055	BRCA1-A complex subunit RAP80	Inf	6.30E-04
gene12955	Probable E3 ubiquitin-protein ligase RNF144A-A	Inf	1.59E-04
gene22005	Putative ribonuclease H protein At1g65750	Inf	1.36E-04
gene31815	Putative phosphoglycerate mutase DET1	Inf	4.03E-05
gene11279	hypothetical protein	Inf	9.52E-06
gene28083	Putative F-box protein At1g30920	Inf	3.63E-06
gene21506	NADPH-dependent diflavin oxidoreductase 1	Inf	3.44E-06
gene23916	Ubiquitin cross-reactive protein, Precursor	791	3.07E-03
gene15763	hypothetical protein	696	1.53E-06
gene25334	Histidine-containing phosphotransfer protein 1	443	8.80E-03
gene02398	UPF0497 membrane protein 1	359	3.34E-07
gene26701	Potassium-transporting ATPase subunit beta	330	1.26E-04

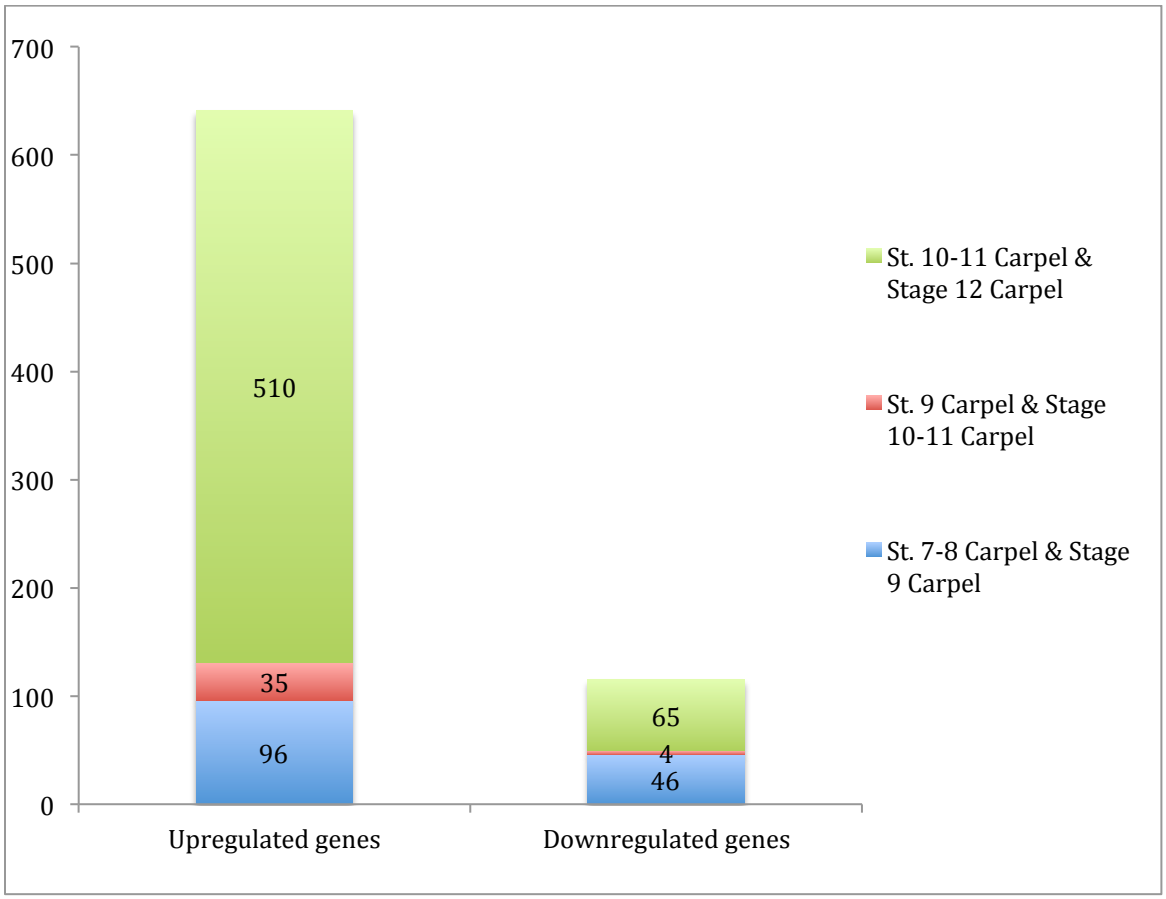

Figure 5-8. Number of differentially expressed genes in *F. vesca* pairwise comparisons of carpels between stages 7-8 and stage 12. Bar on left indicates the number of genes that are upregulated in the older stage carpel of the pairwise comparison. Bar on the right indicates the number of genes that were downregulated in the older stage carpel.

Discussion

The transcriptomes described here, together with those near completion, will provide a valuable molecular resource to the plant biology community in areas of flower development, gamete formation, and fruit initiation. Putative *FvABCE* genes were identified using bioinformatics and their expression levels and floral organ-specificity were analyzed. For the most part, the *FvABCE* genes are expressed in a similar pattern as

their *Arabidopsis* counterparts, with class A gene FvAP1 expressed in young flowers but absent from carpels and anthers. B genes *FvPI* and *FvAP3* are both detected in anthers and stage 1-4 flowers as these flowers are making petals. There is no sepal or petal transcriptomes available at the moment, although one will be generated in the near future. The class C gene *FvAG* is expressed in both anther and carpels and is absent from stage 1-4 flowers, which have not yet developed carpel or stamen primordia. *FvAG* expression in the flower transcriptomes corresponds to the *in situ* hybridization data in Chapter IV. The E class genes, *FvSEP1-3* were appropriately expressed in all the tissues analyzed, with *FvSEP3* and *FvSEP4* having the highest expression. The novel E-class gene, Fv*SEPLIKE1* (which is in its own clade in the phyllogram; Fig. 5-4), might be involved in early stage flower development, as it is expressed most highly in the stage 1-4 flowers, very slightly in the stage 6-7 receptacle, and not at all in later stage carpel and anther tissues (Fig 5-4 and 5-5).

I also examined two non-classically-defined C genes, *CRABSCLAW* (*CRC*) and *HECATE1* (*HEC1*). In *Arabidopsis*, *CRC* promotes longitudinal growth of carpels and restricts their radial growth. *CRC* expression is initiated at the inception of *Arabidopsis* carpel development (Alvarez and Smyth, 2002). *HEC1* promotes stigma and transmitting tract development in the *Arabidopsis* gynoecium (Gremski et al., 2007). In *F. vesca*, these two genes are expressed in late stage carpels consistent with their role in specific tissue formation within the carpel. I searched for *F. vesca* homologs to the C class gene *SPATULA* (*SPT*) (described in Chapters I, II, & III) to use when mining the transcriptomes, but BLAST searches did not turn up any potential matches. However, in

Arabidopsis, *SPT* is primarily involved in the development of stigmatic tissue (See Chapter III), and *F. vesca* carpels have very little stigma. It's possible that there is no *SPT* homolog in *F. vesca,* or that more intensive bioinformatic analysis is needed to find one.

Here, I show that *FvAP2* is expressed at a low level in all floral whorls (Fig 5-5 and 5-6). *AP2* is a class A gene, but is distinct from the other class A gene, *AP1,* on several fronts. First, unlike all the other *ABCE* genes, *AP2* is not a MADS-box protein. AP2 has two AP2 domains and is a founding member of the AP2/EREBP transcription factor family. Second, *AP2* mRNA was initially reported to be present in all floral whorls by several labs (Okamuro et al., 1997a; Würschum et al., 2006; Zhao et al., 2007b), although the genetic evidence of it's A class function in both sepal/petal development and C gene repression cannot be denied (See Chapter I; Bowman et al., 1989). More recently, *Arabidopsis AP2* was shown to be primarily expressed in the sepals and petals, but does have a low level of transient expression in the stamen (Wollmann et al., 2010) due to the post-transcriptional regulation by *miR172* in the inner floral whorls (Chen, 2004; Grigorova et al., 2011). In addition to its role in flower development, *AP2* is also involved in stem cell maintenance (Würschum et al., 2006). Further investigation is need to elucidate the exact role of *FvAP2* in all floral whorls as well as its ability to be negatively regulated by *miRNA172*, *FvAP2* might not be as susceptible to the negative regulation in the inner whorls by a *miR172. Or a miR172* homolog may not be present in *F. vesca*. Similar to *FvAP2*, the petunia *AP2* ortholog is also expressed in all whorls (Maes et al., 2001). Alternatively, the *F. vesca* AP2 protein may have a different

function than its *Arabidopsis* counterpart. Finally, since *FvAP2* was identified only by sequence homology, there is a possibility that this gene is not the true ortholog of *AP2.*

Stage 10 carpel transcriptomes generated from both LCM and HD tissues were compared to assess both the reliability of the LCM transcriptomes as well as discover possible differences that could have resulted from their distinct methods of tissue isolation and RNA-seq library preparation. Quantitatively, gene expression differed between the types of transcriptomes–as shown by the numbers of genes with RPKM ≥ 300 or RPKM ≥ 1000 in LCM vs. HD (Fig 5-3). The quantitative differences between the two types of samples may be partially due to a lack of poly-A selection and the use of amplification for LCM RNA, as well as the a result of the differences between the two types library preparation kits, each manufactured by a different company (Illumina for the HD vs. Nugen for the LCM). Further, the HD samples may contain carpels from stage 11 flowers. Despite the quantitative discrepancies–which were not much greater than differences between the two HD biological replicates–comparable expression trends for *FvABCE* genes were observed in both the HD and LCM stage 10 carpels transcriptomes. (Fig. 5-7). The similarity in the *FvABCE* gene expression values validated that LCM transcriptomes are equally useful in providing relative expression data. However, caution should be exercised in direct quantitative comparisons between data by the two methods due to their very different methods of preparation. Analysis of the additional LCM transcriptomes will give more insight into the differences between the two methods.

Finally, these transcriptomes hold valuable information on the intersection between gene regulation and development. The small amount of data mining presented here is just the beginning of a comprehensive analysis. Future mining of these transcriptomes coupled with experimental testing may lead to the discovery of novel flower development genes as well as the discovery of novel functions of known genes.

Materials and Methods

Hand-dissection of tissue for RNA

Under a dissecting microscope, on a glass side, anther and carpel tissues were hand-dissected from stage 7-12 flowers. Both slide and forceps were cleaned with RNAse-Away (Molecular BioProducts, San Diego CA). Tissues were immediately placed in Arcturus® PicoPure® RNA isolation kit Extraction buffer (Applied Biosystems, Foster City, CA) in the lid of a 1.5 mL microfuge tube and then frozen at -80^{o} C. For each stage, or group of stages, two tubes of tissues, acting as biological replicates, were prepared for RNA isolation and subsequent sequencing. Each biological replicate itself was comprised of tissues from 2-6 individual flowers, according to the table below.

Sample Type		Replicate	Number of flowers contributing to RNA
Stages 7-8	Anther	A	6
Stages 7-8	Anther	B	3
Stages 7-8	Carpel	A	5
Stages 7-8	Carpel	B	5
Stage 9	Carpel	A	2
Stage 9	Carpel	B	2
Stages 10-11	Carpel	A	2
Stages 10-11	Carpel	B	2
Stage 12	Carpel	A	3
Stage 12	Carpel	B	3

Tissue fixation and embedding for LCM samples

Under a dissection microscope, sepals were removed from flowers and the trichomes on the stems were shaved off with forceps and/or a needle before being placed in ice-cold 100% acetone in a glass scintillation vial. The fixation protocol is based on Ohtsu et al. (2007), but contains some modifications. Once in 100% acetone, samples were vacuumed on ice for 40 minutes and then left gently swirling at 4 degrees for ~1 hr. Next, acetone was replaced with fresh ice-cold 100% acetone and vacuum/swirling procedure was repeated. After second swirling, acetone was replaced once more, tissue vacuumed on ice for an additional 30 minutes, and then left overnight at 4 degrees. The next day, after samples equilibrated to room temperature, the acetone was replaced with 50:50 acetone:hemo-de, and incubated at room temperature for ~2 hours, followed by three 100% hemo-de incubations for 2 hours each. After the third 100% hemo-de incubation, the vial was filled halfway with fresh hemo-de, 10 paraplast plus (McCormick Scientific/Leica Microsystems, St. Louis, MO, USA) chips were added, and samples was left overnight at room temperature. The next morning, the vial was transferred to a 60^{o} C incubator and over the course of 1-2 days, 10 additional paraplast chips were added every 2+ hours until full. Once full, half of the wax/hemo-de mix was removed and replaced with 100% molten paraplasts and left for at least 4 hours before being replaced with 100% molten paraplasts. Before pouring wax boats, three more 100% wax changes were done, over the course of 2-3 days. Wax boats were stored indefinitely at room temperature.

Slide preparation and Laser Capture

10-12μm sections were prepared using a rotary microtome and floated on RNAse-free water on Leica PEN-Membrane 2.0 μm slides (Cat # 11505158) placed on a slide warmer set to 40 degrees. After expansion of sections (~5 minutes), the majority of the water was removed and slides were left to completely dry on warmer for 15-30 minutes. Tissue was sectioned and slides were dewaxed on the same day as laser capture. The Leica dewaxing protocol was used (three 20 second incubations in 100% xylene, two 30 second incubations in 100% EtOH, two 30 second incubations in 95% EtOH, followed by two 30 second incubations in 70% EtOH). An average of ~2 x 10^6 μm^2 of tissue (with a range from 1 x 10^6 to 8.7 x 10^6 μm^2) was cut on a Leica ASLMD microscope (Leica). Tissue was dropped into the cap of a 0.2 ml PCR tube containing Arcturus® PicoPure® RNA isolation kit extraction buffer (Applied Biosystems, Foster City CA) and then stored at -80^0 until RNA isolation.

RNA extraction

RNA for both hand dissected and LCM tissue was extracted using the Arcturus® PicoPure® RNA isolation kit (Applied Biosystems, Foster City CA) according to the manufacturers protocol. Immediately prior to RNA extraction, hand dissected samples were ground in extraction buffer with a plastic pestle that was cleaned with RNAse-Away. Extractions incorporated DNAse treatment using Turbo DNA-Free DNAse (Ambion) in between Wash Buffer 1 and Wash Buffer 2 column washes. RNA quality and quantity was measured using the BioRad Experion automatic electrophoresis system.

Sequencing and HD RNA-Seq library preparation

Sequencing libraries for RNA originating from hand dissected tissues were prepared at the Weill Cornell Medical College Genomics Resources Core from ~150 ng of high quality total RNA (Experion RQI values > 7) using the Illumina Truseq RNA-seq library preparation kit after poly-A enrichment. All sequencing was performed by the same facility using Illumina HiSeq2000. 4-5 samples were pooled and sequenced in one lane with Single Read Clustering and 58 Cycles.

RNA-Seq library preparation for RNA from LCM tissues

Sequencing libraries for the RNA from LCM samples were prepared using NuGEN's Ovation® RNA-Seq System V2, which amplified the cDNA after second strand synthesis, followed by NuGEN's Encore® NGS Multiplex Library System I (Nugen Technologies, San Carlos CA) according to manufacturers protocol. Starting amounts of RNA for RNA-Seq System V2 ranged from ~3.5ng to 38 ng. Sonication of cDNA for the NGS Multiplex Library system was done using a Covaris S sonication system with the following parameters: Peak Incident Power 175, Duty cycle 10%, cycles/burse 200, Time 180 seconds, sample volume 130 μl. Prior to using the Encore® NGS Multiplex Library System I, the sonicated cDNA was concentrated using the Qiagen MinElute® PCR purification kit (Qiagen Sciences, Germantown MD) and eluted with 22 μl elution buffer. As per the manufacturer's protocol, approximately 200 ng of sonicated cDNA was used to construct each library. Prior to sequencing, four libraries were pooled in equal molar ratios at the sequencing facility.

RNA-Seq read alignments and analysis

Sequence reads were filtered and aligned to the F. vesca genome (strawberrygenome.org; Shulaev et al 2011) by our collaborator Nadim Alkarhouf, at Towson University. Filtering was done with the FastQ Quality Filter from the Fast X tool kit (http://hannonlab.cshl.edu/fastx_toolkit/) based on a quality score cut-off value of 28 (out of a maximum score of 33) and a probability value of 90. Bowtie (http://bowtie-bio.sourceforge.net/index.shtml) software was used for alignment to the genome. Data was normalized using RPKM values (Reads Per Kilobase of exon model per Million mapped reads). DESeq (http://www-huber.embl.de/users/anders/DESeq/) was used in R (http://www.r-project.org/) to identify differentially expressed genes. The 'heatmap.2' program was used in R to generate heat maps from RPKM values.

Phylogenetic tree construction

Protein alignments were done by MUSCLE (http://www.ebi.ac.uk/Tools/msa/muscle/) and then uploaded to ClustalW2 Phylogeny (http://www.ebi.ac.uk/Tools/phylogeny/), where phylogenetic distance trees were created with the neighbor-joining clustering method and distance correction enabled. In addition to the *F. vesca* protein sequences extracted from strawberrygenome.org, the protein sequences used for the tree are listed in the table below.

Gene Name in Table	Species	TAIR/NCBI protein Accession
AtAP1	*Arabidopsis thaliana*	At1g69120.1
OsAP1	*Oryza sativa* Japonica Group	ABF98925.1
PoplarAP1	*Populus trichocarpa*	EEF02247.1
AtAP3	*Arabidopsis thaliana*	At3g54340.1
OsAP3 (OsMADS16)	*Oryza sativa* Japonica Group	Q944S9.2
PoplarAP3	*Populus tomentosa*	AAO49713.1
AtPI	*Arabidopsis thaliana*	At5g20240.1
OsPI (OsMADS4)	*Oryza sativa* Japonica Group	Q40703.3
AtAG	*Arabidopsis thaliana*	At4g18960
OsAG	*Oryza sativa* Japonica Group	ABG21913.1
PoplarAG	*Populus trichocarpa*	AAC06238.1
AtSEP1	*Arabidopsis thaliana*	At5g15800.1
AtSEP2	*Arabidopsis thaliana*	At3g02310.1
PoplarSEP1/2	*Populus trichocarpa*	XP_002330922.1
AtSEP3	*Arabidopsis thaliana*	At1g24260.2
CrocusSEP3	*Crocus sativus*	ACB69512.1
AtSEP4	*Arabidopsis thaliana*	At2g03710.1

Appendix A: Establishing genetic resources for *F. vesca*

Introduction

The development of *Fragaria vesca* as a model organism requires the availability of genomic and genetic tools for research. One such tool is the creation of a mutagenized population for forward genetics and TILLING lines for reverse genetics. Mutagenesis could yield a plethora of biologically interesting and/or agriculturally desirable phenotypes. Interesting mutants could be further characterized, mapped, and eventually cloned to yield molecular insights into the mutagenized genes and processes. The DNA from the mutagenized population can serve as the starting material for TILLING (Targeting Local Lesions IN Genomes) where mutations in desirable genes are screened for and corresponding mutant plants could be isolated (Comai et al., 2006).

Two preliminary trials of mutagenesis were performed using two mutagens, EMS (Ethyl methanesulfonate ; which produces G→A transitions) and ENU (*N*-ethyl-*N*-nitrosourea; which causes A → T and AT ←→ GC transversions). Seeds were mutagenized with several concentrations of each chemical and for different lengths of exposure. Germination and seedling survival rate of the M1 population were ascertained to assess penetrance of the mutagens. M2 seeds - collected from approximately 600 individual M1 plants - were sent to the Horticulture Institute, Jiangsu Academy of Agricultural Sciences, in Nanjing, China, where they were grown under the supervision of Dr. Jing Wang starting in the winter of 2010. Many M2 plants did not survive due to poor growing conditions, however when ~1000 M2 plants, representing 140 of the initial M1 lines, were phenotyped in June 2011, several mutants with interesting vegetative, floral, and

fruit phenotypes were observed. This work was a preliminary study, laying the foundation for the creation of larger mutagenesis populations that are now in development. It enabled us to determine ideal mutagenesis and growing conditions as well as streamline the basic organizational details of managing such a large-scale project. Though preliminary in nature, this work provided us with small M1 and M2 populations that we can now characterize.

Additionally, genomic DNA was isolated from 518 healthy M2 plants and may be used in the future for TILLING. TILLING is a reverse genetic technique that identifies plants with single nucleotide polymorphisms (SNPs) in genes of interest from mutagenized populations. This technique, which employs high-throughput PCR coupled with DNA digestion analysis, is illustrated in Figure A-1 and described in detail in the legend.

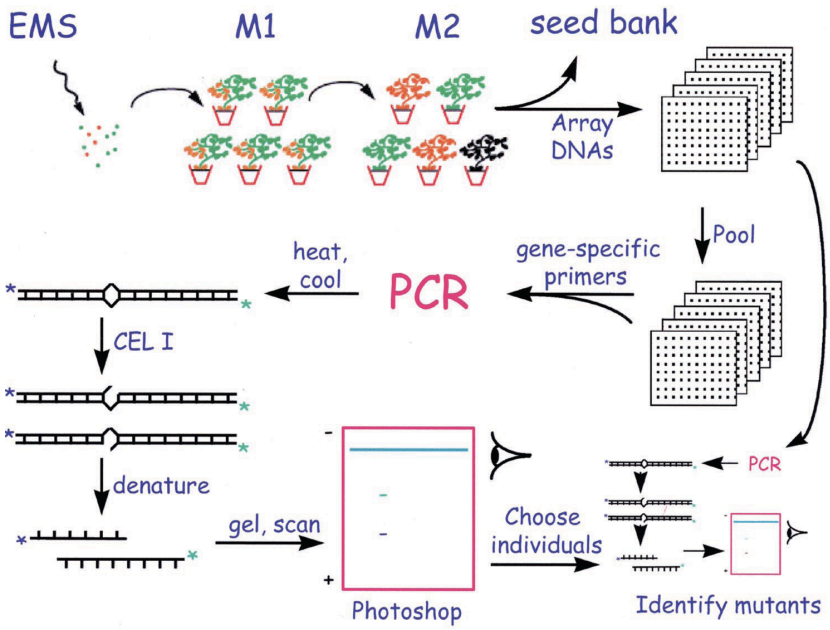

Figure A-1. Diagram of the TILLING process for reverse genetic identification of mutant plants from a large mutagenized population. Image taken from (Colbert et al., 2001)

Figure A-1. Diagram of the TILLING process for reverse genetic identification of mutant plants from a large mutagenized population. This image is taken from (Colbert et al., 2001). Seeds are mutagenized with chemicals such as EMS to induce single base pair mutations, grown for two generations (M1 is the first generation, M2 are the progeny of M1), and M2 seed are stored for future use. DNA from M2 lines is extracted and organized into 96-well plates. Next, to reduce cost and time, pools of DNA are created in 96-well plates, where each well has DNA from several plants (usually 8 or 64). PCR for a region of a gene of interest is done with fluorescently labeled gene-specific primers. In the course of the heating and cooling in the PCR reaction, DNA heteroduplexes form when single base mismatches are present. These mismatched bases are the result of a mutation present in at least one, but not all of the plants in the DNA pool. After the PCR, amplicons are incubated with the single strand endonuclease Cel-I, which cuts heteroduplex DNA wherever there is a mismatch. Gel electrophoresis of the digest enables identification of pools of DNA that contain mutations in the amplified gene. When no mutations are found, the PCR band (visualized by two fluorescent labels, one from each primer) will show the full length of the amplicon, illustrated by the long blue band at the top of the gel. When there is a mutation in this gene in at least one of the plants in the pool, two smaller bands will be present because Cel-I will have digested the amplicon at the site of the mutation. The combined size of each band should equal the total size of the amplicon. After a mutation is identified in a DNA pool, further PCR and digestions will be done on the DNA from the individual lines that made up that pool, and eventually the plant with the mutation will be identified.

Results

Mutagenesis conditions, germination and survival rates, and fruit set

To initiate *Fragaria vesca* mutagenesis, we first needed to determine appropriate mutagen concentrations and treatment conditions. To determine the effect of mutagenesis on the seeds, we examined germination and seedling survival rate in M1 seedlings. To gage mutagenesis efficacy, the rate of chlorotic sectoring in M1 leaves was noted.

In the course of two separate rounds of mutagenesis, *Fragaria vesca* Yellow Wonder 5AF7 seeds were treated for either 4 or 16 hours with either EMS or ENU. The EMS concentrations used were 0.2%, 0.4%, or 0.8% EMS, while the ENU concentrations tested were 2 mM, 4 mM, or 8 mM. Approximately 500 *F. vesca* seeds each were used for each condition as well as for a no mutagen control. After incubation with the mutagen in water (or water alone for the control), seeds were rinsed with sterile water, plated on MS-agar plates, sealed, and vernalized for 5 weeks in the dark at 4^{o}C. The percent seed germination on MS/Agar plates was measured after 7-10 days of growth in light, and the seedling survival rate was noted after the germinated seedlings were transplanted into 12 well bedding flats (Fig. A-2; A-3). Results of all treatments are summarized in Table A-1.

Within the 4-hour mutagen treatments, the 0.4% EMS and 4mM ENU treated plants produced germination rates similar to the 0.2% EMS and the 2mM ENU treated plants (Fig A-2A, Table A-1). We chose to further propagate the 0.4% EMS and 4mM ENU

treated plants, which may have higher mutation rates, and discarded the 0.2% EMS and 2mM ENU plants. The seedlings (of 0.4% EMS and 4mM ENU) were transferred to 12-well bedding pots, and then again to 4-inch pots in the greenhouse. Chlorotic leaf sectoring was observed in these 4-hour treated plants, indicative of somatic chloroplast mutations due to mutagen treatment (Fig A-4 A, B). 1.25% of the 4-hour 0.4% EMS plants showed leaf sectoring (n=399) and 2.84% of the 4-hour 4 mM ENU plants (n=422). Additional abnormal leaf phenotypes, such as extra leaflets or rolled-up leaves, were also observed in a few of the M1 lines (Fig A-3 C, D).

At the time the first M1 plants (four hours with 0.4% EMS or 4mM ENU) were transferred to the greenhouse, a second round of mutagenesis was undertaken to ensure that we would obtain a large enough M1 population. This time, *F. vesca* seeds were exposed to 0.4% and 0.8% EMS and 4 and 8 mM ENU for 16 hours (Figs. A-2, A-3). Hundreds of seeds from the four 16 hours mutagen treatments germinated, however the seedlings of almost all ENU treated seeds didn't survive (Fig. A-2B; Table A-1). In addition, although the plants treated with 0.4% and 0.8% EMS for 16 hours had a high percentage of germination and survival, these plants did not bear fruit or seeds although they flowered normally. We determined that the 16-hour duration of mutagenesis was too severe. The level of chlorotic leaf sectoring in the 0.4% EMS 16-hour population was 56.1%, over ten fold higher than the highest amount of sectoring in the 4-hour treatments. This high rate of sectoring may have been an early indication that the treatment was too caustic, as the plants would not bear fruit (possibly due to a 100% rate

of embryo lethality and embryos are required to produce auxin for fruit set and for seed formation).

Table A-1. Results from 4 and 16-hour EMS and ENU mutagenesis trials. (na: data not available. Dashes represent incalculable data because the plants died or were discarded before that point of analysis. Asterisks indicate M2 plants grown in China.)

Mutagen	Conc.	Mutagenesis length (hours)	Percentage of Germination	Seedling survival Rate	Percent with sectors	Able to produce seeds?
Control	0	4	92.0	100	0	Yes
	0	16	93.3	100	0	Yes
EMS	0.2 %	4	83.1	(discarded)	-	-
	0.4 %	4	83.9	na	1.25	Yes*
	0.4 %	16	85.9	99.6	56.1	No
	0.8%	16	43.0	81.9	na	No
ENU	2mM	4	90.4	(discarded)	-	-
	4mM	4	88.9	na	2.84	Yes*
	4mM	16	91.7	3.6	-	-
	8mM	16	70.7	0.6	-	-

M2 phenotypes

The M2 population from the 4-hour 0.4% EMS and 4mM ENU mutagenesis populations were grown by our collaborator Dr. Jing Wang at the Horticulture Institute, Jiangsu Academy of Agricultural Sciences, in Nanjing, China. Eight seeds from each of the 344 EMS and 251 ENU M1 lines were sown in bedding trays in a greenhouse, though many did not germinate. Seedlings were transferred to an open field in the early spring of 2011. Many M2 plants died in the field, yet in the summer of 2011, members from our lab phenotyped the surviving M2 plants (~1000), which represented 140 lines of the initial M1 population. Several plants from this M2 population had phenotypes worth

further investigation. One plant (Fig A-3 E) produced runners, which are not normally present in Yellow Wonder. Although genotyping needs to be done to confirm that this phenomenon isn't simply due to seed contamination in the field, it would be very exciting to find a runnering Yellow Wonder 5AF7 plant. Runnering has not yet been linked to one gene. The runnering phenotype in *F. vesca* var. Hawaii 4 (H4), is a dominant trait; when YW5AF7 or Ruegen varieties are crossed into H4, the resulting seeds produce plants with runner phenotype (JS, personal communication). However, our runnering YW5AF7 plant is from the M2 population, and the phenotype was not observed in the parental M1 line. This suggests that the mutant allele responsible for runnering in our M2 mutant is recessive. It's possible that mutations in different genes in a meristem identity pathway can result in the ability to produce runners (e.g. genes involved in environmental perception pathways or downstream transcription factors). Isolating any gene in a pathway that could manipulate meristem fate to enable or disable runnering could be useful agriculturally and interesting biologically. Such a gene could be a switch that turns on or off vegetative propagation. Once isolated, it could potentially be used under an inducible promoter to induce or repress vegetative reproduction.

Dwarfism was another phenotype that segregated in the M2 lines (Fig. A-4 F). The small stature may be linked to genes involved in hormone pathways such as the brassinosteroid pathway. Cloning and eventually manipulating genes responsible for plant size could lead to plants that are more favorable to mechanical harvesting. It's also possible that a gene associated with this dwarfism could define novel signaling or developmental pathways.

Several *F. vesca* flower mutants were also identified in the M2 population (Fig. A-4 G, H). These plants may have mutations in the ABCE class of flower development genes. One mutant plant, containing flowers with leaves replacing both sepals and petals, may have defective A and B class genes in the sepal/petal whorls or define novel floral regulatory genes unique to strawberry (Fig A-4 G). Another mutant with a leaf-like organ replacing petals may result from a mutation in a class E gene or may define a novel floral gene (Fig. A-4 H).

A.

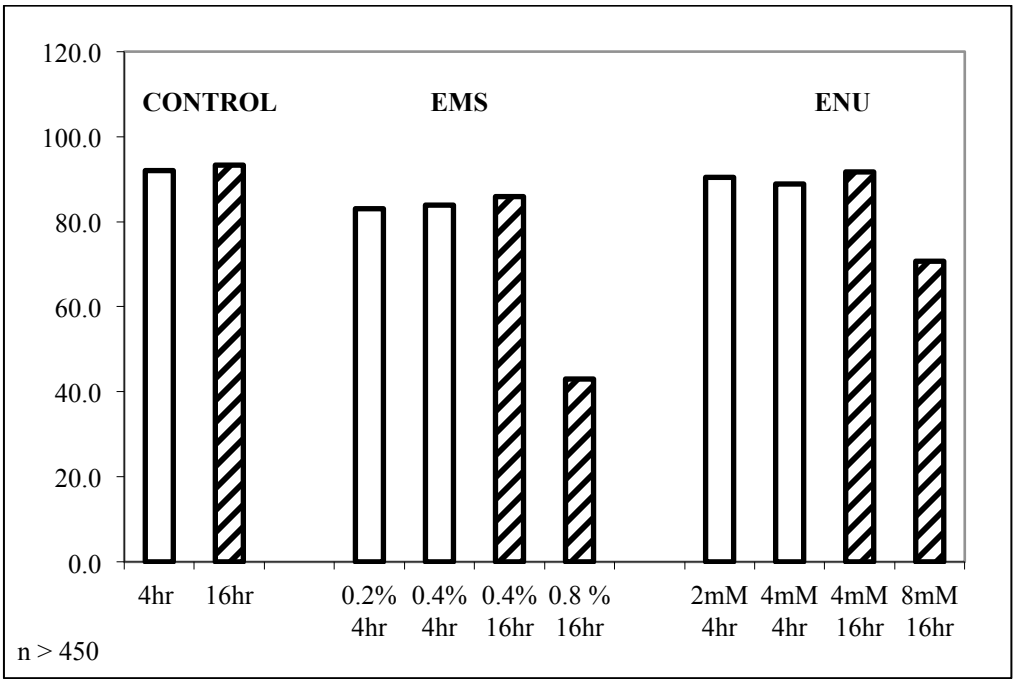

B.

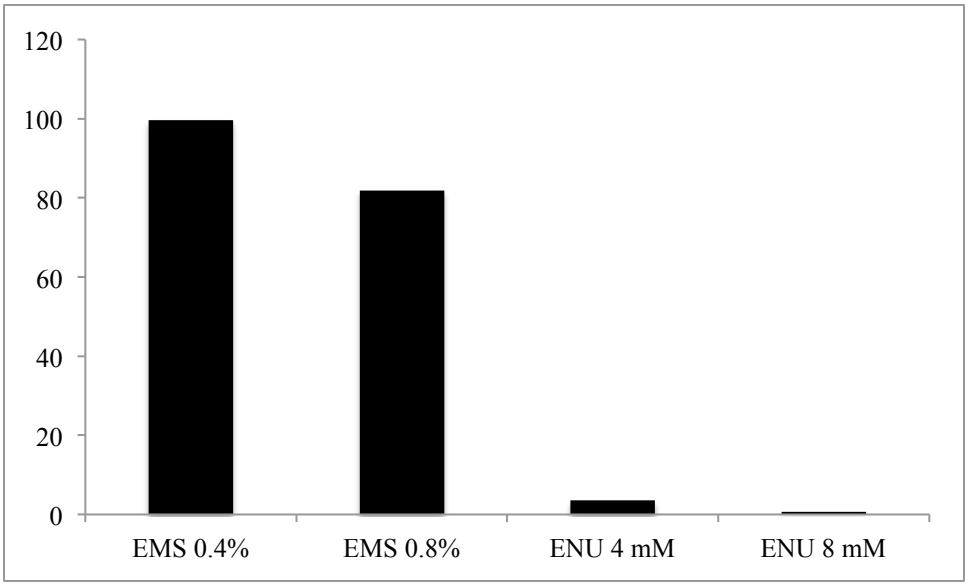

Figure A-2. Germination and seedling survival rates after treatment with different doses of mutagens EMS and ENU. (A) Percent germination on ½ MS-Agar plates after mutagenesis. (B) Percent seedling survival of the 16-hour treated seeds that successfully germinated.

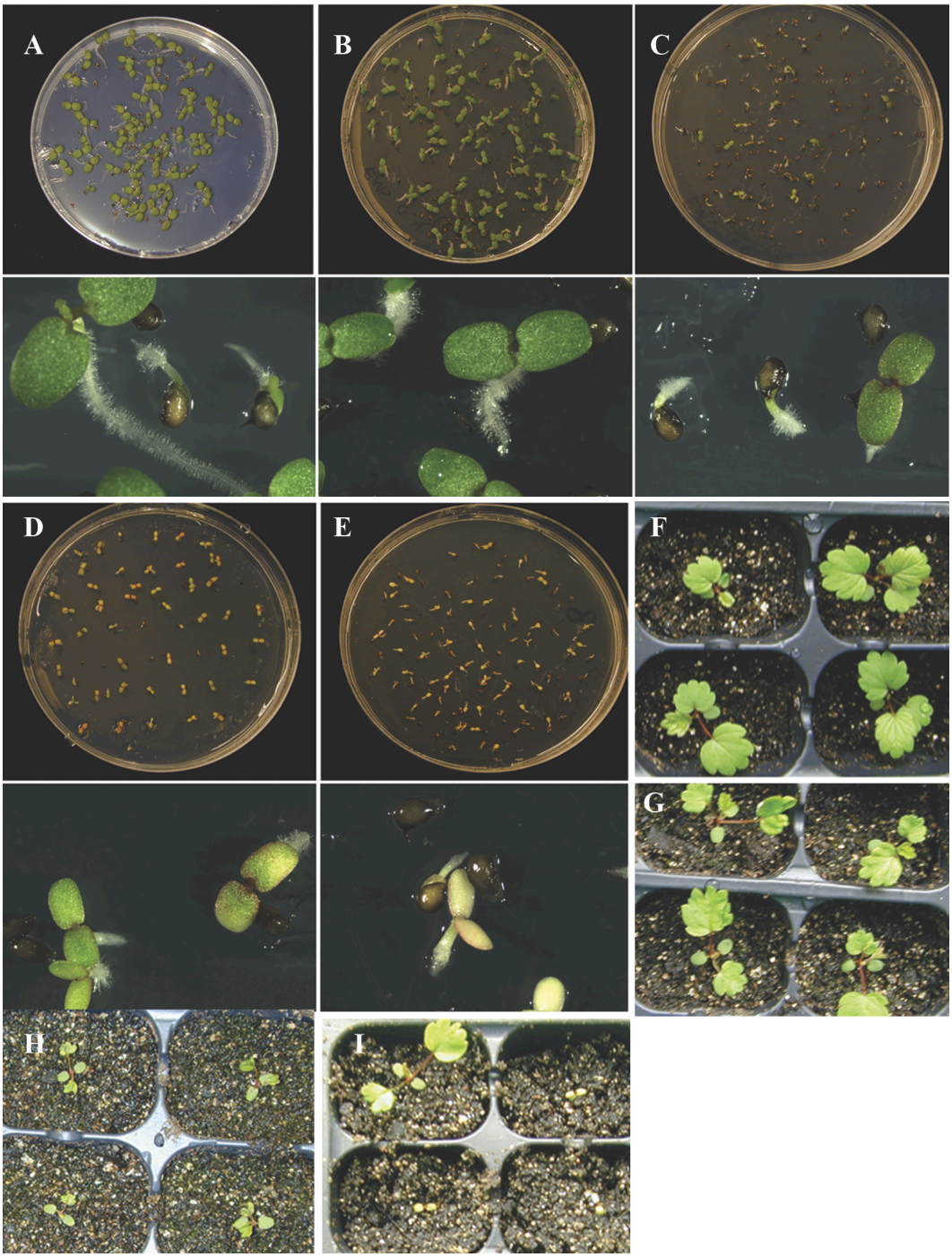

Figure A-3. Mutagenesis lines from 16-hour treatment. (A-E) Germination on ½ MS-Agar plates after approximately one week in a growth chamber. (A) Control. (B) 0.4% EMS. (C) 0.8% EMS. (D) 4 mM ENU. (E) 8 mM ENU. (F-I) seedlings growing in 12 well flats. (F) Control. (G) 0.4% EMS. (H) 0.8% EMS. (I) 4 mM ENU

Figure A-4 Mutagenesis lines from the 4-hour treatments. (A-D) Abnormal leaf phenotypes found in M1 plants. (E-H) Abnormal phenotypes found in M2 plants.

Discussion

With the intent of eventually accruing a *Fragaria vesca* mutagenesis M2 population that is large enough in size for TILLING (M2 ≥ 3000), two small preliminary trials of mutagenesis were performed. *F. vesca* seeds were exposed to the mutagens EMS and ENU at different concentrations and for 4 and 16 hours. Of the conditions tested, it was determined that 4-hour treatments of either 0.4% EMS or 4 mM ENU produced a mutagenesis population that produced viable M2 progeny as well as mutants. None of the 16-hour treated populations could produce M2 seeds, indicating too severe a treatment. It is interesting to note that although both 4-hour and 16-hour treated EMS population showed high germination rates, plants from only the 4-hour populations were able to set fruit. Furthermore, the high germination rate in the 4-hour 0.4% EMS treated seeds was not indication of poor mutagen penetrance in this population, as many mutants were discovered among its M2 population. This data suggests that germination rates are not a good indicator of mutagenesis efficiency. The amount of leaf sectoring in M1 leaves may be a better indicator; our seed bearing 4-hour treatment plants had < 3% sectoring, while the barren 16-hour populations had >50% sectoring. The amount of M1 sectoring that would indicate an optimal, highly mutagenized population, still needs to be determined.

Other ways to assess mutagenesis include measuring rates of albino seedlings in M2, and embryo lethality in M2 seeds (Vishnoi and Gupta 1980; Kurowska et al 2011). Since strawberry fertility and seed germination rates are easily affected by environment, it is difficult to use embryo lethality rates as a measure of mutagenesis success. Additionally,

since *F. vesca* plants take a minimum of 3.5 months for one to produce seed (not including vernalization time), we hoped to find indicators that could be measured well before obtaining M2 seed.

It remains to be determined what parameters are good predictors of successful and efficient mutagenesis. M2 seeds should have some level of seed lethality, but at the same time produce a sufficient fertile population with several mutations per gene (Kurowska 2011). The success of a mutagenesis can only be truly assessed by phenotypic observations and empirical testing approximating the number of mutations per kb of DNA, per plant, and per gene in the entire M2 population. It is difficult to predict the minimum size requirement for a mutagenized population, as the frequency of point mutations is both dependent on the species as well as mutagenesis conditions. An *Arabidopsis* mutagenesis population was able to absorb one mutation per 170 kb of DNA without significantly killing its seed, while a rice population with only 1 mutation per Mb exhibited a 50% seed lethality (Comai and Henikoff, 2006).

As many chemically induced point mutations may be silent, populations with high frequencies of mutations are desirable because they have increased likelihood of containing nonsense and missense mutations for all genes (or your gene of interest). Most published TILLING lines have 1 mutation per 200-500 kb, and M2 populations of 3000-5000 lines (Kurowska et al 2011).

To conclude, the *Fragaria vesca* mutagenesis described here was a preliminary trial to both begin to determine optimal mutagenesis conditions for *F. vesca,* as well to produce a small M2 population with segregating mutant phenotypes that can be further analyzed. The exact mutation frequency in these M2 populations remains to be determined by mining several genes via TILLING. However, seeds treated for 4 hours with either 0.4% EMS or 4 mM ENU produced a small M2 population with several noticeable phenotypes. Treatment methods for creating mutagenized populations with sufficient mutant frequencies for TILLING are still being determined. Currently, a batch of about 1000 M1 seedlings from an 8-hour mutagenesis treatment of 0.4% EMS – under the supervision of Liu lab member Chunying Kang – is growing and successfully producing berries whose seeds will soon be grown by our collaborators in China to generate a new and larger M2 population. In addition, the mutations behind several of the developmentally interesting phenotypes of the 4-hour treatment populations may be further investigated in the future.

Materials and Methods

Approximately 500 seeds for each treatment (determined by weight) were sterilized in the following manner, in order: 5 minutes of shaking with 70% ethanol, five water washes, overnight hydration in water at 4^0 C while rotating, 10 minute shaking with 30% clorox and a drop of dish soap, and then rinsed thoroughly with sterile water (>6 times). After sterilization, seeds for mutagenesis were treated with 2, 4, or 8 mM concentrations of ENU (*N*-ethyl-*N*-nitrosourea) in water (prepared from an 85 mM stock in acetic acid), or with 0.2%, 0.4%, or 0.8% EMS (Ethyl methanesulfonate) in water. Seeds were exposed

to mutagens for either 4 or 16 hours. After treatments, seeds were washed thoroughly with sterile water and then plated on ½ MS/0.8% Agar plates sealed with micropore tape and vernalized for 5 weeks in the dark at 4 degrees.

After cold treatment, plates were transferred to growth chambers at 25^0C with 12-hour light. Approximately 1-1.5 weeks after transfer to chambers, rate of germination was determined and seedlings were transferred to 12 well bedding pots with Metromix 360® soil (Sun Gro Horticulture, Bellevue, WA). Seedlings were grown in these pots until they were large enough (had several immature trifoliate leaves) to be transferred into 4-inch pots and moved into the greenhouse (set to ~20-25^0C). Percent of leaf sectoring and plant survival (for 16-hour treatment only) was recorded.

Seeds from approximately 600 M1 lines from the 4-hour treatments (344 0.4% EMS and 2514mM ENU) were collected and given to our collaborator Dr. Jing Wang at the Horticulture Institute, Jiangsu Academy of Agricultural Sciences, in Nanjing,China. In Nanjing, several seeds per line were germinated in bedding flats in the winter of 2011. Seedlings were then transferred to an open field in early spring of 2011. Many M2 plants died in the field due to poor growing conditions. Of the initial ~600 M1 lines sent to Nanjing, progeny from only 140 of these initial lines, represented by 1039 M2 plants, were alive (but not necessarily healthy) in June 2011 when Janet Slovin and Chunying Kang phenotyped and photographed them. DNA was isolated by JS and CK from 518 healthy M2 plants using the DNeasy kit from Qiagen.

Appendix B: Histone Deacetylase Genes in *Arabidopsis* Development

Preface

In the early stages of my research, I anticipated that my future research projects would revolve around the regulation of developmental genes through histone deacetylases (HDACs). At that time, the literature was lacking an up-to-date review article on the numerous HDACs in *Arabidopsis thaliana* and their various regulatory roles. The following chapter is the article written to fill that void: Hollender and Liu (2008) Histone Deacetylases Genes in *Arabidopsis* Development. *Journal of Integrative Plant Biology* 2008, **50** (7): 875–885.

Abstract

Histone acetylation and deacetylation are directly connected with transcriptional activation and silencing in eukaryotes. Gene families for enzymes that accomplish these histone modifications show surprising complexity in domain organization, tissue-specific expression, and function. This review is focused on the family of histone deacetylases (HDACs) that remove the acetyl group from core histone tails, resulting in a "closed" chromatin and transcriptional repression. In *Arabidopsis*, 18 HDAC genes are divided into three different types – RPD3-like, HD-tuin and sirtuin – with two or more members in each type. The structural feature of each HDAC class, the expression profile of each HDAC gene during development and functional insights of important family members are summarized here. It is clear that HDACs are an important class of global

transcriptional regulators that play crucial roles in plant development, defense, and adaptation.

Introduction

Chromatin, consisting of both DNA and proteins, is responsible for storing heritable and instructional information in a cell. Chromatin is highly organized and consists of nucleosomes. In each nucleosome, four core histone proteins – H2A, H2B, H3 and H4 – are organized into octameric protein complexes containing two molecules of each of the four core histones. Approximately 146 base pairs (bp) of DNA wrap around each nucleosome, and approximately 80bp of DNA link adjacent nucleosomes with the help of histone H1, forming the so-called "beads-on-a-string" organization. This basic level of chromatin packaging is further arranged into higher order conformations (Alberts et al. 2002). Protruding from the nucleosome are the positively charged amino-terminal tails of the core histone proteins that tightly associate with DNA's negatively-charged phosphate backbone. Reversible post-translational modifications of histone H3 and H4 amino-terminal tails, such as methylation, phosphorylation, ubiquitination, adenosine diphosphate (ADP)- ribosylation and acetylation, alter interactions between the DNA and core histones, resulting in changes in chromatin conformation. It was discovered that specific histone modifications at certain residues of the amino-terminal tails of H3 and H4 constitute the "histone code" that instructs the chromatin to adopt either "open" or "closed" configurations, thereby regulating the availability of *cis*-regulatory elements of genes to transcriptional machinery (Jenuwein and Allis, 2001). Some of the histone modifications, such as methylation, are heritable. Therefore, the histone code not only

expands the information-storing capacity of DNA but also offers rapid and reversible changes in chromatin accessibility when organisms are challenged with internal or external stresses. As plants are sessile, the ability to rapidly change their gene expression programs in response to internal or external stresses underlies the very plastic growth and developmental programs in plants.

Histone acetylation is a reversible process that plays vital roles in the epigenetic regulation described above. Therefore, histone acetylation and deacetylation are of particular importance to plant growth, development, defense and adaptation. Histone acetyltransferases (HATs) and histone deacetylases (HDACs) are enzymes required to perform histone acetylation and deacetylation, respectively, acting on the ε-amino group of lysine residues located near the amino-termini of core histone proteins. The prime acetylation targets are H3, lysine (K) residues 9, 14, 18 and 23, and H4 lysine (K) residues 8, 12, 16 and 20 (Fuchs et al., 2006). Although the lysine residues can only accommodate one acetyl group at a time, each nucleosome has over 20 possible targets for acetylation.

The addition of acetyl groups, mediated by HATs, neutralizes the positive charge of histone tails and decreases their affinity for DNA. Growing evidence also indicates that acetylation may help shape the binding surface for activators and repressors (Kurdistani and Grunstein, 2003). Thus, acetylation allows the chromatin to open up and provides transcription factors and RNA polymerases access to the DNA (Mutskov et al., 1998; Puig et al., 1998). This is supported by much experimental data indicating that

hyperacetylation of histone H3 and H4 is associated with transcriptionally active euchromatic regions. Hypoacetylation mediated by HDACs has an opposite effect on the chromatin, enabling the histones to bind more tightly to the negatively-charged DNA. As a result, hypoacetylation is associated with the repression of gene expression (Hebbes et al., 1988; Chen and Pikaard, 1997; Chua et al., 2001; Chua et al., 2003). In order to carry out their intended functions, HDACs and HATS interact with co-repressor or co-activator complexes, respectively, to regulate the expression of target genes (Utley et al., 1998; Gonzalez et al., 2007).

In this review, we will focus on describing the roles HDACs play in *Arabidopsis thaliana* development. These genes are emerging as crucial players in all aspects of plant development, including embryogenesis, abaxial/adaxial polarity determination, flowering and senescence as well as responses to day length and environmental stresses (Tian and Chen, 2001; Devoto et al., 2002; He et al., 2003; Song et al., 2005; Xu et al., 2005; Zhou et al., 2005; Benhamed et al., 2006; Long et al., 2006; Ueno et al., 2007; Tanaka et al., 2008; Wu et al., 2008).

Different HDAC Types

The HDACs can be grouped into three types (Figure 1; Table 1). The first type is homologous to the yeast *RPD3* (reduced potassium deficiency 3), which is present throughout eukaryotes and is most widely studied. The second type, the HD-tuins, appears to be present only in plants (Lusser et al., 1997; Wu et al., 2000a; Dangl et al., 2001). The structurally-distinct third type is homologous to the yeast Sir2, which is a

nicotinamide adenine dinucleotide (NAD)-dependent enzyme.

The type I (RPD3-like) superfamily HDACs in *A. thaliana* consist of 12 putative members (Pandey et al., 2002). All members have a characteristic histone deacetylase domain (Interpro: IPR003084) (Figure 1). Based on sequence similarity, they are further divided into three classes (Figure 1; Table 1)(Pandey et al., 2002). Class I encompasses HDA19, HDA6, HDA7 and HDA9. Class II includes HDA5, HDA15 and HDA18. HDA2 and its two additional isoforms comprise class III. HDA8, HDA14, HDA10 and HDA17 are unclassified members of the RPD3-like superfamily, with both HDA10 and HDA17 bearing similarity to HDA9. There is a lot of structural diversity within this superfamily of proteins. In addition to the conserved HDAC domain, three RPD3 family members (HDA6, 7 and 9) have polyglycine regions, five members (HDA6, 9, 15, 10 and 17) have aspartate-rich regions, one (HDA15) has a RanBP2- type zinc finger, and one (HDA18) has a coiled-coil domain (Figure 1).

The type II (HD-tuins) HDACs are plant-specific HDACs originally identified in maize (Lusser et al., 1997). Expressed sequence tag (EST) homology searches identified four *Arabidopsis* HD-tuins: HDT1–4 (Wu et al., 2000a; Dangl et al., 2001; Pandey et al., 2002). These proteins are structurally distinct from the RPD3 family and possess sequence similarity to the FKBP family peptidyl-prolyl *cis-trans* isomerase (Figure 1) (Aravind, 1998; Dangl et al., 2001). HD-tuins have a conserved amino terminal EFWG amino acid region, required for repression followed by a central acidic region rich in

Table 1. Summary of expression and function of *Arabidopsis* HDACs

Gene	Type	Localization and Expression	Function
HDA19 (At4G38130) (Also HD1, RPD3A)	RPD3 Class I	Globally expressed with highest expression in reproductive tissues (Schmid et al., 2005). Localizes in nucleus (but not nucleolus) (Fong et al., 2006; Long et al., 2006; Zhou et al., 2005)	Global repressor involved in embryonic and flower development, JA and ethylene pathways, stress responses, light responses, and the assimilation of T-DNA in *Agrobacterium*-mediated transformations.(Benhamed et al., 2006; Crane and Gelvin, 2007; Long et al., 2006; Tanaka et al., 2008; Tian and Chen, 2001; Tian et al., 2005; Tian et al., 2003; Wu et al., 2000a; Zhou et al., 2005)
HDA6 (At5G63110) (Also AXE1, RPD3B, Sil1)	RPD3 Class I	Globally expressed with highest level in reproductive tissues (Schmid et al., 2005). Localizes in nucleolus (Earley et al., 2006)	Global repressor involved in regulating flowering, senescence, JA pathway, repression of embryonic fate, and establishment of nucleolar dominance. In addition, it acts in the silencing of transgenes, transposons, and rDNA and maintaining proper DNA methylation patterns (Aufsatz et al., 2002; Devoto et al., 2002; Lippman et al., 2003; Probst et al., 2004; Tanaka et al., 2008; Wu et al., 2008; Zhou et al., 2005)
HDA7 (At5G35600)	RPD3 Class I	Low level expression in all tissues except stage 9 flowers, which show a higher level of expression (Schmid et al., 2005)	
HDA9 (At3G44680)	RPD3 Class I	Most highly expressed in shoot apex, young flower bud, and dry seed (Schmid et al., 2005)	
HDA5 (At5G61060)	RPD3 Class II	Low level expression globally; elevated expression in inflorescence meristem and young floral tissues (Schmid et al., 2005)	An increased root hair density in *hda5* mutants (Xu et al., 2005)
HDA15 (At3G18520)	RPD3 Class II	Low level expression globally; elevated expression in inflorescence meristem and young floral tissue (Schmid et al., 2005)	*hda15* mutant is resistant to Agrobacterium transformation (Crane and Gelvin, 2007)
HDA18 (At5G61070)	RPD3 Class II	Low level expression globally with elevated expression in inflorescence meristem and young flowers as well as pollen (Schmid et al., 2005)	Increased root hair density and altered cellular patterning in the epidermis of *hda18* mutant root (Xu et al., 2005)
HDA2 (At5G26040)	RPD3 Class III	Expressed in developing embryos and dry seeds (Schmid et al., 2005)	
HDA8 (At1G08460)	RPD3 Unclassified	Globally expressed with an increased expression in late stage seeds and a high level in pollen (Schmid et al., 2005)	

HDA14 (At4G33470)	RPD3 Unclassified	Expressed primarily in leaves and pedicels (Schmid et al., 2005).	Increased root hair density in *hda14* mutants (Xu et al., 2005)
HDA10 (At3G44660)	RPD3 Unclassified	Expressed primarily in the inflorescence meristem (Schmid et al., 2005)	
HDA17 (At3G44490)	RPD3 Unclassified	Expressed primarily in the inflorescence meristem (Schmid et al., 2005)	
HDT1 (At3G44750) (Also HD2A, HDA3)	HD-tuin	Expressed in flowers and young siliques (Wu et al., 2000), ovules, embryos, SAM, and primary leaves (Zhou et al., 2004). Localizes to nucleolus (Lawrence et al., 2004; Zhou et al., 2004)	Establishment of abaxial/adaxial leaf polarity, reproductive development, the establishment of nucleolar dominance, and the assimilation of T-DNA in *Agrobacterium*-mediated transformations (Crane and Gelvin, 2007; Lawrence et al., 2004; Pontes et al., 2007; Ueno et al., 2007; Wu et al., 2000b; Zhou et al., 2004)
HDT2 (At5G22650) (Also HD2, HD2B)	HD-tuin	Expressed globally including flowers, stems, leaves, young siliques, ovules, embryos, SAM, and primary leaves (Zhou et al., 2004). Localizes to nucleolus (Lusser et al., 1997; Zhou et al., 2004)	Establishment of abaxial/adaxial leaf polarity, reproductive development,, and the assimilation of T-DNA in *Agrobacterium*-mediated transformations (Crane and Gelvin, 2007; Lawrence et al., 2004; Ueno et al., 2007; Wu et al., 2000b; Zhou et al., 2004)
HDT3 (At5G03740) (Also HD2C)	HD-tuin	Expressed globally including ovules, embryos, SAM, and primary leaves. Localizes to nucleolus (Zhou et al., 2004)	Functions in reproductive development and ABA and abiotic stress response (Lawrence et al., 2004; Ueno et al., 2007; Wu et al., 2000b; Zhou et al., 2004)
HDT4 (At2G27840) (Also, HD2D)	HD-tuin	Expressed in stems, flowers, and young siliques (Zhou et al., 2004)	Increased root hair density in *hdt4* mutants (Xu et al., 2005)
SRT1 (At5G55760)	Sirtuin	Most highly expressed in reproductive tissues (Schmid et al., 2005)	In Arabidopsis, sirtinol (a specific inhibitor of sirtuin) inhibits proper hypocotyls and root development and vascularization. In rice, it plays a key role in hypersensitive responses to (Grozinger et al., 2001; Huang et al., 2007)
SRT2 (At5G09230)	Sirtuin	Globally expressed in all tissues (Schmid et al., 2005)	In Arabidopsis, sirtinol (a specific inhibitor of sirtuin) inhibits proper hypocotyls and root development and vascularization. In rice, it plays a key role in hypersensitive responses to (Grozinger et al., 2001; Huang et al., 2007)

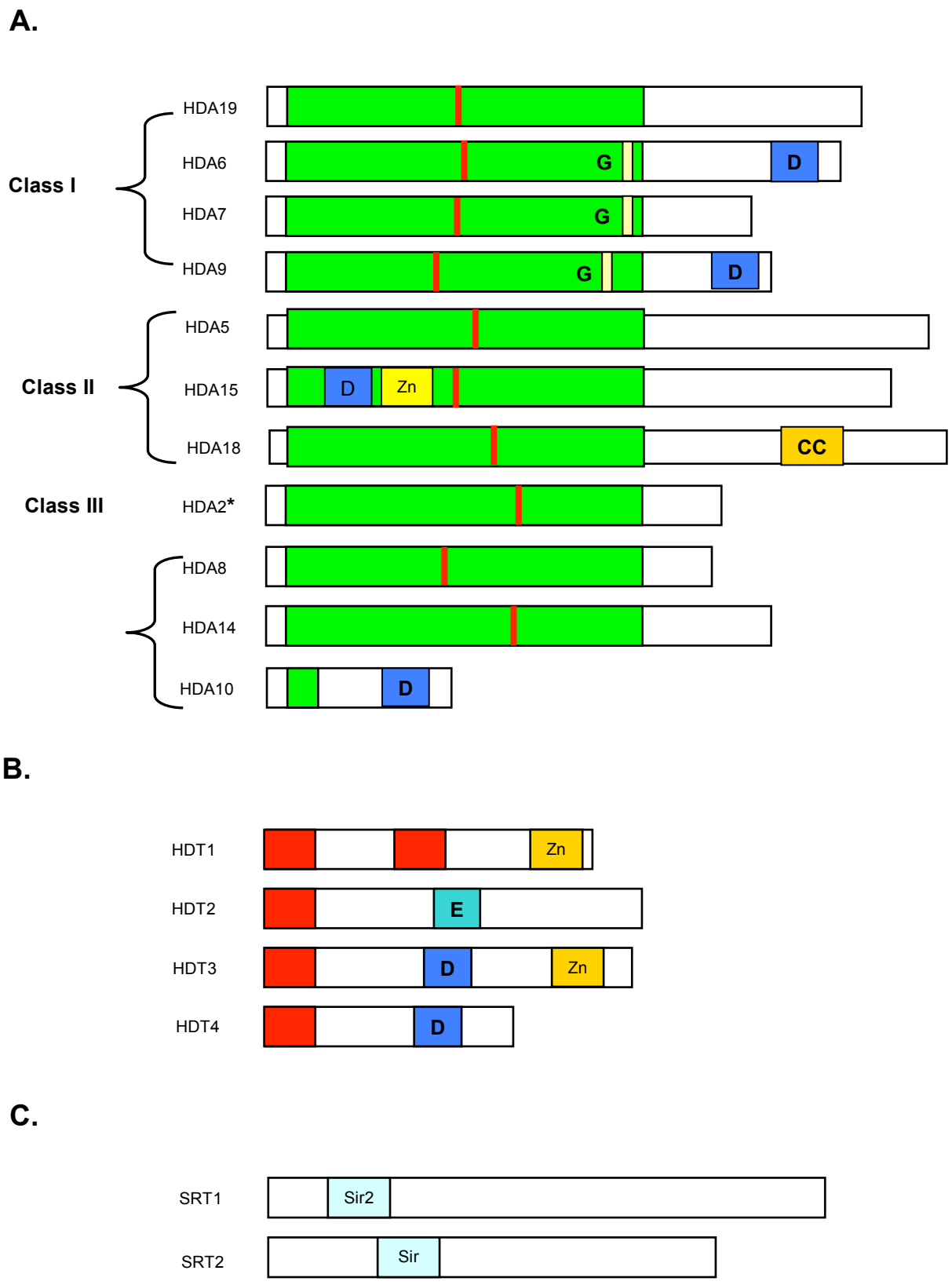

Figure 1. Domain organization of HDACs in *Arabidopsis thaliana*

Figure 1. Domain organization of HDACs in *Arabidopsis thaliana.* (A) Type I (RPD3-like superfamily) HDACs. Green boxes represent the conserved HDAC domain. Red regions are active sites necessary for histone deacetylase activity. *HDA2 isoform 2 is missing residues 268-387 and has a change at residue 253 from NRVYILDMY to SMIKTLYIS. *HDA2 isoform 3 is missing residues 208-235. HDA17 (At3G44490), which is similar to HDA9, is not shown. (B) Type II (HD-tuins) HDACs. The red bar at the amino terminus represents the conserved EFWG region required for repression. The red box in the HDT1 represents an acidic region required for repression. (C) Type III (Sirtuin) HDACs. Light blue boxes represent the conserved Sir2 domain. In all cases, G, D and E represent high glycine-, aspartate-, and glutamate-rich regions, respectively. CC represents a coiled-coil domain, and Zn represents a zinc finger domain. Domain organizations are drawn based on the UniProtKB (beta.uniprot.org).

glutamic and/or aspartic acid. In HDT1, this acidic region is essential for catalytic activity, as its deletion resulted in compromised HDAC activity (Wu et al., 2000a). HDT1 and HDT3 contain a single C2H2 type zinc finger domain in the carboxyl terminus, which may enable high affinity DNA-binding or mediate protein-protein interactions (Aravind, 1998; Wu et al., 2000a; Dangl et al., 2001; Zhou et al., 2004). However, for HDT1, the carboxyl terminal region including the zinc finger was shown to be unnecessary for transcription repression (Wu et al., 2000a).

The type III (sirtuin) HDACs are based on their sequence homology to the yeast silent information regulator 2 (Sir2) protein. They represent a unique group of NAD-dependent HDACs, which, unlike the Rpd3 and HD-tuin types, are not inhibited by trichostatin A (TSA) or sodium butyrate (Jung, 1997; Grozinger et al., 2001). The sirtuins in all organisms are divided into five classes based on sequence motifs within their highly conserved Sir2 domain (Frye, 2000; Imai et al., 2000). *Arabidopsis* has two sirtuin proteins, SRT1 and SRT2, belonging to classes IV and II, respectively. Interestingly, SRT2 has five or more alternate splice variants (Frye, 2000; Pandey et al., 2002). Much needs to be learned about sirtuins in plants.

Expression of HDACs

Because all three types of HDACs consist of two or more family members, one important question is whether these family members play similar or distinct roles. We analyzed the mRNA expression profiles of 16 HDACs using the microarray data from AtGenExpress

(Schmid et al., 2005), which examined mRNA expression in 79 diverse *Arabidopsis* tissues samples with the *Arabidopsis* ATH1 array. As shown in Figure 2, the four HD-tuins family members (HDT1–4) show highly similar expression profiles; all are highly expressed in inflorescences and young floral tissues but are underexpressed in vegetative tissues, pollens, seeds and late-stage flowers. With the exception of HDA7, the RPD3-class I HDAC genes (HDA6, HDA9 and HDA19) also exhibit similar expression profiles with high levels of expression in inflorescences and floral tissues and low levels of expression in vegetative tissues. In contrast, the two sirtuin family members SRT1 and SRT2 exhibit very different expression profiles and may act in different tissues, stages or processes. In addition, the RPD3-class III (HDA2) and RPD3-unclassified (HDA8 and HDA14) HDACs exhibited rather unique expression profiles, with HDA14 the most unique among all HDACs, suggesting a highly distinct function of HDA14

Functions of HDACs RPD3-like HDAC: HDA19

Among all HDACS in *Arabidopsis, HDA19* (also known as HD1 and RPD3A) is the most studied. *HDA19* is expressed in all tissues throughout the life of the plant with high levels of expression in reproductive tissues (Figure 2). Microarray data have revealed that over 7% of the genome is either up- or downregulated in *hda19* mutants, further illustrating the global role of HDA19 (Tian et al. 2005). Loss-of-function via antisense RNA and transferred DNA (T-DNA) insertion as well as overexpression via *35S::HDA19* studies support that HDA19 is a global regulator of gene expression in development and stress responses (Tian and Chen, 2001; Tian et al., 2003; Tian et al., 2005; Zhou et al., 2005). A wide range of developmental abnormalities was observed in these loss-of-function *hda19* lines.

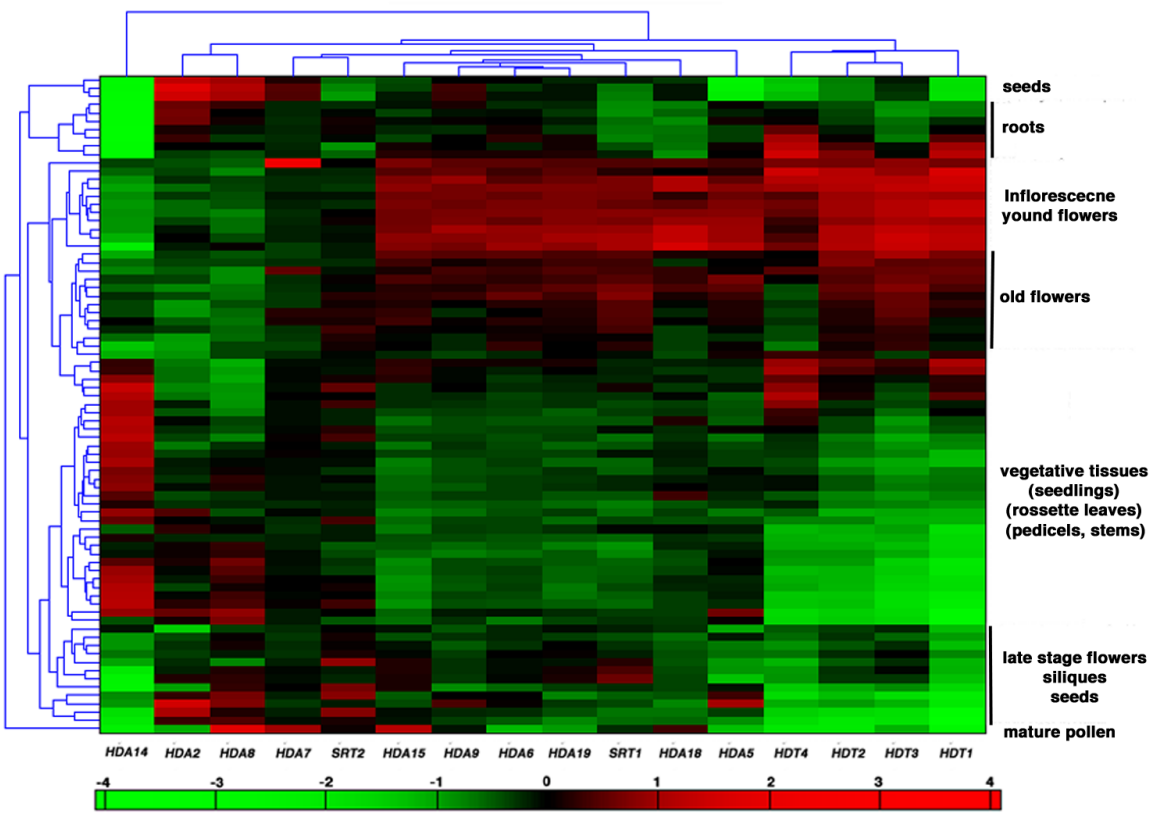

Figure 2. Hierarchal cluster analysis of HDAC expression profile in different tissues and developmental stages. HDAC gene names are indicated below each column; tissue type is indicated on the right. An increase in expression in a specific tissue is indicated by red, a decrease in expression is indicated by green, no change in expression is indicated by black (see the bar below the clustergram for specific fold change). The clustergram was generated with the Matlab RC13 (Mathworks) Bioinformatics Toolbox utilizing the data generated by AtGenExpress (development) (Schmid et al., 2005).

The mutant plants were shorter and flowers were abnormal (Figure 3). *hda19* flowers showed reduced numbers of petals, shorter stamen, reduced male and female fertility, and smaller siliques that often contain aborted seeds. Some showed premature death of seedlings, asymmetrical development of the first two leaves, serrated and narrow leaves, and a prominent left-handed twist of rosette leaves. *hda19-1*, a T-DNA insertion line, is temperature-sensitive. At an elevated temperature (29 ◦C), seedlings developed disorganized root and shoot meristems with shoot meristems forming pin or tubular or single cotyledon phenotype. These phenotypes resemble those of the *Arabidopsis topless* (*tpl*) mutants (Long et al., 2006). Recent experiments illustrated a redundant role of *HDA19* and *HDA6* in the repression of embryonic program and embryogenesis-related genes after germination (Tanaka et al., 2008). In addition, 9% of 151 HDA19 antisense RNA lines experienced embryonic defects with many not surviving past 2 weeks (Tian and Chen, 2001). Many of these early seedling abnormalities could result from ectopic expression of normally silenced genes in germinated seedlings, such as embryogenesis-related genes *LEAFY COTYLEDON1* (*LEC1*) and *FUSCA3* (*FUS3*)(Tanaka et al., 2008), as well as precocious expression of floral-specific gene *SUPERMAN* (*SUP*), and *NO APICAL MERISTEM* (*NAM*) (Tian and Chen, 2001; Tian et al., 2003).

In addition to development, *HDA19* also regulates plants' response to their environment. *Hda19* loss-of-function lines are slightly late flowering under long day (LD) conditions (Tian et al., 2003). While mutants of a histone acetyltransferase GCN5 showed a long-hypocotyl phenotype and a reduced expression of light-inducible genes, *hda19* mutants showed opposite effects. The double *gcn5;hda19* mutants were restored to normal.

Figure 3. Representative phenotypes of *hda19* (Salk_139445) plants. (A) A photo showing *hda19* (left) and wild type (right) plants. Both are in Col-0 background. (B) A wild type flower. (C) A flower from *hda19* plants growing at 20ºC. (C) A flower from *hda19* plants growing at 29ºC. The more severe flower phenotype at 29ºC suggests that the *hda19* mutation is sensitive to high temperature.

Chromatin immunoprecipitation experiments revealed that *gcn5* mutants exhibited reduced histone acetylation on the promoter regions of *CAB2, RBCS-1A* and *IAA3. hda19* mutants, on the other hand, exhibited increased histone acetylation on the pro- moters of the same genes (Benhamed et al., 2006). Therefore, HDA19 works antagonistically with the GCN5 to regulate light- mediated processes.

Using HDA19 promoter-driven reporters, Zhou et al. (2005) showed that *HDA19* transcription is induced by treatment with jasmonic acid (JA), ethylene, wounding, or pathogen infection. Plants expressing *35S::HDA19* not only exhibited generally decreased histone acetylation levels, but also an increased expression of ethylene response factor1 (ERF1) as well as an enhanced resistance to pathogen *A. brassicicola*. Ethylene and JA regulated *PATHOGENESIS- RELATED* (*PR*) genes (basic chitinase and β-1,3-glucanase) were also upregulated (Zhou et al., 2005). *HDA19-RNAi* plants showed opposite phenotypes and reduced expressions of corresponding downstream genes (Zhou et al., 2005). These data suggest that HDA19 regulates gene expression in the JA and ethylene signaling pathways in response to pathogens.

Histone deacetylases often act as part of larger protein complexes. Experimental evidence has linked HDA19 with several such complexes. HDA19 protein was shown to interact with the LEUNIG/SEUSS co-repressor complex, which, among other functions, is involved in the suppression of carpel and stamen identity in the outer two floral whorls by repressing *AGAMOUS* expression (Sridhar et al., 2004; Gonzalez et al., 2007; Liu and Karmarkar, 2008). Interestingly, loss-of-function *hda19* mutants exhibited a floral

phenotype similar to those of *leunig* (Tian and Chen, 2001; Tian et al., 2003). *hda19* was shown to genetically interact with the *tpl* co-repressor, which possesses similar protein domains as the LEUNIG co-repressor. *hda19* mutants also exhibited a similar embryonic phenotype to *tpl-1* (Long et al., 2006).

The defects in acetylation and deacetylation are mostly reversible as phenotypic defects of *hda19* mutant plants were rescued in the heterozygous F1 progeny of a backcross to wild type. These F1 plants exhibited wild type levels of acetylation and showed no change in DNA methylation levels (Wu et al., 2000b; Tian and Chen, 2001; Tian et al., 2003). Interestingly, *hda19/+* plants retain the same reduced levels of H3 lysine 9 methylation as homozygous *hda19/hda19* plants (Tian et al., 2005).

RPD3-like HDAC: HDA6

The *HDA6* gene is required for the silencing of transgenes, transposable elements and ribosomal RNA (rRNA) genes (Murfett et al., 2001; Aufsatz et al., 2002; Lippman et al., 2003; Lawrence et al., 2004; Probst et al., 2004). Several *hda6* mutant alleles were identified in genetic screens designed to isolate mutants with increased expression of transgenes. Both post- transcriptional gene silencing (Murfett et al., 2001) and RNA-directed DNA methylation (Aufsatz et al., 2002) were thought to be involved. It was also shown that, like DNA methyltransferase (MET1) and chromatin remodeling adenosine triphosphatase (DDM1), HDA6 can silence the majority of the transposable element and may act along a similar pathway as MET1 and DDM1 (Lippman et al., 2003). Most interestingly, HDA6 localizes, in part, to the nucleolus and HDA6 was shown to play a

role in the epigenetic mechanism that underlies rRNA gene silencing in nucleolar dominance. Specifically, in *Arabidopsis suecica*, the allotetraploid hybrid of *A. thaliana* and *A. arenosa*, the *A. thaliana*- derived rRNA genes are selectively silenced (Chen et al., 1998), a phenomenon called nucleolar dominance similar to the X-chromosome inactivation in mammals. In HDA6-RNAi knock-down lines, the rRNA genes in the allotetraploid hybrid *Arabidopsis* are derepressed, as is the decondensation of the nucleolus organizer region (NOR), loss of DNA cytosine methylation at the ribosomal DNA (rDNA) promoter, and the loss of histone H3K9 dimethylation that is accompanied with the gain of H3K4 trimethylation, H3K9 acetylation, H3K14 acetylation and histone H4 tetra-acetylation (Lawrence et al., 2004).

Given the highly similar gene expression profiles and sequence similarity between HDA6 and HDA19 (Figure 2), it is not surprising that HDA6 and HDA19 regulate, perhaps redundantly, many of the same processes including suppression of embryonic program after germination, mediation of JA and ethylene signaling pathways, and promotion of flowering and senescence (Devoto et al., 2002; Zhou et al., 2005; Tanaka et al., 2008; Wu et al., 2008). In addition to decreased expression of JA responsive genes, PDF1.2, VSP2, JIN1 and ERF1 in *hda6* loss- of-function mutants or RNA interference (RNAi) lines (Wu et al., 2008), HDA6 protein was found to interact with COI1, a F-box protein involved in JA signal perception or transduction (Devoto et al., 2002). F-box proteins are members of the SCF complexes that target specific proteins for ubiquitination and degradation. It is likely that the COI1-SCF complex regulates JA responsive genes by targeted ubiquitination and degradation of HDA6.

Additional RPD3-like HDACs

In *Arabidopsis*, single-layered root epidermal cells differentiate into hair and non-hair cells in a position-dependent manner. Treatment with TSA, a specific inhibitor of HDAC, and *hda18* loss-of-function mutants showed increases in root hair density in the seedlings (Xu et al., 2005). Therefore, histone deacetylation may regulate key genes in root epidermal cell differentiation by, perhaps, mediating positional cues in roots.

HDA15 is unique among HDACs because it has a RanBP2- type zinc finger, which is known to associate with receptor- mediated transport between the nucleus and cytoplasm. Despite its unique domain, HDA15, like HDA19, HDT1 and HTD2, is involved in the assimilation of T-DNA in *Agrobacterium*-mediated transformations. HDA15-RNAi transgenic lines showed a "resistant to *Agrobacterium* transformation" phenotype (Crane and Gelvin, 2007).

Type II (HD-tuin) HDACs

This is a plant-specific class of HDACs, which is of particular interest because HD-tuins may have evolved to perform plant- specific functions. With the exception of HDT4, the other three HD-tuins have been characterized in further detail. For example, HDT1, HDT2 and HDT3 were shown to repress transcription when they were fused to a GAL4 DNA binding domain and tethered to reporter genes in planta (Wu et al., 2000a; Wu et al., 2003), and the amino-terminal EFWG and the histidine 25 (a potential catalytic residue) were shown to be important for the repressor activity (Zhou et al., 2004). *In situ* hybridization revealed that HDT1, HDT2 and HDT3 were all expressed in ovules,

embryos, shoot apical meristem and leaves. More interestingly, their expression was strongly induced during the process of somatic embryogenesis (Zhou et al., 2004). The *in situ* data is in general agreement with the microarray data (Figure 2), which showed that all family members are expressed in inflorescences and young as well as old flowers. The highly similar mRNA expression profiles among the four HD-tuins (Figure 2) suggest potential functional redundancy.

Consistent with its expression in ovules, embryos and during somatic embryogenesis, HDT1-silencing resulted in aborted seeds (Wu et al., 2000b). In contrast, 35S::GFP-HDT1 lines showed high frequencies of developmental abnormalities such as curved, narrow or branching leaf phenotypes, flowers with shorter filaments, aborted seed development, sterility and late flowering (Wu et al., 2000a; Zhou et al., 2004). This overexpression of *HDT1* also resulted in the repression of genes associated with embryo development (Zhou et al., 2004).

Like HDA6, HDT1 plays a role in rRNA silencing. HDT1-RNAi resulted in the release of silencing of the *Arabidopsis* rRNA, an increase in histone H3K4 methylation, and the loss of cytosine methylation at rDNA in *A. suecica*, the allotetraploid hybrid of *A. thaliana* and *A. arenosa* (Lawrence et al., 2004).

HDT1 and HDT2 act in leaf polarity determination (Ueno et al., 2007). Specifically, HDT1-RNAi and HDT2-RNAi in *asymmetric leaf* 2 (*as2*) or *as1* mutant background caused decreased adaxial gene *PHABULOSA* (*PHB*) expression and increased abaxial

FILAMENTOUS FLOWER (*FIL*) expression, which correlated with the formation of abaxialized and filamentous leaves (Ueno et al., 2007). Further experimental data suggested that HDT1 and HDT2 could interact with AS1 or AS2 to regulate the generation or distribution of microRNA 165/166, which targets the *PHB* transcripts (Kidner and Martienssen, 2004).

Recently, it was shown that HDT3 is involved in abscisic acid (ABA) stress response (Sridha and Wu, 2006). HDT3 expression is repressed by ABA and overexpressing a HDT3-GFP transgene resulted in ABA insensitivity, reduced transpiration, and increased tolerance to salt and drought stresses. The expression of several ABA response genes was affected in these HDT3 overexpression lines (Sridha and Wu, 2006).

Type III (sirtuin) HDACs

In yeast, Sir2 primarily deacetylates H4 lysine16, H3 lysine 56 and H3 lysine 9 and, to a lesser degree, H3 lysine14 (Imai et al., 2000; Xu et al., 2007). In addition to their histone deacetylation ability, yeast Sir2, and its bacterial and mammalian homologs, have NAD-dependent ADP-ribolsyl transferase activity, whose function is distinct from its HDAC activity (Frye, 1999; Imai et al., 2000). Yeast Sir2 is primarily involved in the silencing of telomeres, rRNA, silent mating type loci, and the suppression of rDNA recombination (Rine and Herskowitz, 1987; Gottlieb and Esposito, 1989; Smith and Boeke, 1997; Imai et al., 2000; Xu et al., 2007). Sir2 also has a role in cell longevity. It is involved in preventing the formation of extra-chromosomal rDNA circles associated with cell aging. Sir2 promotes longevity in worms and flies, and mitotically active yeasts lacking Sir2

have reduced life spans, while those with an extra copy live longer (Kaeberlein et al., 1999; Blander and Guarente, 2004). However, Sir2 accelerates aging of cells growing in hypocaloric media (Fabrizio et al., 2005).

In contrast to yeast, there is little experimental data available about plant sirtuin HDACs. Treatment with sirtinol, an inhibitor of sirtuin, inhibits body-axis formation and vascularization in *Arabidopsis* seedlings (Grozinger et al., 2001); these phenotypes resemble those of the *monopterous* mutants defective in auxin signaling (Przemeck et al., 1996; Hardtke and Berleth, 1998). Therefore, SRT1 and SRT2 may have a role in auxin signaling.

In rice, OsSRT1 is highly expressed in rapidly dividing cells, and RNAi knockdown induced DNA fragmentation and cell death, accompanied by an increased hydrogen peroxide production. This phenotype correlated with reduced H3 lysine 9 dimethylation and increase H3 lysine 9 acetylation in transposon and HR gene regions, suggesting a role for plant sirtuins in the HR response (Huang et al., 2007).

Conclusion

HDACs play both global and specific roles in gene regulation through their abilities to modify histones and change chromatin conformation. Much remains unknown as to the functional diversity and functional redundancy among different HDACs. One of the major challenges for plant biologists is the large number of HDAC genes, the possible large variety of HDAC- containing chromatin complexes, and the interactions among

different transcription networks that utilize these HDACs. With the rapid development of new sequencing technologies as well as various tools for transcriptome and proteome analyses and modeling, plant scientists are poised to make major contributions toward understanding the epigenetic regulatory mechanisms underlying the plasticity of plants.

Appendix C: *Arabidopsis* mutant alleles and genotyping primers

Table 1. *Arabidopsis* mutant alleles

Mutant allele	Origin	Ecotype	Strength	Description	Reference
ant-9	Activator (Ac) element insertion	Originally in C24 then crossed into Ler	Strong	Contains an Ac element in the forward orientation in the second intron, which is within the first AP2 domain region.	Elliot et al (1996)
ap2-2	EMS mutagenesis	Ler	Strong	Contains a C to T transition mutation in a splicing acceptor site, and results in a stop codon immediately before the second exon, changing the CAG to a TAG This is likely a null allele, as the stop codon is early on in the gene sequence (base 446 of the 2486bp) genomic DNA sequence.	Meyerowitz et al. (1989); Bowman et al. (1991b)[+]
ett-1	T-DNA mutagenesis	WsO	Strong	Contains a T-DNA insertion (with a non-standard T-DNA sequence) in the second exon in middle of the following sequence: TAT GCT CAA ***insert*** GTC. The T-DNA is in the forward orientation.	Feldmann (1991); Sessions and Zambryski (1995); Sessions et al. (1997)
ett-2	T-DNA mutagenesis	WsO	Weak	Contains a nonsenense mutation created during the T-DNA mutagenesis. There was a transition of a G to an A at the last base of the 5th exon creating a stop codon (CTT TAG in Wt became CTT TAA).	Feldmann (1991); Sessions and Zambryski (1995); Sessions et al (1997)
lug-3	EMS mutagenesis of *ap1-1*	Ler	Strong	Harbors a C to T transition, causing a glutamine to change into a STOP codon in the N-terminal region.	Liu and Meyerowitz (1995); Connor and Liu (2000)
lug-8	EMS mutagenesis	Ler	Weak	This allele has a transition mutation of C to a T in the middle of the 4 exon (at gDNA base 1612), causing CAG CAG CAA to become CAG CAG TAA, and changing the Glutamine at amino acid 153 to become a STOP codon. This stop codon is in the N terminal Q-rich region known for activation.	Liu and Meyerowitz; Hollender (2011) Unpublished[+]

lug-16	EMS mutagenesis of Ler	Ler	Weak	Contains a missense mutation, where a G changed to an A at the splicing acceptor site immediately before the start of the third exon. (tagCTA became taaCTA)	Connor and Liu (2000)
seu-1	EMS mutagenesis of *ufo*-6	Ler	Weak	Contains a C to T transition resulting in a **T**AA Stop codon in in place of a **G**AA glutamine at amino acid 501, which is in the dimerization domain.	Levin et al 1998; Franks el al (2002)
spt-2	EMS mutagenesis of Ler	Ler	Strong	This allele has a R209K missense mutation, within the basic region of a bHLH DNA binding domain. The sequence AGG A**G**G AGA at the beginning of the 3rd exon becomes AGG A**A**G AGA. It is a likely null because the mutated arginine is conserved for bHLH domains and *spt-2* has a similar phenotype to known null *spt-3* (which has a stop codon at amino acid 149). The mutation is at a possible nuclear localization sequence, KRR, thus it could interfere with nuclear localization. *spt-2* is listed as a recessive antimorph on TAIR, but no reference given.	Alvarez and Smyth 2002[+]

[+]Specific base changes in these alleles are not published, but were determined by Courtney Hollender

Table 2. *Arabidopsis* genotyping primers

Genotyping primers					
	Primers	Temp	Band size (bp)	Enz.	Misc.
ap2-2	Ap2-2 fwd CTA GCC ACC GGA TCG TCC GCG GG ap2-2 rev GAT ATC CGC TTC TAC TCC ACG G	55	Wt: 250 & 300 Mut: 550	AlwnI	CAPS primers. AlwnI Cuts Wt sequence. [1]
ant-9	ANT wildtype Fwd 5' GAGGGGACAAGAGGATGTTG 3' ANT wildtype Rev 5' TGAGCTTCATATCTACCAGTCCA *ant*-9 mutant Reverse 5' ACGATAACGGTCGGTCGGTA	55	Wt: 222 Mut: 229		SSLP primers. Do one PCR for Wt and one for mutant. Use 50 cycles and 60s elongation. [2]
ETT wildtype (for ett-1)	Fwd-ett1 genotype Anneals 200 bp upstream of T-DNA insert 5' TCT TCA GTT TTT TCT TTG ATG ATA Rev-ett1 genotype Anneals 200 bp downstream of insert 5' AGG AGT ATT AGA CCT CTT AAG CAC	53	400		Based on T-DNA insertion. Do one PCR for Wt, and one for mutant. [*]
ett-1	Fwd-ett1 genotype 5' TCT TCA GTT TTT TCT TTG ATG ATA LB-ett1 genotype Anneals T-DNA (-) strand 350 bp past insert 5' TAC CGT GAT ATT ATT ATA GAA TCC TG	53	550		
ett-2	ETT Wt primer Fwd 5' GTG ATG CTG TGC TTT TCC TTC G ett-2 mutant forward primer version 2 5' CTG GTG ATG CTG TGC TTT TCC TTT A Reverse primer (version 2) (check tube names) 5' ACT TGG GGT TGT AGG AAA TGC TG	66	258		SAP PCR. Do 2 PCRs, one for Wt (with Wt fwd) and one for mutant (with *ett-2* forward) [*]
GUS	New GUS F.391 ACC GTT TGT GTG AAC AAC GA GUS-reverse GTC TGG CTT TTG GCT GTG AC	55	~400 bp		34 cycles. There is always some background in Wt. [3]

GFP	GFP-F 5' GGTGAAGGTGATGCAACATACGGA GFP-R 5' GGGCCATCGCCAATTGGAGTATTT	65	479		30 cycles. [4]
lug-3	lug3-R2-WT-1979 5' TTG ATG TTG TTG TTG CTG CGG lug3-R1-Mut-1979 5' TTG ATG TTG TTG TTG CTG CCA lug3-F-1678 ACT AAG CTG GAG TAT TTC TAT TT	57	300		SAP primers. Do 2 PCRs, one for Wt, and one for mutant. [5]
For lug-8 genotyping, two versions of Fwd primers exist as well as two versions of dCAPS reverse primers. You can use either Fwd with either reverse, just use the correct enzyme and know if it cuts wt or mutant. Run on a 1.5-2 % gel.					
lug-8	lug8dCapsF3 TTC GTG TGT TTC TTA CAG ACA CAG ATG A	58	261		40 cycles. *
	lug8dCapsF4 CAC AGA TGA TCA AAG CAC GAG	58	242		40 cycles. F4 is a little better than F3 with R2.*
	lug8dCapsR AGG TGG TTG GTT TTG ATG TTG TTG TA			AluI	Wt gets cut. *
	lug8dCaps_R2_RsaI AGG TGG TTG GTT TTG ATG TTG TTG GT			RsaI	Mutant is cut. *
seu-1	*seu-1* dCAPS F 5' ACA ACA GAT TCT GCT CTT CCG GAG GT *seu-1* dCAPS R 5' TTA CCT GCA AAC ACC GAA CA	55		RsaI	dCAPS primers. Wt gets cut.[2]
spt-2	Wt SPT SAP Fwd v4 5' TT TCT TGT AAC AGA GGC G Spt-2 SAP fwd v4 5' CTT TCT TGT AAC AGA GGC A SPT rev SAP 4 5' TAG AAG GTT CCCA AAG CGT A	57	~550		SAP primers. *

* Primer designed by Courtney Hollender
[1] Primer sequence from Jeff Long via Xuemei Chen
[2] Primer sequence from Bob Franks
[3] Primer sequence from Zhongchi Liu and Parsa Hosseni
[4] Primer sequence from Chloe Mara
[5] Primer sequence from Minh Bui

References

Alvarez, J. and Smyth, D. R. (1999) 'CRABS CLAW and SPATULA, two Arabidopsis genes that control carpel development in parallel with AGAMOUS', *Development* 126(11): 2377-86.

Alvarez, J. and Smyth, D. R. (2002) 'CRABS CLAW and SPATULA genes regulate growth and pattern formation during gynoecium development in Arabidopsis Thaliana', *Int. J. Plant Sci.* 163(1): 17-41.

Anderson, H. and Guttridge, C. (1982) 'Strawberry truss morphology and the fate of high-order flower buds', *Crop Res. (Hort. Res)* 22: 105-122.

Aravind, L. (1998) 'Second Family of Histone Deacetylases', *Science* 280(5367): 1167a-1167.

Archbold, D. and Dennis, F. (1985) 'Strawberry receptacle growth and endogenous IAA content as affected by growth regulator application and achene removal.', *Journals of the American Society of Horticultural Science* 110: 816-820.

Archbold, D. D. and Dennis, F. G. (1984) 'Quantification of free ABA and free and conjugated IAA in strawberry achene and receptacle tissue during fruit development ', *Journal of the American Society for Horticultural Science* 109: 330-335.

Aufsatz, W., Mette, M. F., van der Winden, J., Matzke, M. and Matzke, A. J. (2002) 'HDA6, a putative histone deacetylase needed to enhance DNA methylation induced by double-stranded RNA', *EMBO J* 21(24): 6832-41.

Aukerman, M. J. and Sakai, H. (2003) 'Regulation of flowering time and floral organ identity by a MicroRNA and its APETALA2-like target genes', *Plant Cell* 15(11): 2730-41.

Bao, F., Azhakanandam, S. and Franks, R. G. (2010) 'SEUSS and SEUSS-LIKE Transcriptional Adaptors Regulate Floral and Embryonic Development in Arabidopsis', *PLANT PHYSIOLOGY* 152(2): 821-836.

Becker, A. and Theissen, G. (2003) 'The major clades of MADS-box genes and their role in the development and evolution of flowering plants', *Mol Phylogenet Evol* 29(3): 464-89.

Benhamed, M., Bertrand, C., Servet, C. and Zhou, D. X. (2006) 'Arabidopsis GCN5, HD1, and TAF1/HAF2 interact to regulate histone acetylation required for light-responsive gene expression', *Plant Cell* 18(11): 2893-903.

Blander, G. and Guarente, L. (2004) 'The Sir2 family of protein deacetylases', *Annu Rev Biochem* 73: 417-35.

Bowman, J. L., Drews, G. N. and Meyerowitz, E. M. (1991a) 'Expression of the Arabidopsis floral homeotic gene AGAMOUS is restricted to specific cell types late in flower development', *Plant Cell* 3(8): 749-58.

Bowman, J. L., Smyth, D. R. and Meyerowitz, E. M. (1989) 'Genes directing flower development in Arabidopsis', *Plant Cell* 1(1): 37-52.

Bowman, J. L., Smyth, D. R. and Meyerowitz, E. M. (1991b) 'Genetic interactions among floral homeotic genes of Arabidopsis', *Development* 112(1): 1-20.

Buzgo, M., Soltis, D., Soltis, P. and Ma, H. (2004) 'Towards a comprehensive integration of morphological and genetic studies of floral development', *Trends Plant Sci* 9(4): 164-173.

Castillejo, C., de la Fuente, J. I., Iannetta, P., Botella, M. A. and Valpuesta, V. (2004) 'Pectin esterase gene family in strawberry fruit: study of FaPE1, a ripening-specific isoform', *J. Exp. Bot.* 55(398): 909-918.

Chen, X. (2004) 'A microRNA as a translational repressor of APETALA2 in Arabidopsis flower development', *Science* 303(5666): 2022-5.

Chen, Z. J., Comai, L. and Pikaard, C. S. (1998) 'Gene dosage and stochastic effects determine the severity and direction of uniparental ribosomal RNA gene silencing (nucleolar dominance) in Arabidopsis allopolyploids', *Proc Natl Acad Sci USA* 95(25): 14891-6.

Chen, Z. J. and Pikaard, C. S. (1997) 'Epigenetic silencing of RNA polymerase I transcription: a role for DNA methylation and histone modification in nucleolar dominance', *Genes Dev* 11(16): 2124-36.

Chua, Y. L., Brown, A. P. and Gray, J. C. (2001) 'Targeted histone acetylation and altered nuclease accessibility over short regions of the pea plastocyanin gene', *Plant Cell* 13(3): 599-612.

Chua, Y. L., Watson, L. A. and Gray, J. C. (2003) 'The transcriptional enhancer of the pea plastocyanin gene associates with the nuclear matrix and regulates gene expression through histone acetylation', *Plant Cell* 15(6): 1468-79.

Coen, E. (2001) 'Goethe and the ABC model of flower development', *C R Acad Sci III, Sci Vie* 324(6): 523-30.

Coen, E. S. and Meyerowitz, E. M. (1991) 'The war of the whorls: genetic interactions controlling flower development', *Nature* 353(6339): 31-7.

Colbert, T., Till, B. J., Tompa, R., Reynolds, S., Steine, M. N., Yeung, A. T., McCallum, C. M., Comai, L. and Henikoff, S. (2001) 'High-throughput screening for induced point mutations', *Plant Physiol.* 126(2): 480-484.

Comai, L. and Henikoff, S. (2006) 'TILLING: practical single-nucleotide mutation discovery', *Plant J* 45(4): 684-694.

Conner, J. and Liu, Z. (2000) '*LEUNIG*, a putative transcriptional corepressor that regulates *AGAMOUS* expression during flower development', *Proceedings of the National Academy of Sciences U. S. A.* 97: 12902-12907.

Crane, Y. M. and Gelvin, S. B. (2007) 'RNAi-mediated gene silencing reveals involvement of Arabidopsis chromatin-related genes in Agrobacterium-mediated root transformation', *Proc Natl Acad Sci USA* 104(38): 15156-61.

Dangl, M., Brosch, G., Haas, H., Loidl, P. and Lusser, A. (2001) 'Comparative analysis of HD2 type histone deacetylases in higher plants', *Planta* 213(2): 280-5.

Darrow, G. (1966) *The Strawberry: History, Breeding and Physiology*, New York: Holt, Rinehart and Winston.

Davies, B., Egea-Cortines, M., de Andrade Silva, E., Saedler, H. and Sommer, H. (1996) 'Multiple interactions amongst floral homeotic MADS box proteins', *EMBO J* 15(16): 4330-43.

Davis, T. and Yu, H. (1997) 'A linkage map of the diploid strawberry, *Fragaria vesca*', *Journal of Heredity* 88: 215-221.

Deng, C. and Davis, T. M. (2001) 'Molecular identification of the yellow fruit color (c) locus in diploid strawberry: a candidate gene approach', *Theor. Appl. Genet.* 103: 316-322.

Devoto, A., Nieto-Rostro, M., Xie, D., Ellis, C., Harmston, R., Patrick, E., Davis, J., Sherratt, L., Coleman, M. and Turner, J. G. (2002) 'COI1 links jasmonate signalling and fertility to the SCF ubiquitin-ligase complex in Arabidopsis', *Plant J* 32(4): 457-66.

Ditta, G., Pinyopich, A., Robles, P., Pelaz, S. and Yanofsky, M. F. (2004) 'The SEP4 gene of Arabidopsis thaliana functions in floral organ and meristem identity', *Curr Biol* 14(21): 1935-40.

Drews, G. N., Bowman, J. L. and Meyerowitz, E. M. (1991) 'Negative regulation of the Arabidopsis homeotic gene AGAMOUS by the APETALA2 product', *Cell* 65(6): 991-1002.

Dubois, A., Raymond, O., Maene, M., Baudino, S., Langlade, N. B., Boltz, V., Vergne, P. and Bendahmane, M. (2010) 'Tinkering with the C-Function: A Molecular Frame for the Selection of Double Flowers in Cultivated Roses', *PLoS ONE* 5(2): e9288.

Durner, E. F. and Poling, E. B. (1988) 'Strawberry developmental responses to photoperiod and temperature: A review', *Advances in Strawberry Production* 7: 6-14.

Earley, K. W., Haag, J., Pontes, O., Opper, K., Juehne, T., Song, K. and Pikaard, C. S. (2006) 'Gateway-compatible vectors for plant functional genomics and proteomics', *Plant J* 45(4): 616-29.

Egea-Cortines, M., Saedler, H. and Sommer, H. (1999) 'Ternary complex formation between the MADS-box proteins SQUAMOSA, DEFICIENS and GLOBOSA is involved in the control of floral architecture in Antirrhinum majus', *EMBO J* 18(19): 5370-9.

Fabrizio, P., Gattazzo, C., Battistella, L., Wei, M., Cheng, C., McGrew, K. and Longo, V. D. (2005) 'Sir2 blocks extreme life-span extension', *Cell* 123(4): 655-67.

Fahlgren, N., Montgomery, T. A., Howell, M. D., Allen, E., Dvorak, S. K., Alexander, A. L. and Carrington, J. C. (2006) 'Regulation of AUXIN RESPONSE FACTOR3 by TAS3 ta-siRNA affects developmental timing and patterning in Arabidopsis', *Curr Biol* 16(9): 939-44.

Fait, A., Hanhineva, K., Beleggia, R., Dai, N., Rogachev, I., Nikiforova, V. J., Fernie, A. R. and Aharoni, A. (2008) 'Reconfiguration of the achene and receptacle metabolic networks during strawberry fruit development', *Plant Physiol*.

Fan, H. Y., Hu, Y., Tudor, M. and Ma, H. (1997) 'Specific interactions between the K domains of AG and AGLs, members of the MADS domain family of DNA binding proteins', *Plant J* 12(5): 999-1010.

Folta, K. M. and Dhingra, A. (2007) 'Transformation of strawberry: the basis for translational genomics in Rosaceae', *In Vitro Cellular and Developmental Biology - Plant* 42(6): 482–490

Franks, R. G., Liu, Z. and Fischer, R. L. (2006) '*SEUSS* and *Leunig* regulate cell proliferation, vascular development, and organ polarity in *Arabidopsis* petals', *Planta*.

Franks, R. G., Wang, C., Levin, J. Z. and Liu, Z. (2002) 'SEUSS, a member of a novel family of plant regulatory proteins, represses floral homeotic gene expression with LEUNIG', *Development* 129(1): 253-63.

Frye, R. A. (1999) 'Characterization of five human cDNAs with homology to the yeast SIR2 gene: Sir2-like proteins (sirtuins) metabolize NAD and may have protein ADP-ribosyltransferase activity', *Biochemical and Biophysical Research Communications* 260(1): 273-9.

Frye, R. A. (2000) 'Phylogenetic classification of prokaryotic and eukaryotic Sir2-like proteins', *Biochem Biophys Res Commun* 273(2): 793-8.

Fuchs, J., Demidov, D., Houben, A. and Schubert, I. (2006) 'Chromosomal histone modification patterns--from conservation to diversity', *Trends Plant Sci* 11(4): 199-208.

Fujimoto, S. Y., Ohta, M., Usui, A., Shinshi, H. and Ohme-Takagi, M. (2000) 'Arabidopsis ethylene-responsive element binding factors act as transcriptional activators or repressors of GCC box-mediated gene expression', *Plant Cell* 12(3): 393-404.

Galletta, G. J. and Himelrick, D. G. (1990) *Small Fruit Crop Management*, Engelwood Cliffs: Prentice Hall.

Giovannoni, J. (2001) 'Molecular biology of fruit maturation and ripening', *Annu. Rev. Plant Physiol. Plant Mol. Biol.* 52: 725-749.

Gonzalez, D., Bowen, A. J., Carroll, T. S. and Conlan, R. S. (2007) 'The transcription corepressor LEUNIG interacts with the histone deacetylase HDA19 and mediator components MED14 (SWP) and CDK8 (HEN3) to repress transcription', *Mol Cell Biol* 27(15): 5306-15.

Goto, K. and Meyerowitz, E. M. (1994) 'Function and regulation of the Arabidopsis floral homeotic gene PISTILLATA', *Genes Dev* 8(13): 1548-60.

Gottlieb, S. and Esposito, R. E. (1989) 'A new role for a yeast transcriptional silencer gene, SIR2, in regulation of recombination in ribosomal DNA', *Cell* 56(5): 771-776.

Gremski, K., Ditta, G. and Yanofsky, M. F. (2007) 'The HECATE genes regulate female reproductive tract development in Arabidopsis thaliana', *Development* 134(20): 3593-601.

Grigorova, B., Mara, C., Hollender, C., Sijacic, P., Chen, X. and Liu, Z. (2011) 'LEUNIG and SEUSS co-repressors regulate miR172 expression in Arabidopsis flowers', *Development* 138(12): 2451-2456.

Groszmann, M., Bylstra, Y., Lampugnani, E. R. and Smyth, D. R. (2010) 'Regulation of tissue-specific expression of SPATULA, a bHLH gene involved in carpel development, seedling germination, and lateral organ growth in Arabidopsis', *J Exp Bot* 61(5): 1495-508.

Groszmann, M., Paicu, T., Alvarez, J. P., Swain, S. M. and Smyth, D. R. (2011) 'SPATULA and ALCATRAZ, are partially redundant, functionally diverging bHLH genes required for Arabidopsis gynoecium and fruit development', *Plant J* 68(5): 816-29.

Grozinger, C. M., Chao, E. D., Blackwell, H. E., Moazed, D. and Schreiber, S. L. (2001) 'Identification of a class of small molecule inhibitors of the sirtuin family of NAD-dependent deacetylases by phenotypic screening', *J Biol Chem* 276(42): 38837-43.

Guilfoyle, T. J. and Hagen, G. (2007) 'Auxin response factors', *Curr Opin Plant Biol* 10(5): 453-60.

Gutterson, N. and Reuber, T. L. (2004) 'Regulation of disease resistance pathways by AP2/ERF transcription factors', *Curr Opin Plant Biol* 7(4): 465-71.

Hancock, J. F. (1999) *Strawberries*, New York: CABI Publishing.

Hardtke, C. and Berleth, T. (1998) 'The Arabidopsis gene MONOPTEROS encodes a transcription factor mediating embryo axis formation and vascular development ', *The EMBO journal* 17(5): 1405-1411.

Haring, M., Offermann, S., Danker, T., Horst, I., Peterhansel, C. and Stam, M. (2007) 'Chromatin immunoprecipitation: optimization, quantitative analysis and data normalization', *Plant Methods* 3: 11.

Hartmann, H. T. (1947) 'Some effects of temperature and photoperiod on flower formation and runner production in the strawberry', *PLANT PHYSIOLOGY* 22(4): 407-20.

He, Y., Michaels, S. D. and Amasino, R. M. (2003) 'Regulation of flowering time by histone acetylation in Arabidopsis', *Science* 302(5651): 1751-4.

Hebbes, T. R., Thorne, A. W. and Crane-Robinson, C. (1988) 'A direct link between core histone acetylation and transcriptionally active chromatin', *EMBO J* 7(5): 1395-402.

Heisler, M. G., Atkinson, A., Bylstra, Y. H., Walsh, R. and Smyth, D. R. (2001) 'SPATULA, a gene that controls development of carpel margin tissues in Arabidopsis, encodes a bHLH protein', *Development* 128(7): 1089-98.

Hellens, R., Allan, A., Friel, E., Bolitho, K., Grafton, K., Templeton, M., Karunairetnam, S., Gleave, A. and Laing, W. (2005) 'Transient expression vectors for functional genomics, quantification of promoter activity and RNA silencing in plants', *Plant Methods* 1: 13.

Hollender, C. A., Geretz, A. C., Slovin, J. P. and Liu, Z. (2011) 'Flower and early fruit development in a diploid strawberry, Fragaria vesca', *Planta*.

Hollender, C. A. and Liu, Z. (2010) 'Bimolecular fluorescence complementation (BiFC) assay for protein-protein interaction in onion cells using the helios gene gun', *J. Vis. Exp.*(40).

Honma, T. and Goto, K. (2001) 'Complexes of MADS-box proteins are sufficient to convert leaves into floral organs', *Nature* 409(6819): 525-9.

Huang, L., Sun, Q., Qin, F., Li, C., Zhao, Y. and Zhou, D. X. (2007) 'Down-regulation of a SILENT INFORMATION REGULATOR2-related histone deacetylase gene, OsSRT1, induces DNA fragmentation and cell death in rice', *Plant Physiol* 144(3): 1508-19.

Hummer, K. E. and Hancock, J. F. (2009) Strawberry Genomics: Botanical History, Cultivation, Traditional Breeding, and New Technologies. in K. Folta and S. E. Gardiner (eds.) *Genetics and Genomics of Rosaceae, Plant Genetics and Genomic: Crops and Models 6*: Springer Science + Business Media, LLC.

Hytönen, T., Elomaa, P., Moritz, T. and Junttila, O. (2009) 'Gibberellin mediates daylength-controlled differentiation of vegetative meristems in strawberry (*Fragaria* x *ananassa* Duch)', *BMC Plant Biology* 9(1): 18.

Imai, S., Armstrong, C. M., Kaeberlein, M. and Guarente, L. (2000) 'Transcriptional silencing and longevity protein Sir2 is an NAD-dependent histone deacetylase', *Nature* 403(6771): 795-800.

Jenuwein, T. and Allis, C. D. (2001) 'Translating the histone code', *Science* 293(5532): 1074-80.

Jiménez, G., Paroush, Z. and Ish-Horowicz, D. (1997) 'Groucho acts as a corepressor for a subset of negative regulators, including Hairy and Engrailed', *Genes Dev* 11(22): 3072-82.

Jofuku, K. D., den Boer, B. G., Van Montagu, M. and Okamuro, J. K. (1994) 'Control of Arabidopsis flower and seed development by the homeotic gene APETALA2', *Plant Cell* 6(9): 1211-25.

Jung, M., Hoffmann, K, Brosch, G., and Loidl, P. (1997) 'Analogues of Trichostatin A and Trapoxin B as histone deacetylase inhibitors.', *Bioor. Med. Chemm. Lett.* 7: 1655-1658.

Kaeberlein, M., McVey, M. and Guarente, L. (1999) 'The SIR2/3/4 complex and SIR2 alone promote longevity in Saccharomyces cerevisiae by two different mechanisms', *Genes Dev* 13(19): 2570-80.

Kania, W. (1973) 'Entwicklungsgeschichtliche Untersuchungen an Rasaceenbluten', *Bot. Jb. Syst.* 93: 175-246.

Kidner, C. A. and Martienssen, R. A. (2004) 'Spatially restricted microRNA directs leaf polarity through ARGONAUTE1', *Nature* 428(6978): 81-4.

Krizek, B. A. and Fletcher, J. C. (2005) 'Molecular mechanisms of flower development: an armchair guide', *Nat Rev Genet* 6(9): 688-98.

Krizek, B. A. and Meyerowitz, E. M. (1996) 'Mapping the protein regions responsible for the functional specificities of the Arabidopsis MADS domain organ-identity proteins', *Proc Natl Acad Sci U S A* 93(9): 4063-70.

Krizek, B. A. and Sulli, C. (2006) 'Mapping sequences required for nuclear localization and the transcriptional activation function of the Arabidopsis protein AINTEGUMENTA', *Planta* 224(3): 612-21.

Kronenberg, H. (1959) 'Poor fruit setting in strawberries. I', *Euphytica* 8(1): 47-57.

Kurdistani, S. K. and Grunstein, M. (2003) 'In vivo protein-protein and protein-DNA crosslinking for genomewide binding microarray', *Methods* 31(1): 90-5.

Lawrence, R. J., Earley, K., Pontes, O., Silva, M., Chen, Z. J., Neves, N., Viegas, W. and Pikaard, C. S. (2004) 'A concerted DNA methylation/histone methylation switch regulates rRNA gene dosage control and nucleolar dominance', *Mol Cell* 13(4): 599-609.

Lippman, Z., May, B., Yordan, C., Singer, T. and Martienssen, R. (2003) 'Distinct mechanisms determine transposon inheritance and methylation via small interfering RNA and histone modification', *PLoS Biol* 1(3): E67.

Liu, C. M. and Meinke, D. W. (1998) 'The titan mutants of Arabidopsis are disrupted in mitosis and cell cycle control during seed development', *Plant J* 16(1): 21-31.

Liu, Z., Franks, R. G. and Klink, V. P. (2000) 'Regulation of gynoecium marginal tissue formation by LEUNIG and AINTEGUMENTA', *Plant Cell* 12(10): 1879-92.

Liu, Z. and Karmarkar, V. (2008) 'Groucho/Tup1 family co-repressors in plant development', *Trends Plant Sci*.

Liu, Z. and Meyerowitz, E. M. (1995) 'LEUNIG regulates AGAMOUS expression in Arabidopsis flowers', *Development* 121(4): 975-91.

Long, J. A., Ohno, C., Smith, Z. R. and Meyerowitz, E. M. (2006) 'TOPLESS regulates apical embryonic fate in Arabidopsis', *Science* 312(5779): 1520-3.

Lusser, A., Brosch, G., Loidl, A., Haas, H. and Loidl, P. (1997) 'Identification of maize histone deacetylase HD2 as an acidic nucleolar phosphoprotein', *Science* 277(5322): 88-91.

Maes, T., Van de Steene, N., Zethof, J., Karimi, M., D'Hauw, M., Mares, G., Van Montagu, M. and Gerats, T. (2001) 'Petunia Ap2-like genes and their role in flower and seed development', *Plant Cell* 13(2): 229-44.

Mandel, M. A., Bowman, J. L., Kempin, S. A., Ma, H., Meyerowitz, E. M. and Yanofsky, M. F. (1992) 'Manipulation of flower structure in transgenic tobacco', *Cell* 71(1): 133-43.

Mizukami, Y. and Ma, H. (1992) 'Ectopic expression of the floral homeotic gene AGAMOUS in transgenic Arabidopsis plants alters floral organ identity', *Cell* 71(1): 119-31.

Mouhu, K., Hytönen, T., Folta, K., Rantanen, M., Paulin, L., Auvinen, P. and Elomaa, P. (2009) 'Identification of flowering genes in strawberry, a perennial SD plant', *BMC Plant Biol* 9: 122.

Murfett, J., Wang, X. J., Hagen, G. and Guilfoyle, T. J. (2001) 'Identification of Arabidopsis histone deacetylase HDA6 mutants that affect transgene expression', *Plant Cell* 13(5): 1047-61.

Mutskov, V., Gerber, D., Angelov, D., Ausio, J., Workman, J. and Dimitrov, S. (1998) 'Persistent interactions of core histone tails with nucleosomal DNA following acetylation and transcription factor binding', *Mol Cell Biol* 18(11): 6293-304.

Nemhauser, J., Feldman, L. and Zambryski, P. (2000) 'Auxin and ETTIN in Arabidopsis gynoecium morphogenesis', *Development* 127: 3877 - 3888.

Nitsch, J. P. (1950) 'Growth and morphogenesis of the strawberry as related to auxin', *American Journal of Botany* 37: 211-215.

Nole-Wilson, S. and Krizek, B. A. (2000) 'DNA binding properties of the Arabidopsis floral development protein AINTEGUMENTA', *Nucleic Acids Res* 28(21): 4076-82.

Ohme-Takagi, M. and Shinshi, H. (1995) 'Ethylene-inducible DNA binding proteins that interact with an ethylene-responsive element', *Plant Cell* 7(2): 173-82.

Ohtsu, K., Smith, M., Emrich, S., Borsuk, L., Zhou, R., Chen, T., Zhang, X., Timmermans, M., Beck, J., Buckner, B. et al. (2007) 'Global gene expression analysis of the shoot apical meristem of maize (Zea mays L.)', *The Plant Journal* 52(3): 391 - 404.

Okamuro, J. K., Caster, B., Villarroel, R., Van Montagu, M. and Jofuku, K. D. (1997a) 'The AP2 domain of APETALA2 defines a large new family of DNA binding proteins in Arabidopsis', *Proc Natl Acad Sci U S A* 94(13): 7076-81.

Okamuro, J. K., Caster, B., Villarroel, R., Van Montagu, M. and Jofuku, K. D. (1997b) 'The AP2 domain of APETALA2 defines a large new family of DNA binding proteins in Arabidopsis', *Proc Natl Acad Sci USA* 94(13): 7076-81.

Oosumi, T., Gruszewski, H., Blischak, L., Baxter, A., Wadl, P., Shuman, J., Veilleux, R. E. and Shulaev, V. (2006) 'High-efficiency transformation of the diploid strawberry (Fragaria vesca) for functional genomics', *Planta* 223(6): 1219-30.

Pandey, R., Muller, A., Napoli, C. A., Selinger, D. A., Pikaard, C. S., Richards, E. J., Bender, J., Mount, D. W. and Jorgensen, R. A. (2002) 'Analysis of histone acetyltransferase and histone deacetylase families of Arabidopsis thaliana suggests functional diversification of chromatin modification among multicellular eukaryotes', *Nucleic Acids Res* 30(23): 5036-55.

Parenicová, L., de Folter, S., Kieffer, M., Horner, D. S., Favalli, C., Busscher, J., Cook, H. E., Ingram, R. M., Kater, M. M., Davies, B. et al. (2003) 'Molecular and phylogenetic analyses of the complete MADS-box transcription factor family in Arabidopsis: new openings to the MADS world', *Plant Cell* 15(7): 1538-51.

Pelaz, S., Ditta, G. S., Baumann, E., Wisman, E. and Yanofsky, M. F. (2000) 'B and C floral organ identity functions require SEPALLATA MADS-box genes', *Nature* 405(6783): 200-3.

Pelaz, S., Tapia-Lopez, R., Alvarez-Buylla, E. R. and Yanofsky, M. F. (2001) 'Conversion of leaves into petals in Arabidopsis', *Curr Biol* 11(3): 182-4.

Perkins-Veazie, P. M. (1995) 'Growth and ripening of strawberry fruit', *Horticultural Reviews* 17: 267-297.

Perkins-Veazie, P. M., Huber, D. J. and Brecht, J. K. (1995) 'Characterization of ethylene production in developing strawberry fruit', *Plant Growth Regulation* 17: 33-39.

Pfluger, J. and Zambryski, P. (2004) 'The role of SEUSS in auxin response and floral organ patterning', *Development* 131(19): 4697-707.

Pre, M., Atallah, M., Champion, A., De Vos, M., Pieterse, C. M. J. and Memelink, J. (2008) 'The AP2/ERF Domain Transcription Factor ORA59 Integrates Jasmonic Acid and Ethylene Signals in Plant Defense', *PLANT PHYSIOLOGY* 147(3): 1347-1357.

Probst, A. V., Fagard, M., Proux, F., Mourrain, P., Boutet, S., Earley, K., Lawrence, R. J., Pikaard, C. S., Murfett, J., Furner, I. et al. (2004) 'Arabidopsis histone deacetylase HDA6 is required for maintenance of transcriptional gene silencing and determines nuclear organization of rDNA repeats', *Plant Cell* 16(4): 1021-34.

Przemeck, G., Mattsson, J., Hardtke, C., Sung, Z., Berleth and T (1996) 'Studies on the role of the Arabidopsis gene MONOPTEROS in vascular development and plant cell axialization', *Planta* 200(2): 229-237.

Puig, O. M., Bellés, E., López-Rodas, G., Sendra, R. and Tordera, V. (1998) 'Interaction between N-terminal domain of H4 and DNA is regulated by the acetylation degree', *Biochim Biophys Acta* 1397(1): 79-90.

Qin, Y., Teixeira da Silva, J. A., Zhang, L. and Zhang, S. (2008) 'Transgenic strawberry: state of the art for improved traits', *Biotechnol Adv* 26(3): 219-32.

Reganold, J., Andrews, P., Reeve, J., Carpenter-Boggs, L., Schadt, C., Alldredge, J. R., Ross, C., Davies, N. and Zhou, J. (2010) 'Fruit and soil quality of organic and conventional strawberry agroecosystems', *PLoS ONE* 5(9).

Riechmann, J. L., Krizek, B. A. and Meyerowitz, E. M. (1996a) 'Dimerization specificity of Arabidopsis MADS domain homeotic proteins APETALA1, APETALA3, PISTILLATA, and AGAMOUS', *Proc Natl Acad Sci U S A* 93(10): 4793-8.

Riechmann, J. L. and Meyerowitz, E. M. (1997) 'MADS domain proteins in plant development', *Biol Chem* 378(10): 1079-101.

Riechmann, J. L. and Meyerowitz, E. M. (1998) 'The AP2/EREBP family of plant transcription factors', *Biol Chem* 379(6): 633-46.

Riechmann, J. L., Wang, M. and Meyerowitz, E. M. (1996b) 'DNA-binding properties of Arabidopsis MADS domain homeotic proteins APETALA1, APETALA3, PISTILLATA and AGAMOUS', *Nucleic Acids Res* 24(16): 3134-41.

Rine, J. and Herskowitz, I. (1987) 'Four genes responsible for a position effect on expression from HML and HMR in Saccharomyces cerevisiae', *Genetics* 116(1): 9-22.

Rosin, F., Aharoni, A., Salentijn, E., Schaart, J. G., Boone, M. J. and Hannapel, D. (2003) 'Expression patterns of a putative homolog of AGAMOUS, STAG1, from strawberry', *Plant Science*.

Rousseau-Gueutin, M., Lerceteau-Köhler, E., Barrot, L., Sargent, D. J., Monfort, A., Simpson, D., Arús, P., Guérin, G. and Denoyes-Rothan, B. (2008) 'Comparative genetic mapping between octoploid and diploid Fragaria species reveals a high level of colinearity between their genomes and the essential disomic behavior of the cultivated octoploid strawberry', *Genetics* 179(4): 2045-2060.

Sanders, P. M., Bui, A. Q., Weterings, K., Mcintire, K. N., Hsu, Y., Lee, P. Y., Truong, M. T., Beals, T. P. and Goldberg, R. B. (1999) 'Anther developmental defects in Arabidopsis thaliana male-sterile mutants', *Sex Plant Reprod* 11: 297-322.

Sargent, D. J., Davis, T. and Simpson, D. (2009) Strawberry (*Fragaria* spp.) Structural Genomics. in K. Folta and S. E. Gardiner (eds.) *Genetics and Genomics of Rosaceae, Plant Genetics and Genomics: Crops and Models 6*. New York: Springer Science + Business Media, LLC.

Schmid, M., Davison, T., Henz, S., Pape, U., Demar, M., Vingron, M., Scholkopf, B., Weigel, D. and Lohmann, J. (2005) 'A gene expression map of Arabidopsis thaliana development', *Nat Genet* 37: 501 - 506.

Schwab, W., Schaart, J. and Rosati, C. (2009) Functional Molecular Biology Research in *Fragaria*. in K. Folta and S. E. Gardiner (eds.) *Genetics and Genomics of Rosaceae, Plant Genetics and Genomics: Crops and Models 6*. New York,: Springer Science + Business Media, LLC.

Serçe, S. and Hancock, J. F. (2005) 'The temperature and photoperiod regulation of flowering and runnering in the strawberries, *Fragaria chiloensis, F. virginiana,* and *F.* x ananassa.', *Scientia Horticulturae* 103: 167-177.

Sessions, A., Nemhauser, J. L., McColl, A., Roe, J. L., Feldmann, K. A. and Zambryski, P. C. (1997) 'ETTIN patterns the Arabidopsis floral meristem and reproductive organs', *Development* 124(22): 4481-91.

Sessions, R. and Zambryski, P. (1995) 'Arabidopsis gynoecium structure in the wild and in ettin mutants', *Development* 121: 1519 - 1532.

Sheen, J. (2001) 'Signal transduction in maize and Arabidopsis mesophyll protoplasts', *PLANT PHYSIOLOGY* 127(4): 1466-75.

Sheen, J. (2002) A transient expression assay using Arabidopsis mesophyll protoplasts. http://genetics.mgh.harvard.edu/sheenweb/.

Shulaev, V., Korban, S. S., Sosinski, B., Abbott, A., Aldwinckle, H. S., Folta, K. M., Iezzoni, A., Main, D., Arús, P., Dandekar, A. M. et al. (2008) 'Multiple models for Rosaceae genomics', *Plant Physiol.* 147(3): 985-1003.

Shulaev, V., Sargent, D. J., Crowhurst, R. N., Mockler, T. C., Folkerts, O., Delcher, A. L., Jaiswal, P., Mockaitis, K., Liston, A., Mane, S. P. et al. (2011) 'The genome of woodland strawberry (Fragaria vesca)', *Nat Genet* 43(2): 109-16.

Sitaraman, J., Bui, M. and Liu, Z. (2008) 'LEUNIG_HOMOLOG and LEUNIG perform partially redundant functions during Arabidopsis embryo and floral development', *PLANT PHYSIOLOGY* 147(2): 672-81.

Slovin, J. and Michael, T. (2011) Strawberry. Part 3 Structural and Functional Genomics. in K. Folta and C. Kole (eds.) *Genetics, Genomics and Breeding of Berries.* Enfield, New Hampshire.: Science Publishers.

Slovin, J. and Rabinowicz, P. D. (2007) *Fragaria vesca*, a useful tool for Rosaceae genomics. in F. Takeda (ed.) *6th North American Strawberry Symposium*. Ventura, CA: American Society for Horticultural Science.

Slovin, J. P., Schmitt, K. and Folta, K. M. (2009) 'An inbred line of the diploid strawberry Fragaria vesca f. semperflorens for genomic and molecular genetic studies in the Rosaceae', *Plant Methods* 5: 15.

Smaczniak, C., Immink, R. G. H., Muiño, J. M., Blanvillain, R., Busscher, M., Busscher-Lange, J., Dinh, Q. D. P., Liu, S., Westphal, A. H., Boeren, S. et al. (2012) 'Characterization of MADS-domain transcription factor complexes in Arabidopsis flower development', *Proc Natl Acad Sci USA* 109(5): 1560-5.

Smith, J. and Boeke, J. (1997) 'An unusual form of transcriptional silencing in yeast ribosomal DNA', *Genes Dev* 11(2): 241-54.

Smyth, D. R., Bowman, J. L. and Meyerowitz, E. M. (1990) 'Early flower development in Arabidopsis', *Plant Cell* 2(8): 755-67.

Song, C. P., Agarwal, M., Ohta, M., Guo, Y., Halfter, U., Wang, P. and Zhu, J. K. (2005) 'Role of an Arabidopsis AP2/EREBP-type transcriptional repressor in abscisic acid and drought stress responses', *Plant Cell* 17(8): 2384-96.

Sridha, S. and Wu, K. (2006) 'Identification of AtHD2C as a novel regulator of abscisic acid responses in Arabidopsis', *Plant J* 46(1): 124-33.

Sridhar, V. V., Surendrarao, A., Gonzalez, D., Conlan, R. S. and Liu, Z. (2004) 'Transcriptional repression of target genes by *LEUNIG* and *SEUSS*, two interacting regulatory proteins for *Arabidopsis* flower development', *Proceedings of the National Academy of Sciences* 101(31): 11494-11499.

Sridhar, V. V., Surendrarao, A. and Liu, Z. (2006) 'APETALA1 and SEPALLATA3 interact with SEUSS to mediate transcription repression during flower development', *Development* 133(16): 3159-66.

Stangeland, B. and Salehian, Z. (2002) 'An improved clearing method for GUS assay in Arabidopsis endosperm and seeds ', *Plant Molecular Biology Reporter* 20: 107-114.

Taiz, L. and Zeiger, E. (2006) Ethylene: The Gaseous Hormone *PLANT PHYSIOLOGY*. Sunderland, Massachusetts: Sinauer Associates, Inc.

Tanaka, M., Kikuchi, A. and Kamada, H. (2008) 'The Arabidopsis histone deacetylases HDA6 and HDA19 contribute to the repression of embryonic properties after germination', *Plant Physiol* 146(1): 149-61.

Teale, W. D., Paponov, I. A. and Palme, K. (2006) 'Auxin in action: signalling, transport and the control of plant growth and development', *Nat Rev Mol Cell Biol* 7(11): 847-859.

Theissen, G., Becker, A., Di Rosa, A., Kanno, A., Kim, J. T., Münster, T., Winter, K. U. and Saedler, H. (2000) 'A short history of MADS-box genes in plants', *Plant Mol Biol* 42(1): 115-49.

Theissen, G. and Saedler, H. (2001) 'Plant biology. Floral quartets', *Nature* 409(6819): 469-71.

Tian, L. and Chen, Z. J. (2001) 'Blocking histone deacetylation in Arabidopsis induces pleiotropic effects on plant gene regulation and development', *Proc Natl Acad Sci USA* 98(1): 200-5.

Tian, L., Fong, M. P., Wang, J. J., Wei, N. E., Jiang, H., Doerge, R. W. and Chen, Z. J. (2005) 'Reversible histone acetylation and deacetylation mediate genome-wide, promoter-dependent and locus-specific changes in gene expression during plant development', *Genetics* 169(1): 337-45.

Tian, L., Wang, J., Fong, M. P., Chen, M., Cao, H., Gelvin, S. B. and Chen, Z. J. (2003) 'Genetic control of developmental changes induced by disruption of Arabidopsis histone deacetylase 1 (AtHD1) expression', *Genetics* 165(1): 399-409.

Tiwari, S. B., Hagen, G. and Guilfoyle, T. (2003) 'The roles of auxin response factor domains in auxin-responsive transcription', *Plant Cell* 15(2): 533-43.

Trainotti, L., Pavanello, A. and Casadoro, G. (2005) 'Different ethylene receptors show an increased expression during the ripening of strawberries: does such an increment imply a role for ethylene in the ripening of these non-climacteric fruits?', *J. Exp. Bot.* 56(418): 2037-2046.

Tröbner, W., Ramirez, L., Motte, P., Hue, I., Huijser, P., Lönnig, W. E., Saedler, H., Sommer, H. and Schwarz-Sommer, Z. (1992) 'GLOBOSA: a homeotic gene which interacts with DEFICIENS in the control of Antirrhinum floral organogenesis', *EMBO J* 11(13): 4693-704.

Ueno, Y., Ishikawa, T., Watanabe, K., Terakura, S., Iwakawa, H., Okada, K., Machida, C. and Machida, Y. (2007) 'Histone deacetylases and ASYMMETRIC LEAVES2 are involved in the establishment of polarity in leaves of Arabidopsis', *Plant Cell* 19(2): 445-57.

Ulmasov, T., Hagen, G. and Guilfoyle, T. J. (1999a) 'Activation and repression of transcription by auxin-response factors', *Proc Natl Acad Sci U S A* 96(10): 5844-9.

Ulmasov, T., Hagen, G. and Guilfoyle, T. J. (1999b) 'Dimerization and DNA binding of auxin response factors', *Plant J* 19(3): 309-19.

Utley, R. T., Ikeda, K., Grant, P. A., Côté, J., Steger, D. J., Eberharter, A., John, S. and Workman, J. L. (1998) 'Transcriptional activators direct histone acetyltransferase complexes to nucleosomes', *Nature* 394(6692): 498-502.

Walter, M., Chaban, C., Schütze, K., Batistic, O., Weckermann, K., Näke, C., Blazevic, D., Grefen, C., Schumacher, K., Oecking, C. et al. (2004) 'Visualization of protein interactions in living plant cells using bimolecular fluorescence complementation', *Plant J* 40(3): 428-38.

Weberling, F. (1989) *Morphology of Flowers & Influorescences*, Cambridge: Cambridge University Press.

Williamson, S. C., Yu, H. and Davis, T. M. (1995) 'Shikamate dehydrogenase allozymes: inheritance and close linkage to fruit color in the diploid strawberry', *Journal of Heredity* 86(1): 74-76.

Wollmann, H., Mica, E., Todesco, M., Long, J. A. and Weigel, D. (2010) 'On reconciling the interactions between APETALA2, miR172 and AGAMOUS with the ABC model of flower development', *Development* 137(21): 3633-42.

Wu, K., Malik, K., Tian, L., Brown, D. and Miki, B. (2000a) 'Functional analysis of a RPD3 histone deacetylase homologue in Arabidopsis thaliana', *Plant Mol Biol* 44(2): 167-76.

Wu, K., Tian, L., Malik, K., Brown, D. and Miki, B. (2000b) 'Functional analysis of HD2 histone deacetylase homologues in Arabidopsis thaliana', *Plant J* 22(1): 19-27.

Wu, K., Tian, L., Zhou, C., Brown, D. and Miki, B. (2003) 'Repression of gene expression by Arabidopsis HD2 histone deacetylases', *Plant J* 34(2): 241-7.

Wu, K., Zhang, L., Zhou, C., Yu, C. W. and Chaikam, V. (2008) 'HDA6 is required for jasmonate response, senescence and flowering in Arabidopsis', *J Exp Bot*.

Würschum, T., Gross-Hardt, R. and Laux, T. (2006) 'APETALA2 regulates the stem cell niche in the Arabidopsis shoot meristem', *Plant Cell* 18(2): 295-307.

Wynne, J. and Treisman, R. (1992) 'SRF and MCM1 have related but distinct DNA binding specificities', *Nucleic Acids Res* 20(13): 3297-303.

Xu, C. R., Liu, C., Wang, Y. L., Li, L. C., Chen, W. Q., Xu, Z. H. and Bai, S. N. (2005) 'Histone acetylation affects expression of cellular patterning genes in the Arabidopsis root epidermis', *Proc Natl Acad Sci USA* 102(40): 14469-74.

Xu, F., Zhang, Q., Zhang, K., Xie, W. and Grunstein, M. (2007) 'Sir2 deacetylates histone H3 lysine 56 to regulate telomeric heterochromatin structure in yeast', *Molecular Cell* 27(6): 890-900.

Xu, Z.-S., Chen, M., Li, L.-C. and Ma, Y.-Z. (2011) 'Functions and application of the AP2/ERF transcription factor family in crop improvement', *Journal of Integrative Plant Biology* 53(7): 570-85.

Yanofsky, M. F., Ma, H., Bowman, J. L., Drews, G. N., Feldmann, K. A. and Meyerowitz, E. M. (1990) 'The protein encoded by the Arabidopsis homeotic gene agamous resembles transcription factors', *Nature* 346(6279): 35-9.

Zhao, L., Kim, Y., Dinh, T. T. and Chen, X. (2007a) 'miR172 regulates stem cell fate and defines the inner boundary of APETALA3 and PISTILLATA expression domain in Arabidopsis floral meristems', *Plant J* 51(5): 840-9.

Zhao, L., Kim, Y., Dinh, T. T. and Chen, X. (2007b) 'miR172 regulates stem cell fate and defines the inner boundary of *APETALA3* and *PISTILLATA* expression domain in *Arabidopsis* floral meristems', *The Plant Journal* 51: 840-849.

Zhou, C., Labbe, H., Sridha, S., Wang, L., Tian, L., Latoszek-Green, M., Yang, Z., Brown, D., Miki, B. and Wu, K. (2004) 'Expression and function of HD2-type histone deacetylases in Arabidopsis development', *Plant J* 38(5): 715-24.

Zhou, C., Zhang, L., Duan, J., Miki, B. and Wu, K. (2005) 'HISTONE DEACETYLASE19 is involved in jasmonic acid and ethylene signaling of pathogen response in Arabidopsis', *Plant Cell* 17(4): 1196-204.